Ministère de l'Enseignement Supérieur et de la Recherche Scientifique
Université Hassiba Benbouali de Chlef
Faculté de Technologie
Département d'Electrotechnique

THÈSE

Présentée pour l'obtention du diplôme de

DOCTORAT

Filière : Electrotechnique
Spécialité : Réseaux Electriques

Par
SELMA Belkacem

Thème :

OPTIMISATION ÉNERGÉTIQUE D'UN SYSTÈME ÉOLIEN BASÉ SUR UN GÉNÉRATEUR À RELUCTANCE SYNCHRONE (SYNRM)

"ENERGY OPTIMIZATION OF A WIND SYSTEM BASED ON A SYNCHRONOUS RELUCTANCE GENERATOR (SYNRM)"

Soutenue le **12/12/2024**, devant le jury composé de :

DJAHBAR Abdelkader	Professeur	Université de Chlef	Président
BELMADANI Bachir	Professeur	Université de Chlef	Directeur de thèse
BOUNADJA Elhadj	MCA	Université de Chlef	Co- Directeur de thèse
HELAIMI M'hamed	Professeur	Université de Chlef	Examinateur
DJERIRI Youcef	MCA	Université de Sidi Belabès	Examinateur
BESSAAD Taieb	MCA	Université de Chlef	Examinateur
BOUDJEMA Zinelaabidine	Professeur	Université de Chlef	Invité

Abstract

ملخص:

تلعب طاقة الرياح دوراً حيوياً في التحول العالمي نحو الطاقة المتجددة. وقد أدى النمو الصناعي السريع لهذا القطاع إلى جعل توربينات الرياح أساسية في تزويد شبكات الكهرباء بالطاقة النظيفة. من بين التقنيات المستخدمة في توليد طاقة الرياح، تعد الماكينات المتزامنة ذات المغناطيس الدائم (PMSM) والمولدات الحثية ذات التغذية المزدوجة (DFIG) من الحلول الشائعة، إلا أنها تواجه تحديات مثل الاعتماد على المواد النادرة وحدود الأداء عند السرعات العالية.

تتناول هذه الأطروحة دراسة استخدام المولدات التزامنية بالتحريض (SynRG) كحل بديل لأنظمة تحويل طاقة الرياح، لما توفره من مزايا مثل التشغيل الخالي من المغناطيس وكفاءة الأداء على نطاق واسع من السرعات. الهدف الأساسي هو تحسين كفاءة تحويل الطاقة وتعزيز التحكم في أنظمة طاقة الرياح من خلال دمج أساليب التحكم المتقدمة.

من خلال تطوير استراتيجية تحكم جديدة تجمع بين التحكم غير المعتمد على النماذج (MFC) وخوارزميات تحسين مستوحاة من سلوك النمل(ACO) ، تهدف هذه الدراسة إلى تحسين الطاقة المستخرجة من توربينات الرياح مع تقليل التذبذبات في القدرة والتشوهات التوافقية. تقدم الأطروحة نمذجة تفصيلية ومحاكاة والتحقق من نظام طاقة الرياح المعتمد على SynRG، مما يُظهر تحسناً في متانة النظام ودقته وكفاءته. تقدم النتائج رؤى واعدة حول إمكانات SynRG لتحسين استدامة وأداء أنظمة طاقة الرياح.

الكلمات المفتاحية:

طاقة الرياح، المولد التزامني بالتحريض، التحكم المتقدم، الطاقة المتجددة، التحكم غير المعتمد على النماذج، خوارزمية النمل، MATLAB/Simulink.

Abstract:

Wind energy plays a crucial role in the global transition to renewable energy. Its rapid industrial growth has made wind turbines essential for supplying electrical grids with clean energy. Among the technologies used for wind power generation, permanent magnet synchronous machines (PMSM) and double-fed induction generators (DFIG) are commonly adopted but present challenges such as reliance on rare-earth materials and performance limitations at high speeds.

This thesis investigates the use of synchronous reluctance generators (SynRG) as an alternative solution for wind energy conversion systems, offering advantages like magnet-free operation and efficient performance across a broad speed range. The primary objective is to improve energy conversion efficiency and enhance the control of wind power systems by integrating advanced control methods.

Through the development of a novel control strategy combining model-free control (MFC) and ant colony optimization (ACO) algorithms, this research aims to optimize the energy extracted by wind turbines while reducing power fluctuations and harmonic distortions. The thesis presents detailed modeling, simulation, and validation of the SynRG-based wind power system, demonstrating improved system robustness, precision, and efficiency. The results provide promising insights into the potential of SynRG to improve the sustainability and performance of wind energy systems.

Keywords:

Wind Energy, Synchronous Reluctance Generator, Advanced Control, Renewable Energy, Model-free control, Ant Colony Optimization, MATLAB/Simulink.

Résumé :

L'énergie éolienne joue un rôle crucial dans la transition mondiale vers les énergies renouvelables. Sa croissance industrielle rapide a rendu les éoliennes indispensables pour alimenter les réseaux électriques en énergie propre. Parmi les technologies utilisées pour la production d'énergie éolienne, les machines synchrones à aimants permanents (PMSM) et les générateurs à induction à double alimentation (DFIG) sont couramment adoptés, mais elles présentent des défis tels que la dépendance aux matériaux rares et des limitations de performance à haute vitesse.

Cette thèse explore l'utilisation des générateurs à réluctance synchrone (SynRG) comme solution alternative pour les systèmes de conversion d'énergie éolienne, offrant des avantages tels que l'absence d'aimants et une performance efficace sur une large plage de vitesses. L'objectif principal est d'améliorer l'efficacité de conversion énergétique et d'optimiser le contrôle des systèmes éoliens en intégrant des méthodes de contrôle avancées.

Grâce au développement d'une stratégie de contrôle innovante combinant le contrôle sans modèle (MFC) et les algorithmes d'optimisation par colonies de fourmis (ACO), cette recherche vise à maximiser l'énergie extraite par les éoliennes tout en réduisant les fluctuations de puissance et les distorsions harmoniques. La thèse présente la modélisation, la simulation et la validation détaillées du système éolien basé sur le SynRG, démontrant une amélioration de la robustesse, de la précision et de l'efficacité du système. Les résultats offrent des perspectives prometteuses sur le potentiel du SynRG à améliorer la durabilité et la performance des systèmes d'énergie éolienne.

Mots clés :

Énergie éolienne, Générateur à réluctance synchrone, Contrôle avancé, Énergie renouvelable, Contrôle sans modèle, Optimisation par colonies de fourmis, MATLAB/Simulink.

List of Publications

[1] SELMA, B., BOUNADJA, E., BELMADANI, B., SELMA, B., & FLIESS, M. (2024). A novel intelligent control approach for wind energy conversion systems with synchronous reluctance generators. International Journal of Circuit Theory and Applications, 52(8), 3967-3987.

[2] KACEMI, W. M., BOUNADJA, E., BELHADJ DJILALI, A., & SELMA, B. (2024). Enhancing Wind Energy Conversion Efficiency with Parallel Hybrid Excitation Synchronous Generators based on Second-Order Sliding Mode Control. Przeglad Elektrotechniczny, 2024(4).

[3] SELMA, B., BOUNADJA, E., BELMADANI, B., SELMA, B. (2024). Improving dynamic response and stability of three-phase synchronous reluctance machines with a novel higher-order field-oriented sliding mode control. International Journal of Dynamics and Control, 1-10.

[4] SELMA, B., BOUNADJA, E., BELMADANI, B., SELMA, B. (2024). Improved performance and robustness of synchronous reluctance machine control using an advanced sliding mode and direct vector control. Advanced Control for Applications: Engineering and Industrial Systems, 6(1), e178.

[5] SELMA, B., BOUNADJA, E., BELMADANI, B., SELMA, B., & ABOUAISSA, H. (2023). Model-free control-based vector control of synchronous reluctance motor. International Journal of Dynamics and Control, 11(6), 3062-3073.

List of Conferences

[1] Selma B, Bounadja E, Belmadani B, et al. L'application d'une commande sans modèle aux machine synchrone a réluctance. The Second Doctoral Technology Symposium, 2022.

[2] Selma B, Bounadja E, Belmadani B, et al. MATLAB/Simulink Modeling and Control of Two Synchronous Reluctance Generators for a Grid Connected Wind Farm. The first International Conference on Renewable Solutions for Ecosystems: Towards a Sustainable Energy Transition (ICRSEtoSET), 2023.

[3] Selma B, Bounadja E, Belmadani B, et al. Enhancing Performance and Robustness of Vector Control for Three-Phase Synchronous Reluctance Machine Using Second-Order Sliding Mode. The first international Conference on Advances in Electronics, Control and Computer Technologies ICAECCT'23, 2023.

[4] Selma B, Bounadja E, Belmadani B, et al. Modeling and Control of Variable Structure Scheme for Grid-Connected Wind Power Production System with Parallel-Connected Synchronous Reluctance Generators. The first international Conference on Advances in Electronics, Control and Computer Technologies ICAECCT'23, 2023.

[5] Selma B, Bounadja E, Belmadani B, et al. Exploring the Potential of Synchronous Reluctance Generator in Grid-Connected Wind Energy Conversion Systems: A Comprehensive Feasibility Study and Control Analysis. The second International Conference on Electronics, Energy and Measurement (IC2EM 2023), 2023.

[6] Selma B, Bounadja E, Belmadani B, et al. A Novel Intelligent Control Approach for WPCS with Synchronous Reluctance Generator. The Third Doctoral Technology Symposium, 2023.

[7] Selma B, Bounadja E, Belmadani B, et al. COMBINING ACO AND MFC FOR EFFICIENT WIND ENERGY SYSTEMS USING SynRG. The Fourth Doctoral Technology Symposium, 2024.

Contents

List of figures

GENERAL INTRODUCTION

CHAPTER 1: FUNDAMENTAL PRINCIPLES OF WIND ENERGY

CHAPTER 2: AN1LYTICAL MODELING AND CONVENTIONAL CONTROL OF SynRG-BASED WPS

CHAPTER 3: MODEL-FREE CONTROL STRATEGY OF SynRG-BASED WPS

CHAPTER 4: ENERGY OPTIMIZATION USING ADVANCED CONTROL OF SynRG-BASED WPS

List of tables

CHAPTER 1: FUNDAMENTAL PRINCIPLES OF WIND ENERGY

CHAPTER 2: AN1LYTICAL MODELING AND CONVENTIONAL CONTROL OF SynRG-BASED WPS

CHAPTER 4: ENERGY OPTIMIZATION USING ADVANCED CONTROL OF SynRG-BASED WPS

Dedication

I dedicate this to my parents, whose love and support have been my foundation.

To my brother and sisters, for their companionship and encouragement.

To all my friends, for their unwavering presence and understanding.

To everyone who holds a special place in my heart.

And to those who have helped me, whether from near or far, your guidance and assistance have made all the difference.

Belkacem SELMA.

Acknowledgments

This work presents in detail the research I conducted for my doctoral thesis at the Laboratory of Electrical Engineering and Renewable Energies (LGEER), Hassiba Benbouali University of Chlef.

First and foremost, I thank God, the Almighty, for granting me the strength and willpower to endure all these years of study.

I would like to express my deepest gratitude and sincere thanks to Professor Bachir BELMADANI and Elhadj BOUNADJA, both Professors at Hassiba Benbouali University of Chlef, for their constant support, their positive outlook on the progress of my work, and their invaluable guidance throughout this research. I have learned so much while working with them.

I am also profoundly grateful to the following professors for accepting to examine this work and for their participation in the defense jury:

Professor DJAHBAR Abdelkader, Hassiba Benbouali University of Chlef

Professor HELAIMI M'hamed, Hassiba Benbouali University of Chlef

MCA DJERIRI Youcef, University of Sidi Belabès

MCA BESSAAD Taieb, Hassiba Benbouali University of Chlef

Professor BOUDJEMA Zinelaabidine, Hassiba Benbouali University of Chlef

I extend my heartfelt thanks to my fellow doctoral students at Hassiba Benbouali University of Chlef for the enriching discussions and exchanges we have shared.

I would also like to thank all the members of my family and my friends. Your love, encouragement, and presence have meant the world to me throughout this journey.

To everyone, a sincere and heartfelt thank you.

Nomenclature

SynRG	Synchronous reluctance generator
WPS	Wind power systems
VC	Vector control
MFC	Model-free control
ACO	Ant colony optimization
PI	Proportional-integral
iP	Intelligent proportional
BTB	Back-to-back converters
MPPT	Maximum power point tracker
MSC	Machine-side converter
GSC	Grid-side converter
PWM	Pulse width modulation
$V_{s\ d,q}$	dq stator voltages
$i_{s\ d,q}$	dq stator currents
R_s	Stator resistance
$L_{s\ d,q}$	dq stator inductances
Ω_r	Generator electrical speed
$\Phi_{s\ d,q}$	dq flux linkage
T_{em}	Electromechanical torque
P_t	Aerodynamic power
ρ	Air density
C_p	Power coefficient
R	Radius of the turbine
V_ω	Wind speed.
λ	Tipspeed ratio
β	Blade-pitch angle
P_g	Active grid power
Q_g	Reactive grid power
Ω_t	Mechanical speed of the turbine
Ω_m	Mechanical speed of the generator
J	Inertia
$V_{g\ d,q}$	dq grid voltages
$i_{g\ d,q}$	dq grid currents
$V_{f\ d,q}$	dq filter voltages

$i_{f\,d,q}$	dq filter currents
ω_g	Grid pulsation.
R_f	Filter resistance
L_f	Filter inductance
V_{DC}	DC-bus voltage
C	Capacitance of DC-bus voltage
α	A non-physical constant parameter
u_{MFC},y	Represent the input and output of the control system.
F	Groups all the unknown signals

GENERAL INTRODUCTION

General introduction

0.1 Introduction to wind energy and global significance

Wind energy, derived from atmospheric temperature differences due to solar heating and the Earth's rotation, has emerged as a powerful source of renewable energy. It plays a critical role in the global transition towards sustainable and environmentally friendly energy sources. Unlike fossil and nuclear energy, wind energy is both local and decentralized, making it widely accessible across diverse regions. This decentralization enables countries to enhance energy independence and mitigate reliance on finite hydrocarbon resources, significantly contributing to global energy security [1,2].

In the past few decades, the wind energy sector has witnessed remarkable growth, evolving from a limited-scale industry into a major contributor to electrical grids worldwide. The transition from smaller turbines producing tens of kilowatts to today’s large-scale systems generating several megawatts underscores the rapid technological advancements and scalability of wind energy solutions [3-5]. Beyond promoting energy independence, wind energy aligns with critical environmental goals, including reducing air pollution and combating climate change, thus reinforcing its position as a central pillar of the global energy transition [6,7].

0.2 Evolution of wind power technologies: an overview

Historically, wind turbine technologies have progressed from fixed-speed systems to the variable-speed topologies that dominate today. Among these, the double-fed induction generator (DFIG) and permanent magnet synchronous generator (PMSG) topologies have emerged as primary configurations. Both designs prioritize efficiency and reliability while addressing the cost and maintenance challenges associated with conventional gearboxes [8]. DFIG technology allows for power converters rated at a fraction of the machine’s capacity, reducing costs but limiting the speed range [9]. In contrast, PMSGs provide higher efficiency and power density but face challenges under high-speed and short-circuit conditions due to fixed excitation from permanent magnets [10,11].

The reliance on rare-earth materials, such as neodymium, within PMSG systems adds complexity due to fluctuating material costs and concentrated global production. Consequently, researchers are exploring new alternatives, including reluctance machines that forgo permanent magnets. These innovations aim to optimize performance and reduce dependencies on rare materials while providing high efficiency, fault tolerance, and compact design for modern wind applications [12-14]. Direct-drive switched reluctance generators (SRG) and synchronous reluctance machines (SynRM) exemplify promising directions in the development of magnet-free, high-efficiency solutions for the wind energy sector [15,16]. The unpredictable nature of wind speeds often prevents wind power generator research from reaching optimal performance, leading to reduced efficiency in using wind energy and diminishing the benefits of wind turbines. Furthermore, frequent fluctuations and the inherent instability of wind power can disrupt the power grid when wind farms are connected, potentially destabilizing the entire system.

0.3 Challenges in wind power generation and grid stability

Despite technological advancements, the integration of wind power into electrical grids poses significant challenges due to the unpredictable nature of wind speeds. The intermittent and fluctuating power output from wind turbines can disrupt grid stability, creating potential issues for balancing supply and demand. Optimal performance in wind power generation is often unattainable due to these irregular wind patterns, limiting the overall efficiency of energy conversion and diminishing the potential benefits of wind energy systems [3,7].

The inherent instability of wind power further complicates its integration, as frequent fluctuations can induce power quality issues and compromise grid reliability. Consequently, addressing these challenges requires innovative control strategies that can enhance energy conversion efficiency, stabilize output, and ensure a seamless interface between wind farms and the larger electrical grid.

0.4 Advances in control strategies for wind power systems

Control strategies play a pivotal role in optimizing wind power systems (WPS) to maximize output, enhance reliability, and improve integration with the grid. Traditionally, vector control (VC) and proportional-integral (PI) controllers have been the most implemented methods in WPS due to their straightforward design and ease of application [2,7]. However, the nonlinear characteristics of WPS and the variability of wind conditions often limit the performance of these traditional controllers, which may fail to respond adequately to the dynamic challenges of wind energy systems.

In response, nonlinear control techniques, such as model-based control (MBC) and model predictive control (MPC), have been introduced to improve robustness and flexibility in WPS management. MBC methods require detailed system modeling and a deep understanding of system dynamics to manage control objectives. Yet, they may falter under conditions of parametric uncertainty or unexpected fluctuations, both of which are prevalent in industrial wind power applications. MPC, on the other hand, offers rapid dynamic response and safety but introduces computational complexity due to continuous prediction steps at each sampling interval, closely tying its success to model accuracy [17-19].

0.5 The rise of model-free control techniques and ant colony optimization

As a solution to the challenges posed by MPC and MBC techniques, researchers have introduced a control principle known as model-free control (MFC) [20,21]. MFC provides a solution by eliminating the dependency on a detailed system model, thus reducing the associated complexities, and increasing adaptability to changing environmental conditions. Unlike model-based methods, MFC utilizes a continuously updated local linear approximation that is valid within a short time window. This approach allows MFC to adjust to new data points rapidly, making it particularly well-suited for wind energy applications where environmental conditions can fluctuate significantly. By incorporating a fast estimator, MFC continuously recalibrates itself in response to changing system states, making it an attractive choice for enhancing the performance and stability of WPS in the face of wind variability.

To further optimize MFC parameters and enhance control performance, we have integrated ant colony optimization (ACO) as a tuning mechanism. ACO is a nature-inspired optimization algorithm that models the foraging behavior of ants to find optimal paths [22]. In the context of MFC, ACO systematically searches for optimal parameter configurations by simulating the pheromone-laying and path-following behaviors observed in ant colonies. This enables the control system to identify ideal control parameters for MFC, which might otherwise be challenging to determine manually.

This innovative MFC-ACO strategy thus presents a promising solution for overcoming the limitations of traditional model-based control methods, achieving enhanced adaptability, optimized control performance, and robustness for WPS applications. Through this approach, the potential of wind energy as a sustainable resource can be further optimized, supporting global efforts to transition towards renewable energy sources in a stable and efficient manner.

0.6 Objectives of the thesis

This thesis focuses on enhancing the control performance of wind power systems using SynRG through an innovative approach that combines MFC with an optimization algorithm. Specifically, the integration of MFC with an ACO algorithm presents a novel solution for maximizing WPS efficiency, stability, and resilience against fluctuating wind conditions. The core objectives of this research include:

- Developing a robust, efficient control strategy for SynRG-based WPS that minimizes reliance on precise modeling.
- Reducing the amplitude of oscillations in currents and the active and reactive power injected into the grid.
- Ensuring the proposed control strategy’s adaptability to across variable wind scenarios.

0.7 Methodological approach

To achieve these objectives, the thesis employs a multi-faceted methodology involving:

- **Literature review:** Analyzing existing control strategies for wind energy systems and recent advancements in reluctance-based generator technologies.
- **System modeling and simulation:** Creating a detailed model of the wind power system, including SynRG and converter dynamics, followed by simulations to validate the control performance.
- **Control strategy development:** Integrating MFC with ACO to design a resilient control strategy capable of adapting to variable wind conditions without detailed modeling.

- **Performance validation:** Comparing the proposed control method against traditional techniques through simulated scenarios that reflect real-world wind variability.

0.8 Thesis structure

This thesis aims to improve the control system performance of a WPS-SynRG by introducing a novel control strategy. This approach integrates an MFC method with an ant colony optimization (ACO) algorithm, offering a new direction for enhancing system efficiency.

The work of this thesis is divided into four chapters as follows (as shown in Figure 1):

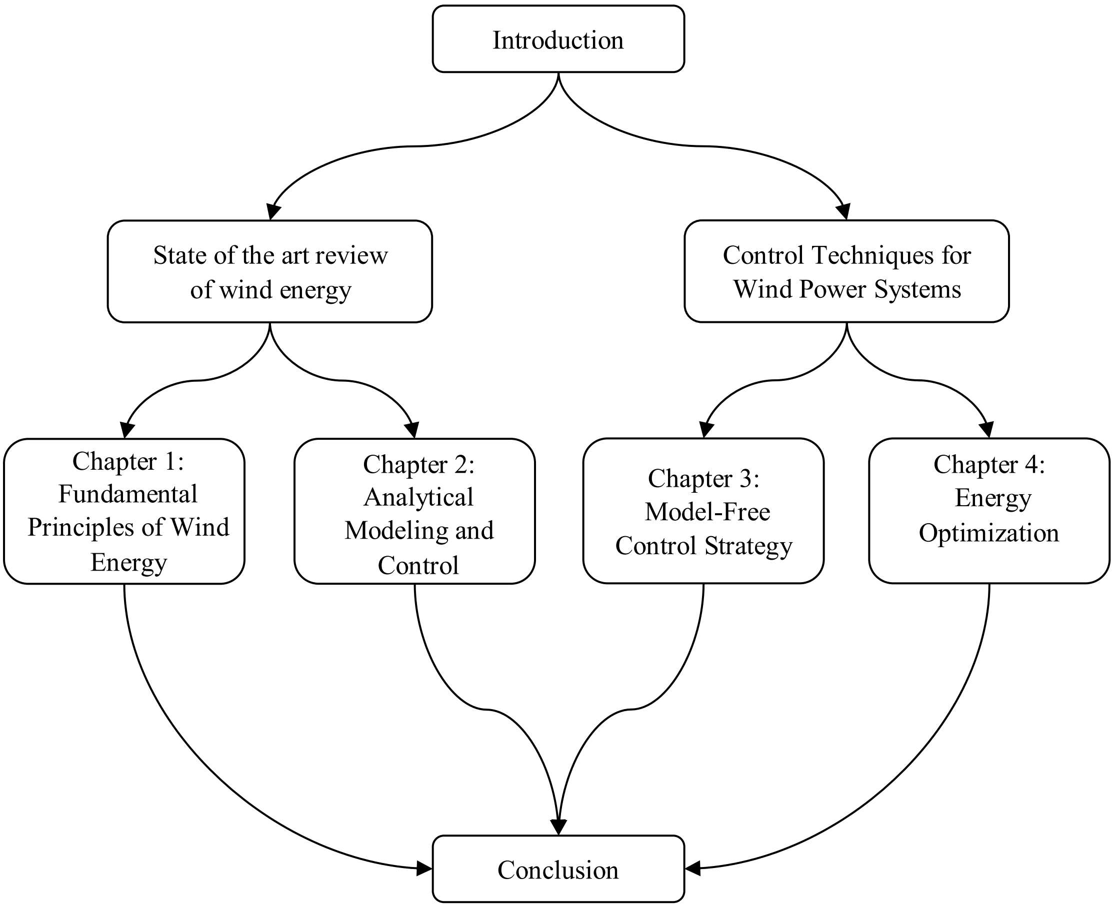

Figure 0. 1 Structure of the thesis.

- Chapter 1 covers the fundamental principles of wind energy, offering a concise overview of the various types of wind turbines. It will then explore the different components that constitute a wind turbine. Following this, the advantages of the synchronous reluctance machine will be highlighted. The chapter will conclude with a summary of Algeria's renewable energy development program and an outline of the objectives of this doctoral thesis. In essence, the opening section of the thesis will summarize the findings of a literature review on the core principles of wind energy and the current advancements in synchronous reluctance machines.

- Chapter 2 focuses on key concepts and aspects related to the analytical modeling of various elements within the wind energy conversion chain addressed in this work. It covers the modeling and maximum power point tracking (MPPT) control of a wind turbine, the modeling of the SynRG in the Park reference frame, and both machine-side converter (MSC) and grid-side converter (GSC) control using classical PI controllers. Additionally, it discusses the modeling of power converters and the DC bus. The chapter concludes with the presentation of simulation results to validate.
- Chapter 3 proposes a control strategy that eliminates the need for modeling or identification procedures of the wind power system (WPS) while ensuring robustness against both endogenous disturbances (where control performance remains unaffected by internal changes) and exogenous disturbances (such as variable wind speed). To achieve this, the WPS structure is divided into two parts as discussed in Chapter 2: the GSC and the MSC, with each part being controlled by an MFC. We then provide conclusive results that demonstrate the practical stability of the proposed control method in comparison to the classical control approach. The effectiveness of our control strategy is validated under two scenarios with variable wind speed.
- Chapter 4 This chapter focuses on minimizing the ripples in the currents and the active and reactive powers injected into the grid, which are observed with traditional control methods. We propose a new method based on a combination of two different techniques: the MFC algorithm and the ACO algorithm. This approach ensures the control and regulation of active and reactive powers. This new strategy differs from many other works in terms of principle, simplicity, ease of implementation, and sustainability. The simulation results of the WPS, controlled using the optimized MFC-ACO controller, demonstrate good robustness and a significant reduction in the oscillations of the currents and powers injected into the electrical grid.

We conclude our work with a general conclusion that provides a summary of the findings and perspectives for future research.

CHAPTER 1: FUNDAMENTAL PRINCIPLES OF WIND ENERGY

Chapter 1: Fundamental principles of wind energy

1.1 Introduction

For centuries, humans have harnessed the power of wind to propel ships, grind grain, and pump water [23]. Today, this energy source is used to generate electricity. Wind energy has seen significant industrial growth in recent years due to its numerous advantages, particularly as a renewable, non-polluting energy source that helps improve air quality and combat the greenhouse effect [24].

In this chapter, we will explore various aspects related to the general structure of wind energy conversion systems, the different types of wind turbines, and their operation. Additionally, this chapter will discuss Algeria's renewable energy development program and the objectives of this thesis, which aim to enhance the performance of wind turbines equipped with synchronous reluctance generator (SynRGs) and connected to the electrical grid.

1.2 Overview of wind energy

1.2.1 Definition of wind energy

Wind energy is defined as the process of converting the kinetic energy of the wind into mechanical energy using a wind turbine. This mechanical energy is then converted into electrical energy through an electric generator, making wind power a renewable and sustainable source of electricity [25,26].

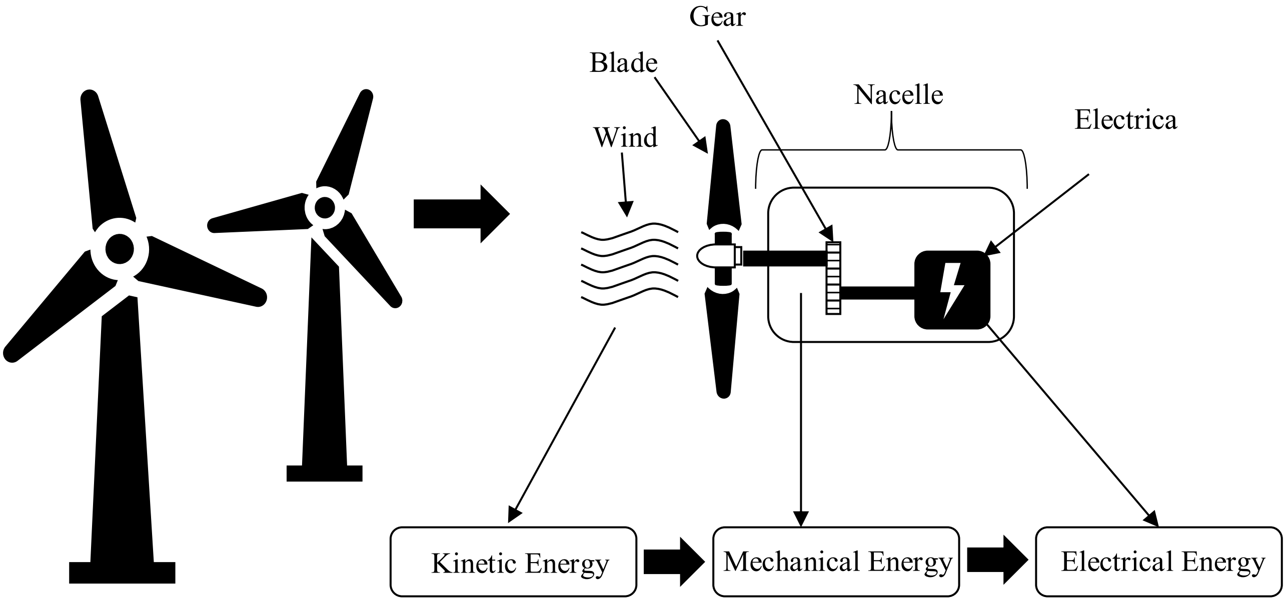

Figure 1.1 Conversion of wind kinetic energy into electrical energy.

Figure 1.1 shows how wind energy is converted into electrical energy. The conversion chains involve many fields of physics such as aerodynamics, mechanics, electricity, power electronics, automation, computer science, etc [24].

1.2.2 Different types of wind turbines

There are two fundamental types of wind turbines, based on the geometry of the shaft on which the blades are mounted [27]:

- Horizontal-axis wind turbines.
- Vertical-axis wind turbines.

1.2.2.1 Vertical-axis wind turbines

Research on this type of wind turbines is extensive because it offers the advantage of not requiring a blade orientation system, and its conversion chain (gear box and generator) is located at ground level, making maintenance easier. Three designs have reached the stage of industrialization, namely: the Savonius rotor, the Darrieus rotor, and the H-rotor, Figure 1.2, [28,29].

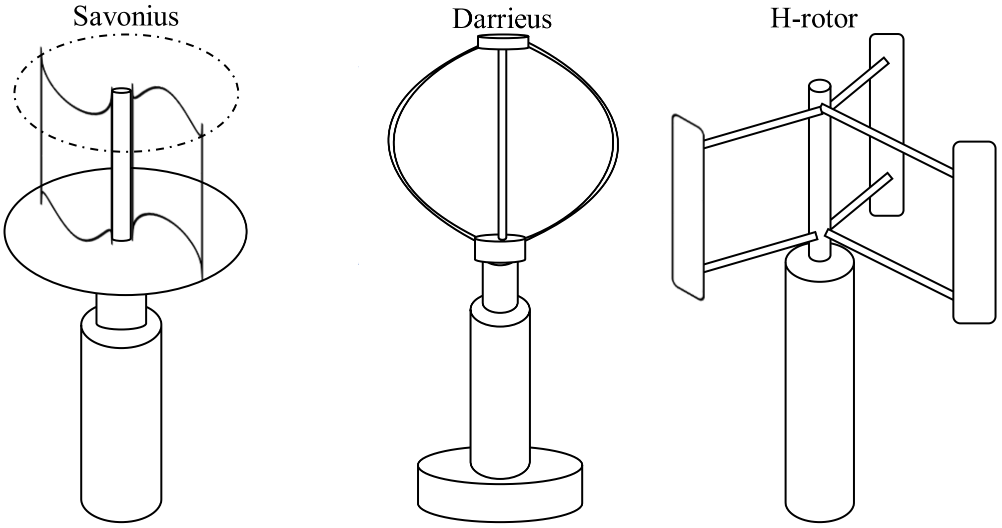

Figure 1.2 Vertical-axis wind turbine

However, some of these wind turbines need to be externally started, and the mast, often very heavy, is subject to significant mechanical stresses. Additionally, the efficiency of these turbines is lower compared to horizontal-axis wind turbines.

These drawbacks have forced manufacturers to abandon this technology for medium and large-scale onshore wind farms. However, it is still used for very low-power applications and large-scale floating offshore wind turbines, [27,30].

1.2.2.2 Horizontal-axis wind turbines

Horizontal-axis wind turbines are much more widely used, even though they often require a blade orientation mechanism and a nacelle that houses the entire conversion chain. The main advantage of this design is its higher aerodynamic efficiency compared to vertical-axis wind turbines. Additionally, it can start autonomously and occupies minimal space at ground level. Different designs of horizontal-axis wind turbines use two-bladed, three-bladed (the most common, Figure 1.3), or multi-bladed rotors [31,32].

There are two categories of horizontal-axis wind turbines, Figure 1.4 [33]:

- Upwind: The wind blows on the front of the blades towards the nacelle. The blades are rigid, and the rotor is oriented according to the wind direction by a device (rudder for very low-power turbines and an active system for high-power turbines).
- Downwind: The wind blows on the back of the blades from the nacelle. Although the rotor of this structure is self-orienting, the upwind configuration is more commonly used because it is simpler, provides better efficiency, and offers good stability for high-power applications. In the downwind position, the wind passes through the nacelle and the tower before reaching the blades, causing wind disturbance [33].

Figure 1.3 Horizontal-axis wind turbine
(https://img.archiexpo.fr/images_ae/photo-g/62400-11048784.jpg)

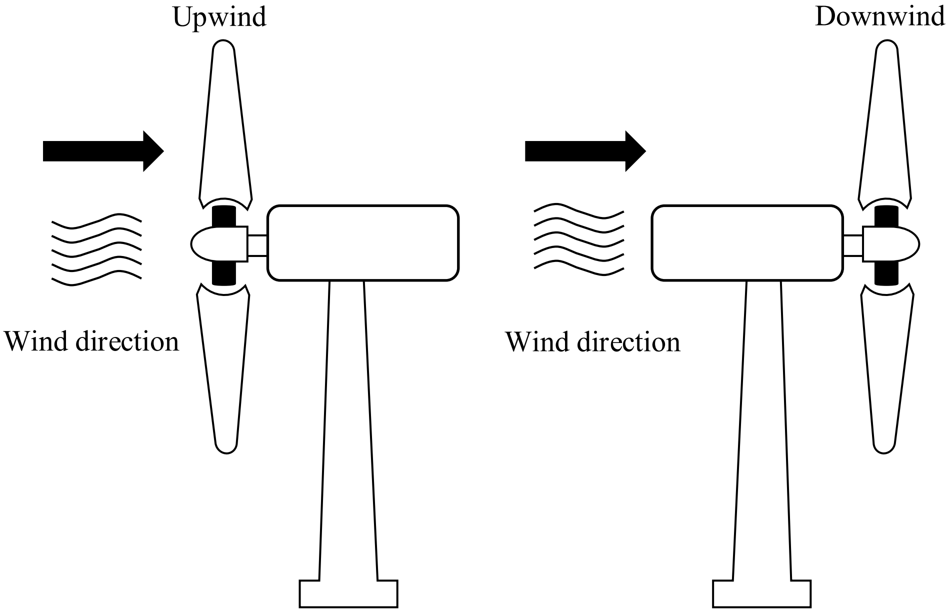

Figure 1.4 Types of horizontal-axis wind turbines

Wind turbines are classified into three groups based on the power output and the diameter of the turbine blades [33]:

- Small: Blade diameter less than 12 meters, with a power output of less than 40 kW.
- Medium: Blade diameter between 12 meters and 45 meters, with a power output ranging from 40 kW to 1 MW.
- Large: Blade diameter 46 meters and above, with a power output of 1 MW and more.

1.2.2.3 Components of horizontal-axis wind turbine

Figure 1.5 illustrates the main components of horizontal-axis wind turbine. We describe some of these components in the paragraphs below, [24,32-35].

- **The tower (Mast)**

The tower, also known as the mast or pylon, is a support structure whose height depends on the turbine's rated power. It must be tall enough to avoid ground-level wind disturbances and to provide sufficient clearance for the blades. The mast is typically made of metal (steel, aluminum, etc.) or concrete and can be cylindrical or conical in shape for high-power turbines [35]. For lower-power applications, a low-cost lattice tower may be used. In addition to supporting the nacelle and rotor, the mast houses the access ladder to the nacelle, the grid connection equipment, control components, and electrical cables.

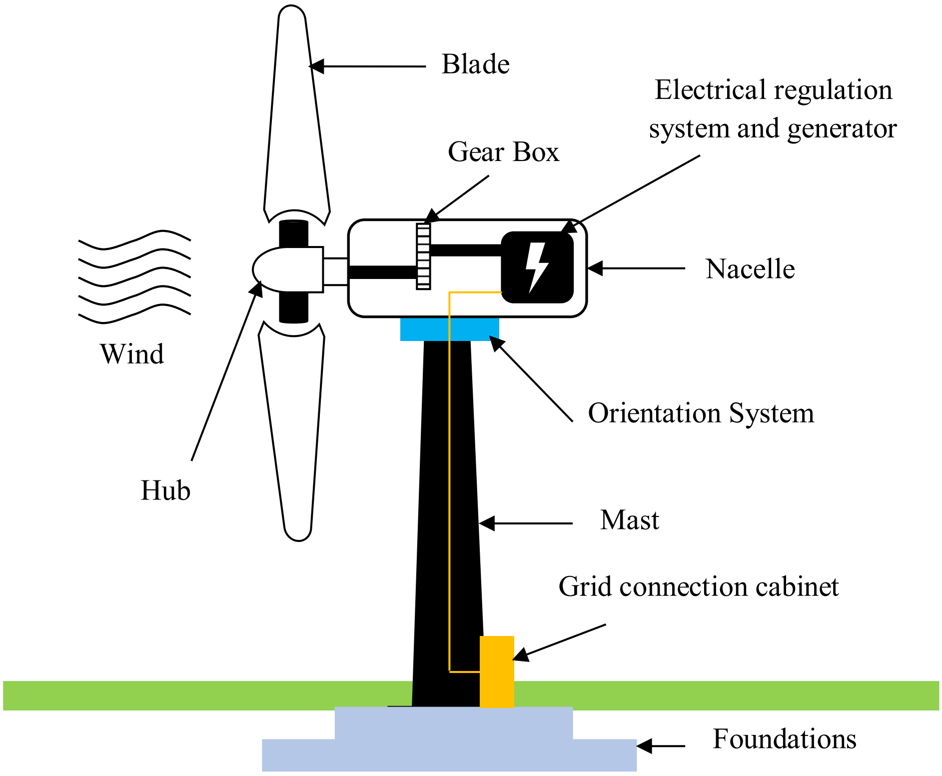

Figure 1.5 Components of horizontal-axis wind turbine

- **The rotor**

The rotor generally consists of two, three, or more blades attached to a hub [32,35]. It is driven by the wind force captured by the blades, and it is connected to an electrical generator, either directly or indirectly through a mechanical gearbox.

- **Blades**

The blades capture the wind's energy and transmit it to the rotor. Most wind turbines have three blades, as this number provides a balance between stability, turbine performance, and manufacturing costs [32,35].

- **The hub**

The hub is the component that holds the blades and their orientation system. It must be able to withstand strong vibrations and shocks, especially during the turbine’s startup or when wind speeds change suddenly.

- **The nacelle**

The nacelle houses mechanical, pneumatic components, the generator, and some electronic control systems. It is mounted at the top of the tower, and it is designed to always face the wind. The electrical energy produced by the generator is transmitted through electrical cables that run down inside the tower of the wind turbine [23].

- **The gearbox**

The gearbox is used to increase the rotational speed between the rotor shaft (slow shaft) and the generator shaft (fast shaft). This gearbox can have a fixed or variable mechanical ratio to ensure that the generator operates at a constant speed.

- **The generator**

The generator is the key component responsible for converting the mechanical energy produced by the wind rotor into electrical energy. There are different types of generators based on the design of the wind turbine [24]:

- ❖ Synchronous Generator: In this case, the generator is directly coupled to the rotor, which means that the turbine blades are mounted directly onto the generator’s shaft. This eliminates the need for a gearbox, simplifying the system and reducing maintenance costs.
- ❖ Induction Generator: Here, the generator is connected to the rotor via a gearbox, which adjusts the rotational speed to match the generator's requirements. This type of configuration is common in wind turbines requiring variable speed control to maximize efficiency.

1.2.3 Wind energy conversion chain configurations

The electrical configuration of a wind turbine plays a crucial role in determining its performance and operation. The ability of a turbine to function at either fixed or variable speeds is primarily influenced by its electrical setup [36-38]. Proper configuration and control help optimize energy capture, especially in low to medium wind conditions.

1.2.3.1 Fixed-speed wind turbine configuration

In this setup, the generator, typically an induction machine (IG), operates at a fixed speed or experiences minimal variation by adjusting the machine's slip. Two types of generators are used in this configuration: one designed for lower power during lower wind speeds, and another for higher power during stronger winds. The main drawback of this configuration is the complexity and mass of the system, which increases its cost and maintenance requirements. An alternative involves altering the stator wiring to modify the number of poles, allowing the turbine to switch between fast daytime rotation and slower nighttime operation to minimize noise.

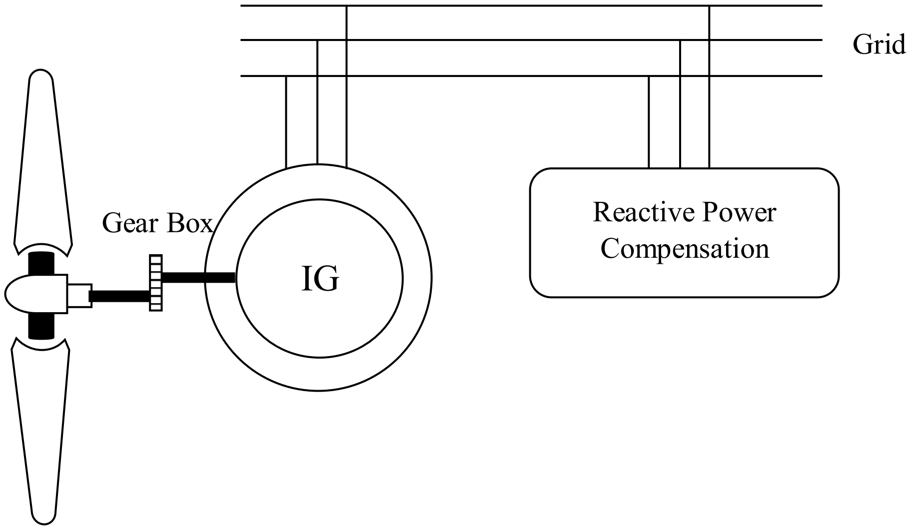

Figure 1.6 Fixed-speed wind turbine using an induction generator.

Early large-scale wind turbines used a squirrel-cage induction generator directly connected to the electrical grid (Figure 1.6). This generator is driven by a gearbox and maintains an almost constant speed with the help of a mechanical blade pitch control system.

1.2.3.2 Variable-speed wind turbine configuration

Variable-speed wind turbines are now the dominant choice in the industry. The term "variable speed" refers to the turbine's ability to operate independently of the grid's frequency. This flexibility maximizes energy capture from the wind, making the system more efficient.

Three types of generators are commonly used in variable-speed wind turbines: synchronous generators, induction generators, and doubly-fed induction generators (DFIG).

- **Induction generator in variable-speed wind turbines**

In this configuration, the turbine drives an induction generator that connects to the grid via a power converter on the stator circuit (Figure 1.7). Unlike fixed-speed turbines, the output voltage and frequency are not controlled by the grid, allowing for turbine speed regulation. The inverter system ensures a stable DC bus voltage, maintaining efficient operation.

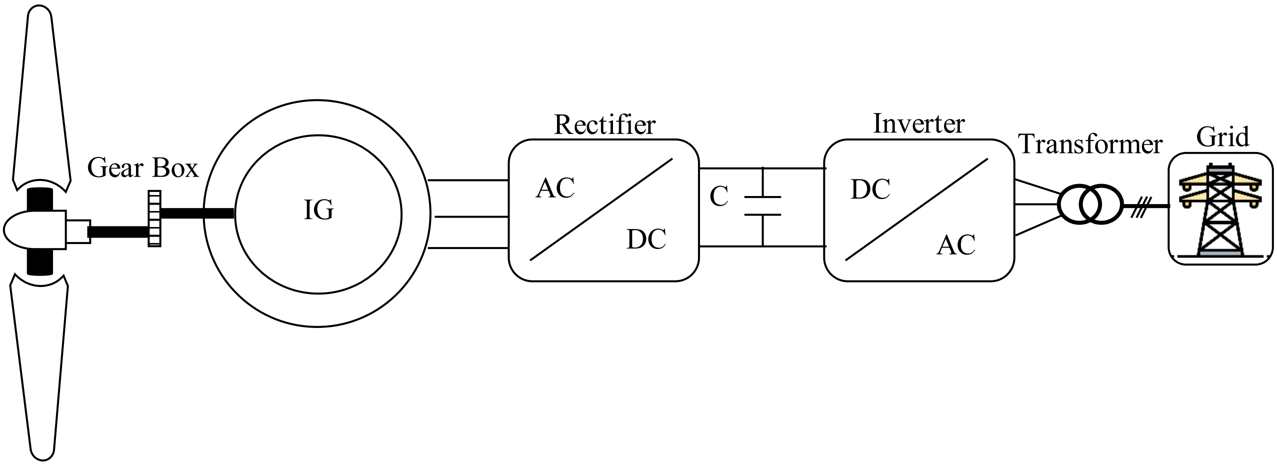

Figure 1.8 Variable-speed wind turbine using an induction generator.

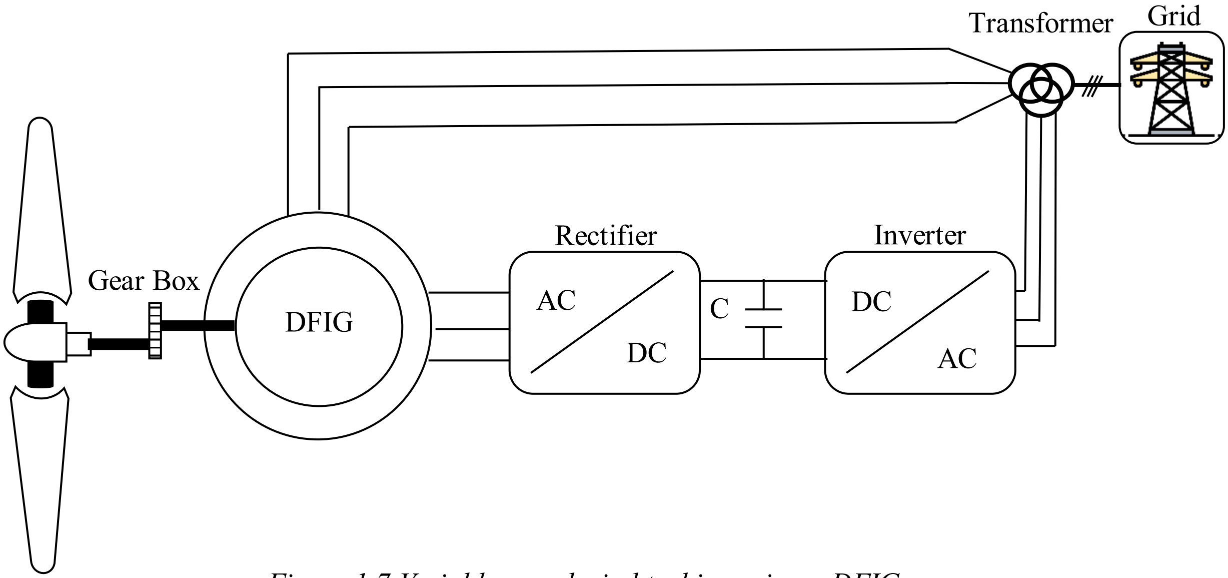

Figure 1.7 Variable-speed wind turbine using a DFIG.

- **Doubly-fed induction generator in wind turbines**

In this configuration, the stator of the DFIG is connected directly to the grid, while a power converter is linked to the rotor circuit (Figure 1.8). The rectifier controls the rotor voltage, allowing precise control over the generator's operation. The inverter keeps the DC bus voltage stable, ensuring continuous and reliable energy output from the turbine.

- **Synchronous generator in variable-speed wind turbines**

In a synchronous generator setup, the rotor's magnetic field must rotate at the same speed as the stator's magnetic field. If the generator is connected to the grid, its speed must be multiple of the stator's current frequency. This presents challenges in maintaining a stable turbine speed and ensuring smooth synchronization with the grid. To address this, a power electronics interface is used between the stator and the grid, enabling variable-speed operation over a broad wind range (Figure 1.9).

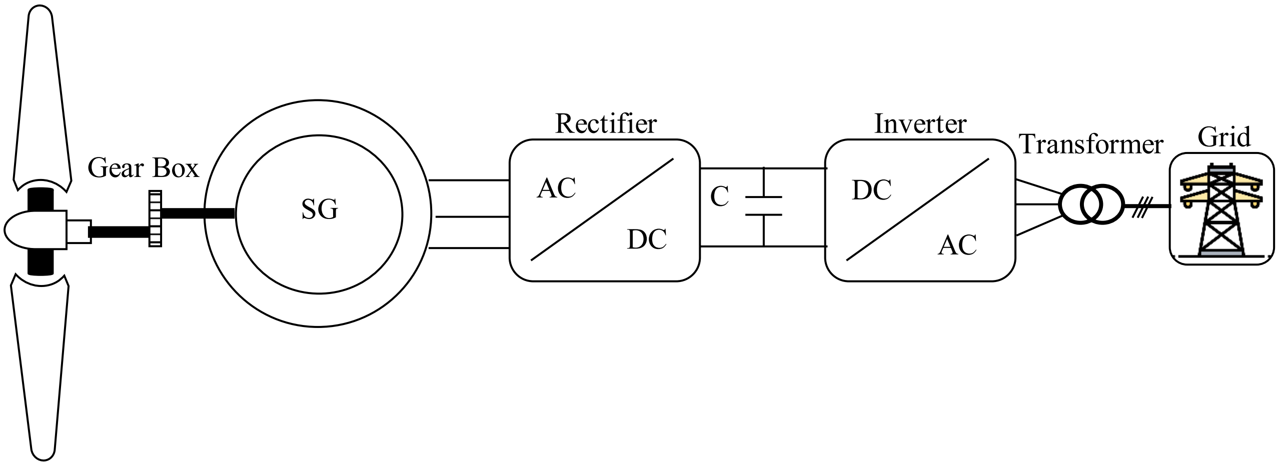

Figure 1.9 Variable-speed wind turbine using a synchronous generator.

1.2.3.3 Comparison between the two types of operations

A comparison between the two types of electricity generations, fixed-speed, and variable-speed, is presented in Table 1.1.

This comparison highlights the trade-offs between the simpler, cost-effective fixed-speed system and the more efficient, but complex, variable-speed system.

Table 1.1 Comparison between operation types

Fixed-Speed Wind Turbine	Variable-Speed Wind Turbine
• Lower cost.	• Operates at variable speed.
• Simple electrical system.	• Improved energy efficiency.
• Lower efficiency.	• Reduced torque fluctuations.
• Regular maintenance required for the gearbox.	• Generates higher-quality electrical energy.

1.3 Synchronous reluctance machines (SynRM)

In recent years, significant progress in wind power systems (WPS) has been fueled by the development of various generator technologies, such as PMSG and DFIG [39-43]. However, the high cost of rare earth materials in PMSGs and rotor losses in DFIGs have driven researchers to explore alternative solutions. One promising option is the synchronous reluctance generator (SynRG), which combines robustness, simplicity, and cost-effectiveness [44].

The history of the SynRM dates back to 1923, when J.K. Kostko introduced the first model. Key advancements occurred in the 1960s with the introduction of line-start synchronous AC motors, and by the 1990s, significant research aimed at enhancing the design and control of these machines. Recent improvements have made the SynRM a commercially viable, high-efficiency alternative to induction motors. Thanks to their cost-efficiency, lower maintenance needs, and improved durability, SynRGs are increasingly favored for modern wind power systems [44].

What differentiates SynRGs from other generators is their innovative design, which eliminates the rotor cage, windings, and magnets found in traditional generators (Figure 1.10). This reduces both costs and maintenance requirements while increasing the generator's durability—an essential attribute in wind power applications [45-47]. Although synchronous reluctance machines (SynRMs) have primarily been used as motors in various industries [48-51], their use as generators in wind power systems is a relatively new and promising development [46,47,52,53].

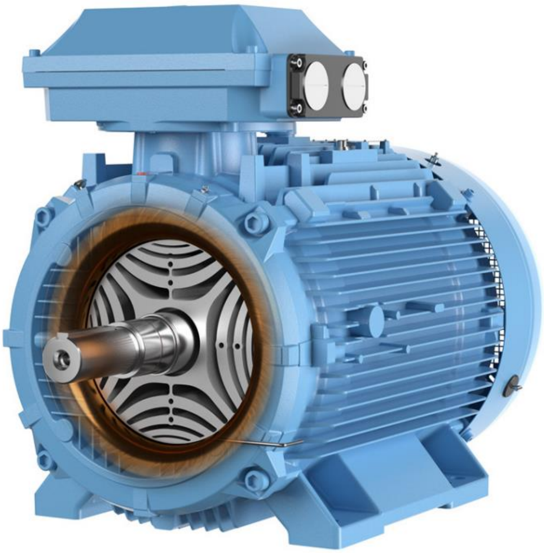

Figure 1.10 Synchronous reluctance machines.
(https://www.elprocus.com/wp-content/uploads/Synchronous-Reluctance-Motor-or-SRM.jpg)

1.3.1 Operating principle

The SynRM operates based on the principles of reluctance torque, which arises due to the tendency of magnetic flux to follow a path of least reluctance.

The SynRM is structurally a synchronous machine without excitation. The classic form of the machine has a salient rotor equipped with a squirrel cage; it contains neither magnets nor excitation windings (see Figure 1.11). The stator has the same structure as that of an asynchronous machine. The cage ensures direct start from the power grid and helps improve operational stability in synchronism (for example, during a sudden load torque).

This machine has the advantage of maintaining a constant speed under load up to a certain value of the resistant torque, which an asynchronous machine cannot do due to slip [54,55].

1.3.1.1 Rotor design

The rotor in a SynRM has no windings or permanent magnets. It is designed with materials that create paths of varying reluctance (resistance to magnetic flux). This typically involves laminations with air gaps or flux barriers, making the rotor anisotropic (having different properties in different directions).

1.3.1.2 Stator and magnetic field

The stator is similar to that in other synchronous machines and is equipped with a three-phase winding. When three-phase AC power is supplied to the stator, it produces a rotating magnetic field.

1.3.1.3 Reluctance torque

The rotor experiences torque due to the tendency of the magnetic field to align with the path of least reluctance. As the stator's rotating magnetic field interacts with the rotor, the rotor moves to minimize the reluctance of the magnetic circuit. This creates a synchronous torque that drives the rotor to follow the rotating magnetic field.

1.3.1.4 Energy conversion

In generator mode, the rotor is driven by a mechanical prime mover (like a turbine), which causes it to rotate at synchronous speed. As the rotor rotates, it causes changes in the reluctance of the magnetic circuit, which in turn modulates the magnetic flux. This changing magnetic flux induces an electromotive force (EMF) in the stator windings, generating a voltage.

1.3.2 Types of SynRM

There are three primary types of SynRM, each featuring distinct anisotropic rotor structures (Figure 1.11):

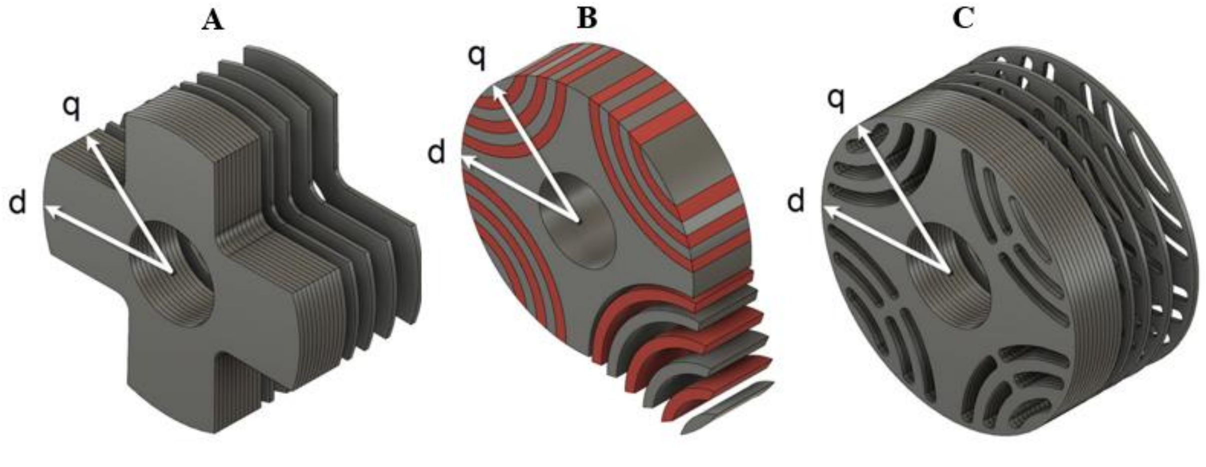

Figure 1.11 SynRM rotor configurations.

1.3.2.1 Salient pole rotor (Type A)

The salient pole rotor design involves removing some iron material from each rotor in the transversal region. This design enhances the magnetic characteristics, making the rotor anisotropic, which helps improve the machine's performance.

1.3.2.2 Axially laminated rotor (Type B)

In the axially laminated rotor, the iron laminations are shaped at each pole and insulated from each other using electrically and magnetically passive materials. These laminated stacks are connected to the central shaft via pole holders. This design reduces losses and allows for better control of the machine's magnetic flux.

1.3.2.3 Punched laminated rotor (Type C)

In this rotor type, laminations are punched in a traditional manner, leaving thin ribs that connect various rotor segments. These ribs provide structural integrity while allowing the rotor to maintain the desired anisotropic magnetic properties.

Table 1.2 summarizes the characteristics of different rotors in terms of performance, mechanical strength, price, and manufacturing complexity [56].

Table 1.2 Comparison between SynRM types

Type	Performance	Mechanical Strength	Price	Manufacturing Complexity
Salient pole rotor	☹	😀	😀	😀
Axially laminated rotor	😀	☹	😀	☹
Punched laminated rotor	🙂	🙂	😀	😀

Legend:

☹ = bad 🙂 = good 😀 = very good

1.3.3 The advantages and disadvantages of SynRM

This table summarizes the key strengths and limitations of SynRM in different applications.

Table 1.3 Advantages and disadvantages of SynRM

Advantages	Disadvantages
• No need for permanent magnets or excitation windings	• Lower power factor compared to permanent magnet synchronous machines
• Simple rotor construction (robust and easy to manufacture)	• Reduced efficiency compared to high-end permanent magnet machines
• Cost-effective due to lack of magnets and copper in the rotor	• Limited torque density compared to machines with magnets or windings
• High reliability and lower maintenance (no brush wear)	• Can have higher noise and vibration due to saliency effects
• Direct start capability using a squirrel cage	• Lower starting torque than induction motors without optimized design

• Constant speed operation up to a certain load • Improved operational stability in synchronism	• Limited dynamic performance without control systems • Requires control strategies to maintain synchronization under varying loads

1.4 Algeria's renewable energy development program

Algeria has initiated an ambitious program to enhance energy efficiency and develop renewable energies, with a goal of installing approximately 22,000 MW of renewable energy capacity by 2030. The program also aims to save around 63 million tons of oil equivalent (TOE) by integrating advanced technologies. As a result, it is expected to reduce CO2 emissions by 193 million tons [57].

1.4.1 Renewable energy potential

Algeria aims to establish itself as a key player in renewable energy production by leveraging various sectors such as photovoltaic, wind, biomass, cogeneration, and geothermal energy. The goal is for 37% of the installed capacity by 2030, and 27% of electricity production for national consumption, to come from renewable sources. While solar energy remains the primary focus, Algeria is also planning numerous wind energy projects, as well as initiatives in biomass, geothermal, and cogeneration sectors [58, 59].

1.4.1.1 Solar potential

Algeria has significant solar potential due to its geographical location, with more than 2,000 hours of annual sunshine across almost the entire country. In the southern regions, solar energy levels exceed 5.6 kWh/m^2, highlighting the country's capacity for large-scale solar energy production [58,60].

1.4.1.2 Wind potential

Algeria has a diverse wind resource due to its varied topography and climates. The northern region is characterized by a 1,200 km coastline and mountain ranges, while the south experiences a Saharan climate. Wind speeds in the southern region, particularly in the southeast and around Tamanrasset, are generally higher than those in the north. Although average wind speeds are lower in northern areas, there are microclimates along coastal sites such as Oran, Bejaïa, and Annaba, as well as on the high plateaus of Tébessa, Biskra, M'sila, and El Bayadh, and in the vast southern regions, offering potential for wind energy projects [60].

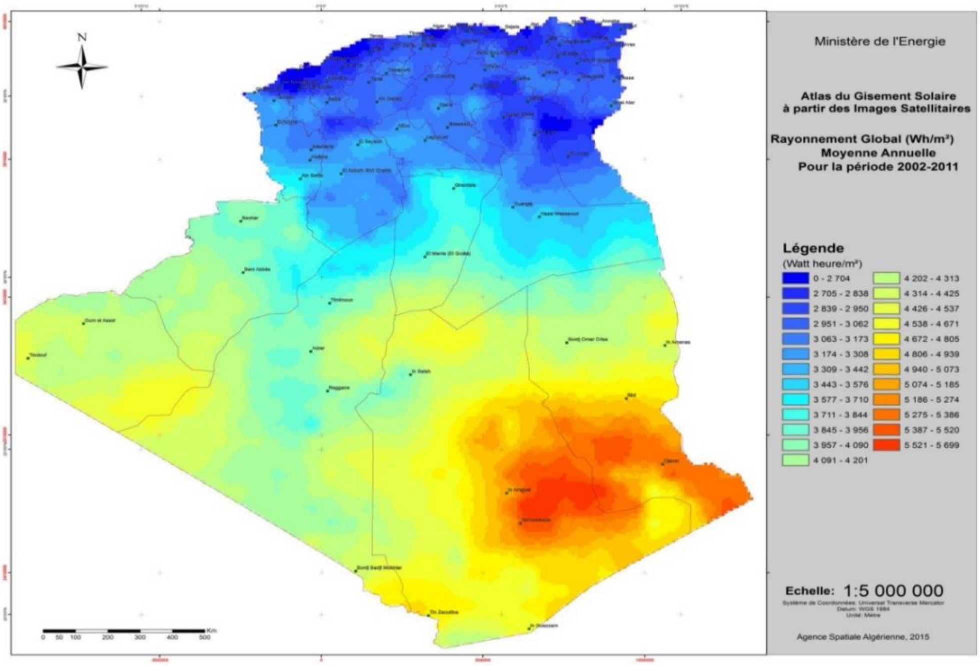

Figure 1.12 Map of average annual global direct solar irradiation (Period 2002-2011)
(https://www.energy.gov.dz/Media/upload/image//1528888901_Carte-de-l-Irradiation-Globale-Directe-Annuelle-Moyenne.jpg)

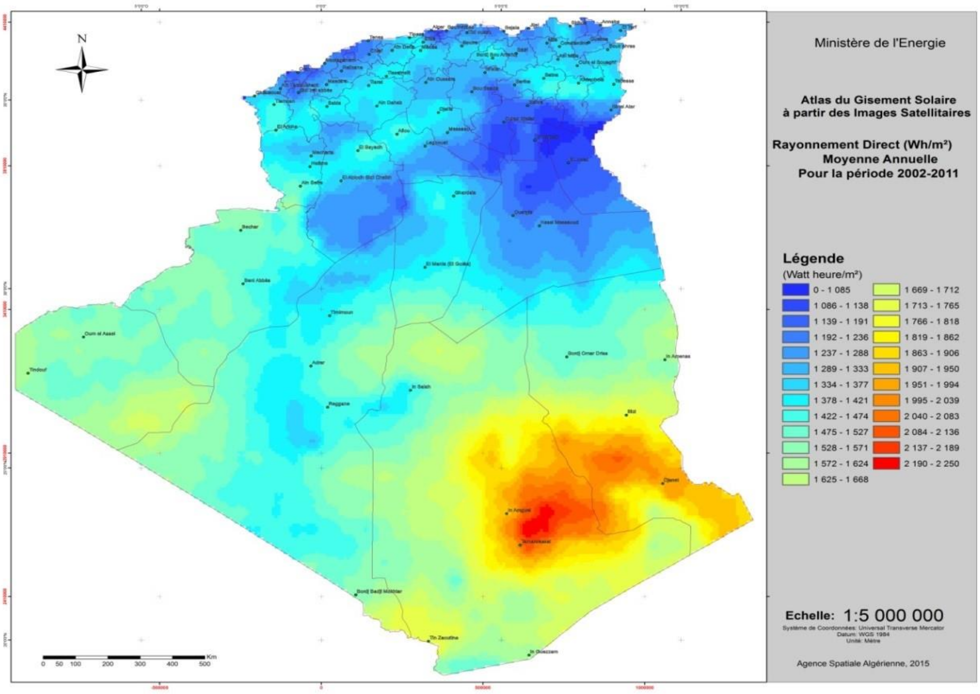

Figure 1.13 Map of average annual direct solar irradiation (Period 2002-2011)
(https://www.energy.gov.dz/Media/upload/image//1528889038_Carte-de-l-Irradiation-Directe-Annuelle-Moyenne.jpg)

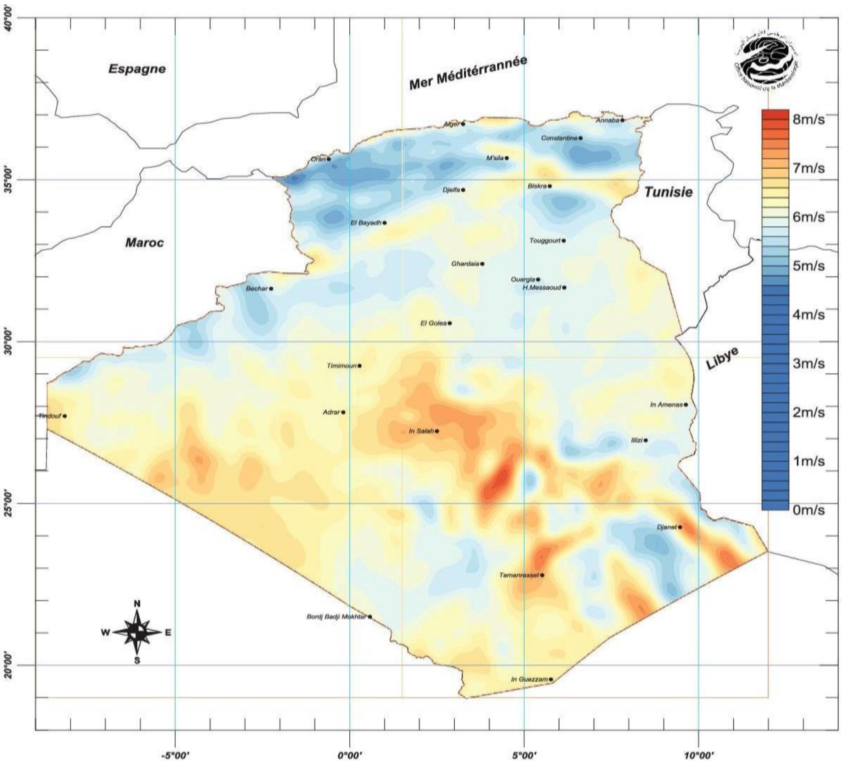

Figure 1.14 Map of average annual direct wind irradiation (Period 2002-2010) (https://www.energy.gov.dz/Media/upload/image//1528889302_Carte-du-Vent-Annuel-Moyen-a-50m.jpg)

1.4.1.3 Geothermal energy potential

Based on geological, geochemical, and geophysical data analysis, more than 200 hot springs have been identified in northern Algeria. Approximately one-third (33%) of these sources have temperatures exceeding 45°C, with some reaching very high levels, such as the hot spring in Biskra, which can reach up to 118°C. Thermal gradient studies have identified three zones where the gradient exceeds 5°C per 100 meters: the Relizane and Mascara zone, the Aïne Boucif and Sidi Aïssa zone, and the Guelma and Djebel El Onk zone [60].

1.4.1.4 Hydropower potential

Although Algeria receives an estimated 65 billion cubic meters of annual precipitation, the country benefits little from this resource due to factors such as a limited number of rainy days, geographically concentrated rainfall, high evaporation rates, and rapid runoff to the sea. Surface water resources generally decrease from north to south, with an estimated renewable and usable resource total of around 25 billion cubic meters, of which approximately two-thirds are surface water. Specifically, there are 103 dam sites in Algeria, with over 50 currently in operation [58-60].

1.4.2 Renewable energy development program

The renewable energy (EnR) projects dedicated to electricity production for the national market will be carried out in two phases [58, 61]:

- First phase (2015 - 2020): During this phase, a capacity of 4,010 MW will be achieved through photovoltaic and wind energy projects, along with 515 MW from biomass, cogeneration, and geothermal energy.
- Second phase (2021 - 2030): The development of electrical interconnections between the northern regions and the Sahara (Adrar) will enable the installation of large renewable energy power plants in regions such as In Salah, Adrar, Timimoune, and Bechar, integrating them into the national energy system. By this time, solar thermal energy is expected to become economically viable.

Algeria's strategy aims to develop a robust renewable energy industry, accompanied by a training program and knowledge capitalization to promote local employment. The scope of the renewable energy program for the national market between 2015 and 2030 is set at 22,000 MW, distributed across various sectors as follows [62,63]:

Table 1.4 Breakdown of the renewable energy development program

Energy Source (Unit: MW)	1st Phase (2015-2020)	2nd Phase (2021-2030)	TOTAL
Photovoltaic	3,000	10,575	13,575
Wind	1,010	4,000	5,010
Concentrated Solar Power (CSP)	-	2,000	2,000
Cogeneration	150	250	400
Biomass	360	640	1,000
Geothermal	5	10	15
TOTAL	4,525	17,475	22,000

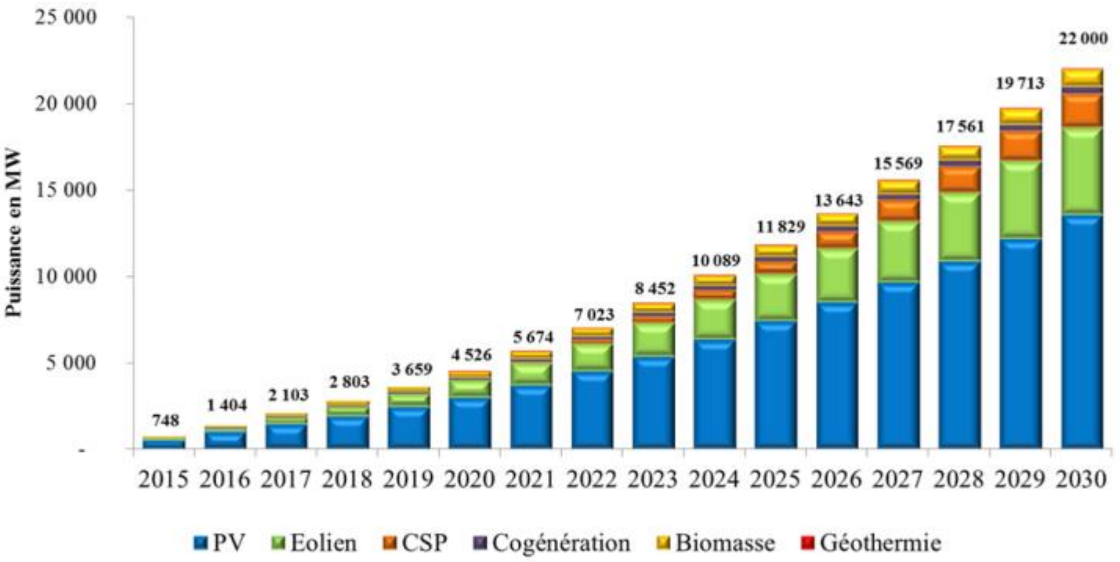

Figure 1.15 Breakdown of the renewable energy development program.

1.5 Methods for improving wind turbines using SynRG

Despite the progress made in wind energy control systems, there remains a notable gap in research regarding the untapped potential of SynRG within these systems [44,46,47,52,53]. This gap highlights the need for more concentrated academic focus. Current research aims to improve the performance of SynRG-equipped wind turbines by focusing on the following objectives:

- ❖ Maximizing power extraction: Ensuring maximum power extraction across a wide range of wind speeds to optimize energy capture.
- ❖ Improving energy quality: Significantly enhancing the quality of the generated energy by reducing total harmonic distortion (THD) in the current, leading to cleaner and more stable output.
- ❖ Addressing traditional limitations: Overcoming the limitations of traditional control strategies, thereby improving the overall performance and robustness of the system.
- ❖ Efficient power generation: Utilizing SynRGs in WPS to efficiently generate electrical energy from wind, ensuring optimal performance.
- ❖ Performance validation: Validating the effectiveness and practicality of SynRGs in real-world applications to ensure their feasibility for broader deployment.
- ❖ Increasing durability and reliability: Extending the lifespan and reliability of wind energy systems, reducing maintenance needs, and ensuring consistent long-term operation.

These research efforts aim to bridge the existing gaps and further enhance the role of SynRGs in the future of wind energy systems.

Vector control strategies using traditional proportional-integral (PI) controllers are favored for their simplicity and ease of implementation. However, the dynamic and nonlinear characteristics of wind power generation can lead to suboptimal performance with PI controllers. To address these challenges, nonlinear control methods have emerged as more effective solutions, offering enhanced robustness and better handling of the unpredictable nature of wind energy systems.

Among the proposed solutions, model-free control (MFC) emerges as a recent and innovative approach developed by M. Fliess and C. Join [20]. This technique is originally applied in robotics and automotive control systems [64,65], aims to streamline processes and boost efficiency. MFC stands out for its ability to enhance WPS performance by removing the need for a precise mathematical model [20], which can be difficult to acquire for complex systems like wind turbines. Its capacity to adapt in real-time to varying conditions, such as fluctuating wind power, and its resilience to disturbances make MFC a promising and effective control strategy for WPS.

1.6 Objectives of our thesis

The main objectives of this doctoral thesis aim to address some of the previously identified issues. Specifically, the goals are:

- To model and simulate a wind power conversion system connected to the electrical grid, equipped with a SynRG and a back-to-back converter.
- To develop a model-free control method to enhance vector control and reduce power and current oscillations.
- To create a more effective approach by combining model-free control with the ant colony optimization algorithm to further improve vector control.
- To compare the performance of the proposed methods with the traditional PI controller method in terms of tracking accuracy and robustness.

MATLAB/Simulink will be used to simulate the control techniques developed in this thesis.

1.7 Conclusion

In this chapter, we presented an extensive review of the diverse types of wind turbines and their operational principles in the context of wind energy conversion. By delving into the fundamental mechanics of wind energy harnessing, we underscored the critical importance of this renewable resource in addressing the pressing energy demands of our time. Wind energy, as a clean and sustainable alternative, plays a vital role in reducing greenhouse gas emissions and fostering energy independence for nations worldwide.

We began by examining various wind turbine designs, highlighting the significant advancements in technology that have propelled the industry forward. From horizontal-axis turbines, which dominate the market, to vertical-axis designs that offer unique advantages in specific environments, the evolution of turbine technology reflects the ongoing innovation in this field. The comparison of different turbine configurations emphasized their distinct operational efficiencies, capacities, and suitability for various wind conditions, illustrating how these factors influence energy production.

Additionally, we explored the range of electrical generators used in wind energy systems, focusing on their respective advantages and limitations. This analysis included a detailed look at synchronous reluctance generators (SynRG), which have emerged as a promising solution due to their high efficiency and reduced reliance on rare-earth materials.

Furthermore, we discussed the objectives of Algeria's national renewable energy development program, which aims to significantly enhance the country's energy portfolio by integrating renewable sources like wind. This initiative not only highlights Algeria's commitment to sustainable energy development but also serves as a model for other nations seeking to transition to cleaner energy solutions.

The chapter culminated in outlining the primary goals of this thesis. By identifying the critical areas for research, we aim to address the existing challenges in wind energy systems, particularly those related to control strategies and the performance of SynRGs. Our objectives focus on modeling and simulating a wind power conversion system, developing innovative control methodologies, and ultimately enhancing the overall efficiency and reliability of wind energy generation.

In summary, this chapter has laid a robust foundation for the subsequent exploration of analytical modeling and advanced control techniques in wind energy systems. By thoroughly reviewing the various turbine types, generator configurations, and national initiatives, we have framed the context and significance of our research. This sets the stage for the following chapters, where we will delve deeper into the intricacies of wind power technology and propose solutions that aim to optimize performance in the face of evolving energy demands.

CHAPTER 2: AN1LYTICAL MODELING AND CONVENTIONAL CONTROL OF SynRG-BASED WPS

Chapter 2: Analytical modeling and conventional control of SynRG-Based WPS

2.1 Introduction

This chapter focuses on the modeling and control of a wind power conversion system based on a synchronous reluctance machine (SynRM) connected to the electrical grid. The chapter is divided into three main parts:

Mechanical modeling and MPPT: The first part addresses the modeling of the mechanical components, including the turbine, gearbox, and mechanical shaft, as well as their maximum power point tracking (MPPT).

Modeling of the SynRM and Vector Control: The second part involves modeling the SynRG in the park reference frame to develop a simplified model for vector control. This method utilizes classic proportional-integral (PI) controllers and the pulse width modulation (PWM) technique for the machine-side converter (MSC) to ensure the system follows the wind speed reference generated by the MPPT algorithm, thereby maximizing power output.

Modeling and control of the DC bus and power Conversion: The third part covers the modeling and control of the DC bus, as well as the active and reactive power management and the grid-side converter (GSC), which is also controlled using the PWM technique.

Finally, the chapter will present and discuss simulation validation using MATLAB/Simulink, along with a robustness study of the techniques employed.

2.2 Modeling of WPS

2.2.1 Wind turbine modeling and MPPT control

The wind energy conversion system is one of the most developed and widely adopted systems in recent years due to its lack of toxic gas emissions, environmental preservation, and reduction in the use of traditional energy sources. The wind power system based on a SynRG (Maximum Available Demand Analysis) can be represented by Figure 2.1.

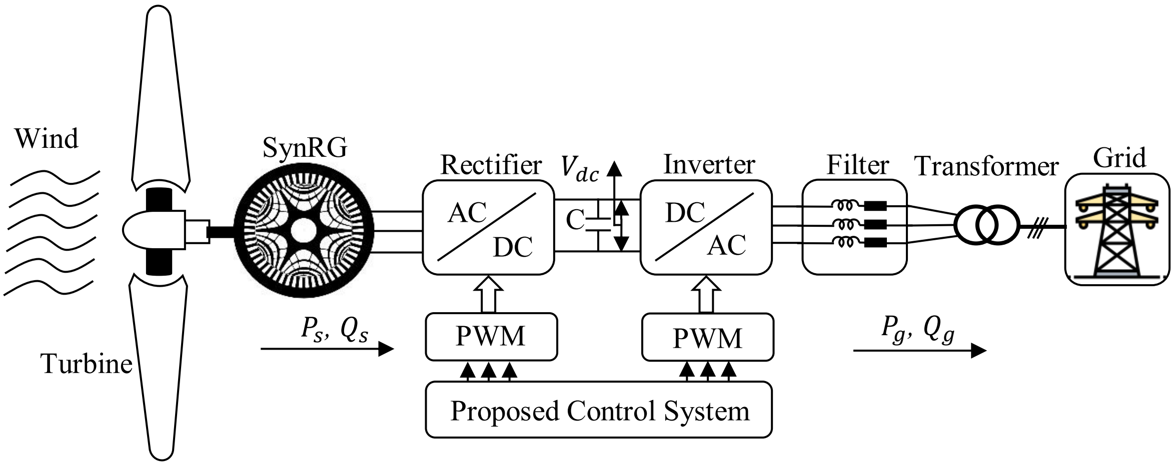

Figure 2.1 Functional diagram of a wind turbine based on SynRG connected to the grid.

To generate electrical energy from wind, turbines and electrical generators are used. Additionally, a power converter is often connected to the generator to facilitate the control of the conversion chain.

In this chapter, an aerodynamic model based on the power coefficient C_p is presented. For high-power turbines, the power coefficient depends on the blade pitch angle β and the tip-speed ratio λ. The aerodynamic torque T_t is calculated using the rotor radius R, wind speed V, air density ρ, and the power coefficient, as described by the following equation [46,66]:

$$\begin{cases} T_t = P_t/\Omega_t = \frac{1}{2\Omega_t}\rho C_p(\lambda,\beta) A {V_\omega}^3 \\ A = \pi R^2 \end{cases} \tag{2.1}$$

The power coefficient C_p of a wind turbine reflects its efficiency in converting wind kinetic energy into mechanical power. This coefficient is affected by the tip speed ratio λ and the pitch angle β. It is generally expressed through a specific nonlinear function, as detailed below [67]:

$$\begin{cases} C_p(\lambda,\beta) = C_1.\left[\frac{C_2}{\lambda_i} - C_3.\beta - C_4\right] exp\left(\frac{-C_5}{\lambda_i}\right) + C_6.\lambda \\ \frac{1}{\lambda_i} = \frac{1}{\lambda+0.08.\beta} - \frac{0.035}{\beta^3+1} \\ \lambda = \frac{R.\Omega_t}{V_\omega} \end{cases} \tag{2.2}$$

The mechanical torque generated by the wind turbine can be determined using:

$$T_m = T_t/G \tag{2.3}$$

The shaft speed on the generator side of the gearbox can be calculated as follows:

$$\Omega_m = \Omega_t.G \tag{2.4}$$

A MPPT algorithm is used to ensure maximum power extraction from a wind turbine, regardless of variations in wind speed. By continuously adjusting the operating point to match the turbine's maximum power point, this algorithm guarantees optimal power generation, thereby maximizing energy output [67, 68].

The wind turbine's reference speed, determined through the MPPT approach, is given by Equation (2.2):

$${\Omega_t}^* = \frac{\lambda_{opt}.V_\omega}{R} \tag{2.5}$$

The turbine model and MPPT control system are developed based on Equations (2.1) to (2.5) and are illustrated in Figure 2.2.

2.2.2 SynRG modeling

Considering simplified conditions, fundamental physical laws, and key assumptions, the dynamic model of SynRG in the dq-axis reference frame can be represented [46]. The formulation provides a mathematical framework that captures the essential behavior of the SynRG, while incorporating necessary simplifications to focus on the key dynamics of the system. By using these assumptions, the model allows for a more tractable analysis of the SynRG's performance in practical applications. The following equations describe the electrical and mechanical dynamics of the generator, laying the groundwork for further control and optimization strategies within the $\boldsymbol{dq}$-axis reference system.

- Stator voltage equations

$$\begin{cases} V_{sd} = R_s i_{sd} + \frac{d\Phi_{sd}}{dt} - p\Omega_r \Phi_{sq} \\ V_{sq} = R_s i_{sq} + \frac{d\Phi_{sq}}{dt} + p\Omega_r \Phi_{sd} \end{cases} \tag{2.6}$$

- Magnetic flux linkage relations

$$\begin{cases} \Phi_{sd} = L_{sd} i_{sd} \\ \Phi_{sq} = L_{sq} i_{sq} \end{cases} \tag{2.7}$$

- Electromagnetic torque expression

$$T_{em} = \frac{3}{2} p \left(\left(L_{sq} - L_{sd} \right) i_{sd} i_{sq} \right) \tag{2.8}$$

- Mechanical dynamics equation

$$J.\frac{d\Omega_m}{dt} = T_m - T_{em} - f.\Omega_m \tag{2.9}$$

Figure 2.3 shows the dq-axis equivalent electrical circuit, which is derived from the stator voltage equations in Equation (2.6).

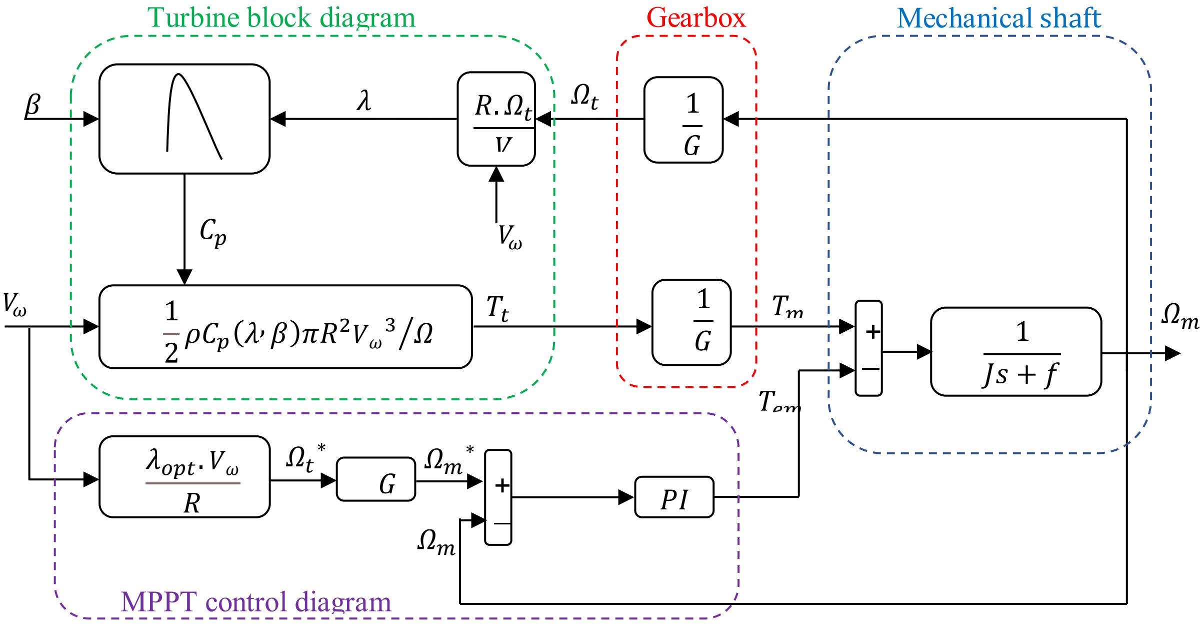

Figure 2.2 Block diagram of the turbine model alongside the MPPT control system diagram.

2.2.3 Power converters and DC bus modeling

Traditionally, the power electronics converter used to connect the generator voltages to the grid consists of two three-phase inverters arranged in a Back-to-Back configuration. A capacitor is placed between the two converters to filter the DC bus voltage (as shown in Figure 2.1).

As illustrated in Figure 2.1, the power conversion system connecting the machine side to the grid side primarily consists of the following components:

- The MSC (machine side converter), which controls the speed and currents.
- A DC bus.
- The GSC (grid side converter), which regulates the DC bus voltage and manages the active and reactive power exchanged between the generator and the grid.
- These converters are controlled using a pulse width modulation (PWM) technique.

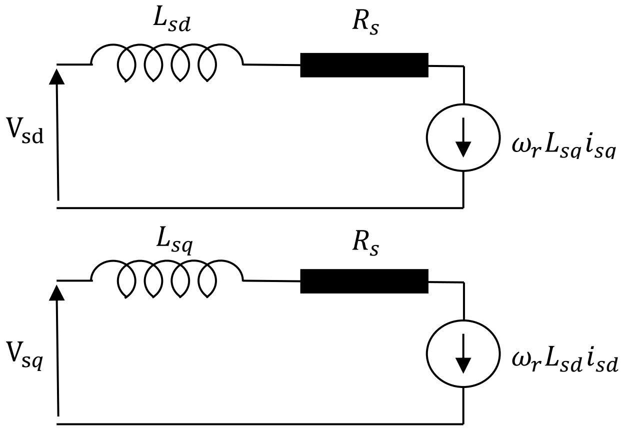

Figure 2.3 The dq-axis equivalent circuit of the SynRG

2.2.3.1 Grid-side converter (GSC)

The GSC plays a critical role in the energy conversion process, particularly when interfacing with the electrical grid. In this system, the GSC utilizes an inverter to convert the DC bus voltage into AC voltage, which allows the controlled transfer of electrical energy from the DC bus to the grid. This conversion process is essential for maintaining synchronization with the grid frequency and ensuring that the generated energy can be efficiently fed into the grid.

To optimize the performance and ensure that the current injected into the grid is smooth and free of distortions, a passive R-L filter is typically placed between the grid and the GSC. This filter helps mitigate harmonics and ensures compliance with grid standards, enabling the converter to function efficiently without causing disturbances in the grid.

As shown in Figure 2.4, the overall system connecting to the electrical grid consists of several key components, including the low-pass filter, the DC bus, and the GSC. These components work in tandem to regulate power flow, filter out unwanted noise, and maintain the stability of the energy conversion process, ensuring that energy flows seamlessly between the converter and the grid.

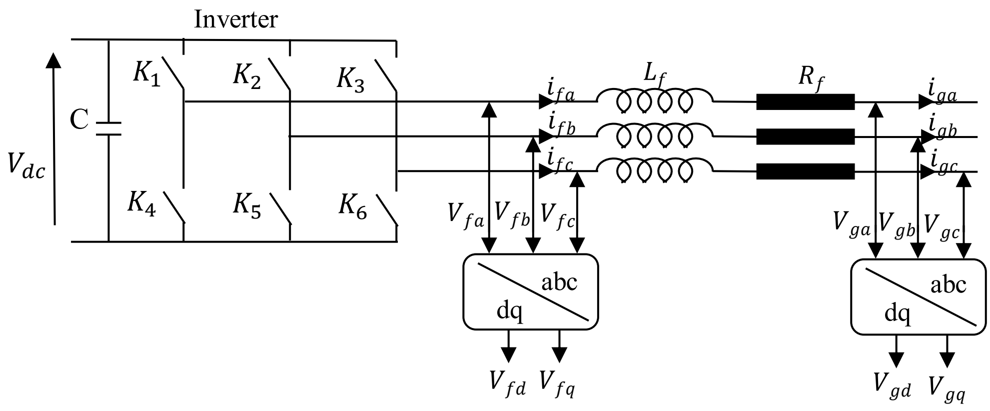

Figure 2.4 Connection of the GSC.

The voltage equations in the dq reference frame can be formulated as follows [69]:

$$\begin{cases} V_{gd} = V_{fd} + R_f i_{gd} - L_f \frac{di_{gd}}{dt} + \omega_g L_f i_{gq} \\ V_{gq} = V_{fq} + R_f i_{gq} - L_f \frac{di_{gq}}{dt} - \omega_g L_f i_{gd} \end{cases} \tag{2.10}$$

The equations for calculating the active and reactive power of the grid are given as follows [69]:

$$\begin{cases} P_g = \frac{3}{2}(V_{gd} i_{gd} + V_{gq} i_{gq}) \\ Q_g = \frac{3}{2}(V_{gq} i_{gd} - V_{gd} i_{gq}) \end{cases} \tag{2.11}$$

The DC-link serves as the connection between the MSC and the GSC. By applying the principle of power balance and neglecting converter losses, the dynamic characteristics of the DC-bus voltage can be described as follows [70,71]:

$$P_s - P_g = \frac{1}{2}\left[C \frac{dV^2{}_{DC}}{dt}\right] \tag{2.12}$$

2.2.3.2 Machine-side converter (MSC)

The MSC is responsible for managing the electrical energy generated by the machine (Figure 2.5). Its primary function is to regulate the generated power and control the machine's operation to ensure optimal energy production and stability under varying operational conditions. The MSC converts the variable frequency and amplitude AC power generated by the turbine into a DC voltage, which is fed into the DC-link that connects it to the GSC.

The MSC uses pulse width modulation (PWM) control strategies to modulate the AC signal generated by the machine, allowing precise control over the generator’s torque and speed. By adjusting these parameters, the MSC ensures that the machine operates at its maximum power point (MPP), maximizing energy extraction, especially in variable wind conditions.

To facilitate modeling and reduce simulation time, the rectifier is modeled using a set of ideal switches. These switches exhibit zero resistance in the conducting state, infinite resistance in the blocked state, and respond instantaneously to control signals.

For the dynamic model of the system, the analysis of the converter is divided into three parts: the AC side, the discontinuous section comprising the switches, and the DC side. In this context, the switches serve to establish a link between the AC side and the DC bus. Since these switches are complementary, their state is governed by the following function:

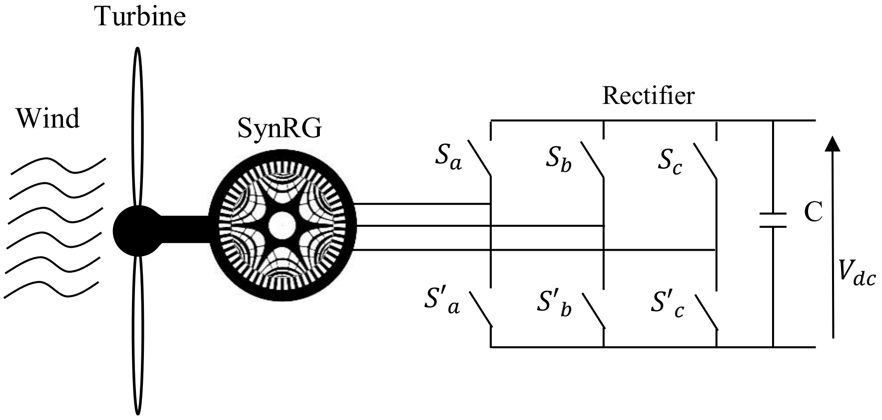

Figure 2.5 Connection of the MSC.

$$S_i = \begin{cases} +1 & \overline{S_i} = -1 \\ -1 & \overline{S_i} = +1 \end{cases} \qquad \text{with i} = \text{a, b, c} \tag{2.13}$$

Then, the input phase voltages and the output current can be expressed as functions of S_i, V_{DC}, and the input currents i_a, i_b, i_c.

$$i_a + i_b + i_c = 0 \tag{2.14}$$

The voltages at nodes a, b, and c with respect to the virtual midpoint of the inverter (a point that divides the DC voltage in half) are expressed as follows [25]:

$$\begin{cases} V_{a0} = \frac{V_{DC}}{2} S_a \\ V_{b0} = \frac{V_{DC}}{2} S_b \\ V_{c0} = \frac{V_{DC}}{2} S_c \end{cases} \tag{2.15}$$

To obtain the instantaneous values of these voltages, starting from the node voltages V_{a0}, V_{b0}, and V_{c0}, we have the following expressions:

$$\begin{cases} V_a = \frac{1}{3}(2V_{a0} - V_{b0} - V_{c0}) \\ V_b = \frac{1}{3}(2V_{b0} - V_{a0} - V_{c0}) \\ V_c = \frac{1}{3}(2V_{c0} - V_{b0} - V_{a0}) \end{cases} \tag{2.16}$$

The voltages V_{a0}, V_{b0}, and V_{c0} necessarily have a sum of zero. In this case, the expressions for the voltages V_a, V_b, and V_c can be expressed using the connection functions as follows:

$$\begin{bmatrix} V_a \\ V_b \\ V_c \end{bmatrix} = \frac{V_{DC}}{3} \begin{bmatrix} 2 & -1 & -1 \\ -1 & 2 & -1 \\ -1 & -1 & 2 \end{bmatrix} \begin{bmatrix} S_a \\ S_b \\ S_c \end{bmatrix} \tag{2.17}$$

The system (2.17) represents the simplified mathematical model of the inverter, which allows the calculation of the voltages V_a, V_b, and V_c based on the inverter's control signals S_a, S_b, and S_c.

2.2.3.3 Sinusoidal-triangle pulse width modulation (PWM)

Sinusoidal-triangle pulse width modulation (PWM), also known as intersective modulation, derives its name from the intersection between a high-frequency switching carrier wave (often triangular or sawtooth) and a low-frequency modulation wave, known as the reference voltage. When the reference is sinusoidal, two parameters characterize this control method [72]:

- The modulation index m, which defines the ratio between the carrier frequency f_p and the reference frequency f_r, is a crucial parameter. The selection of this ratio is important as it must balance a good harmonic suppression (with a high m) and efficient inverter performance (with a low m to reduce switching losses). It is given by the equation:

$$m = \frac{f_p}{f_r} \tag{2.18}$$

- The modulation rate $\boldsymbol{r}$ (also referred to as the voltage modulation index or duty cycle) defines the ratio of the amplitude of the modulation signal $\boldsymbol{V_r}$ to the peak value $\boldsymbol{V_p}$ of the carrier signal. It is expressed as:

$$r = \frac{V_r}{V_p} \tag{2.19}$$

The switching instants of the switches are defined by the intersections between the two waves, while the switching frequency is determined by the frequency of the carrier wave.

We note that there are other, more advanced PWM techniques than sinusoidal PWM, such as space vector modulation (SVM), optimized PWM, dual-carrier PWM, and PWM with third harmonic injection, among others. However, the objective of our work is to improve control laws by replacing traditional PI controllers with more robust ones. For these reasons, we opted for the simpler sinusoidal PWM, which is easier to program.

2.2.4 Application of PI controller to SynRG-based WPS

When wind speed fluctuates, it becomes crucial to regulate the active and reactive power, as well as the voltage and frequency delivered to the grid. This regulation is achieved by controlling the frequency converters, which consist of a PWM rectifier and a PWM inverter [71], to meet the desired control objectives. As a result, the state vector and control vector are defined as follows:

- The state vector is expressed as:

$$[X] = \left[i_{sd}, i_{sq}, \Omega_m, i_{gd}, i_{gq}\right]^T \tag{2.20}$$

- The control variable is expressed as:

$$[U] = \left[V_{sd}, V_{sq}, V_{fd}, V_{fq}\right]^T \tag{2.21}$$

2.2.4.1 Control of the MSC

On this side, three PI controllers are implemented to regulate the stator's direct and quadrature current components (i_{sd} and i_{sq}), as well as the speed (Ω_m), as illustrated in Figure 2.6. These controllers provide accurate control of both the machine's electrical and mechanical performance.

The control errors selected for regulating the MSC are defined as follows:

$$e(i_{sd}) = i^*{}_{sd} - i_{sd} \tag{2.22}$$

$$e(i_{sq}) = i^*{}_{sq} - i_{sq} \tag{2.23}$$

$$e(\Omega_m) = \Omega^*{}_m - \Omega_m \tag{2.24}$$

In the PI control strategy, the reference values for the direct and quadrature stator voltages, are as follows:

$$V^*{}_{sd} = K_P e(i_{sd}) + \int K_I e(i_{sd}) \tag{2.25}$$

$$V^*{}_{sq} = K_P S(i_{sq}) + \int K_I S(i_{sq}) \tag{2.26}$$

The reference values for the quadrature stator current, are as follows:

$$i^*{}_{sq} = K_P e(\Omega_m) + \int K_I e(\Omega_m) \tag{2.27}$$

2.2.4.2 Control of the GSC

To stabilize the DC-link voltage, a PI controller was implemented to ensure that the measured voltage V_{DC} tracks its reference value $V^*{}_{DC}$. Furthermore, two additional PI controllers were designed to regulate the direct and quadrature current components (i_{gq}, i_{gq}) of the GSC, as shown in Figure 2.6.

For GSC, the errors are defined as follows:

$$e(i_{gd}) = (i^*{}_{gd} - i_{gd}) \tag{2.28}$$

$$e(i_{gd}) = (i^*{}_{gd} - i_{gd}) \tag{2.29}$$

$$e(V_{DC}) = (V^*{}_{DC} - V_{DC}) \tag{2.30}$$

Similarly, to the approach used for MSC control, the controller design for the GSC will be structured as follows:

$$V^*{}_{fd} = K_P e(i_{gd}) + \int K_I e(i_{gd}) \tag{2.31}$$

$$V^*{}_{fq} = K_P S(i_{gq}) + \int K_I S(i_{gq}) \tag{2.32}$$

$$i^*{}_{gd} = K_P e(V_{DC}) + \int K_I e(V_{DC}) \tag{2.33}$$

In this design, the reference quadrature current $i^*{}_{gq}$ is determined by the reactive power $Q^*{}_g$, which is set to zero to achieve unity power factor control, as illustrated in Figure 2.6.

2.3 Results and simulation

In this section, we present the simulation results for the control of a wind power system using SynRG. The entire wind system and its control were simulated using MATLAB/SIMULINK. This simulation aims to analyze the performance of vector control strategy using PI controller for the generator, the MPPT technique applied, the control of the DC bus, and the system's robustness. The numerical values for the parameters of the wind turbine and SynRG are listed in Table 2.1.

The wind speed varies between 6.43 m/s and 11.4 m/s over a 5-second period, as shown in Figure 2.7.

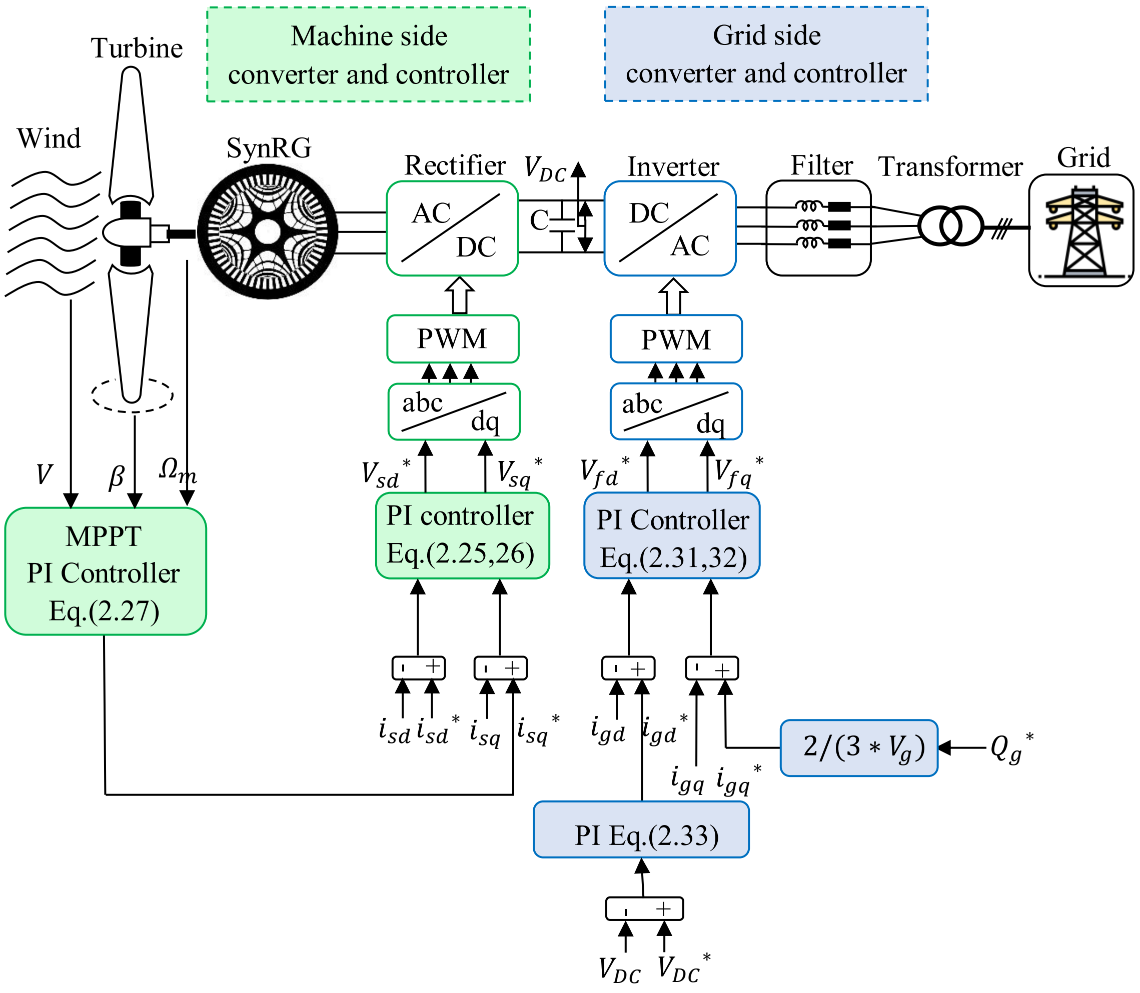

Figure 2.6 System control configuration using PI controller.

Table 2.1 Parameters of the WPS

	Parameters value	Units
SynRG Generator		
$\boldsymbol{R_s}$	0.3	Ohm
$\boldsymbol{L_d}$	0.155	H
$\boldsymbol{L_q}$	0.015	H
Rated power	11	KW
Rated current	25	A
Rated speed	1000	rpm

Number of poles	6	
Wind turbine		
Maximum mech. speed	600	rpm
Rated wind speed	10	m/s
Radius	2.25	m
$\boldsymbol{\lambda_{opt}}$	8.1	
$\boldsymbol{C_{p\ max}}$	0.47	

Table 2.2 The PID parameters

K_P (Ω_m)	K_I (Ω_m)	K_P (i_{sd})	K_I (i_{sd})	K_P (i_{sq})	K_I (i_{sq})	K_P (V_{DC})	K_I (V_{DC})	K_P (i_{gd})	K_I (i_{gd})	K_P (i_{gq})	K_I (i_{gq})
-500	10	1200	200	500	1	-1500	10	-200	-120	-200	-120

2.3.1 MSC control results

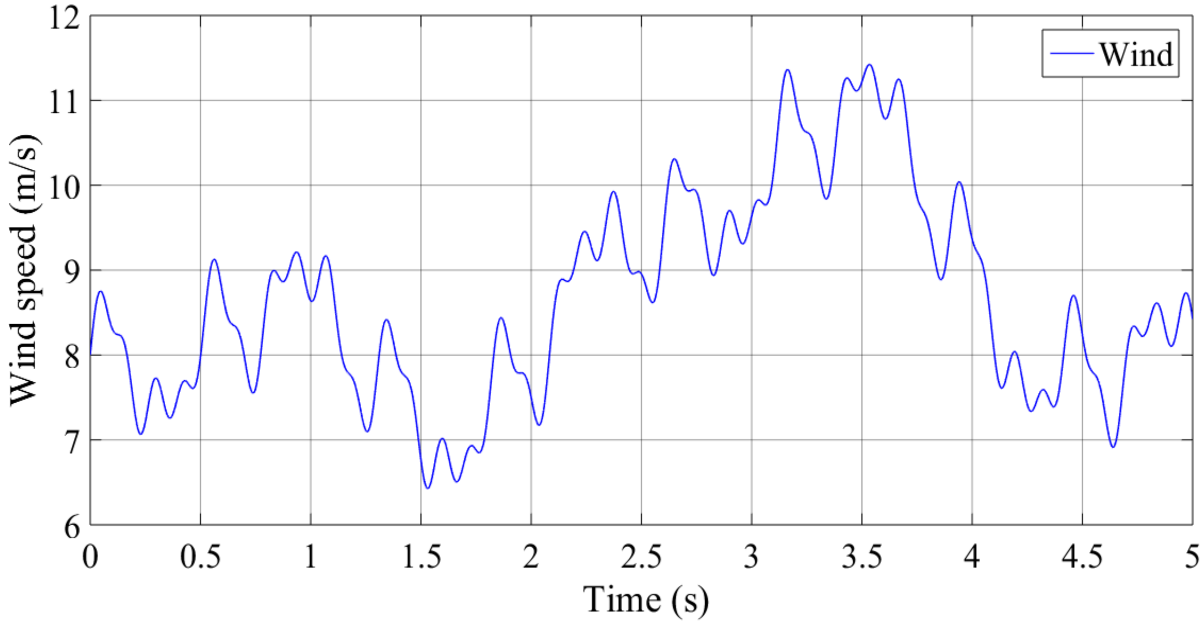

Figure 2.7 Wind speed profile.

Figures 2.8(a,b) clearly show that the tip speed ratio (λ) and the power coefficient (C_p) closely follow their optimal reference values of 8.1 and 0.47, respectively, throughout the simulation period. This accurate alignment demonstrates that the system operates at maximum aerodynamic efficiency, which is essential for optimizing energy extraction from the wind.

Figure 2.8(c) illustrates that the electromagnetic torque (T_{em}) accurately tracks the optimal torque dictated by the MPPT algorithm. This precise torque control is crucial for ensuring optimal power transfer from the wind turbine to the generator, thus maximizing the electrical power output.

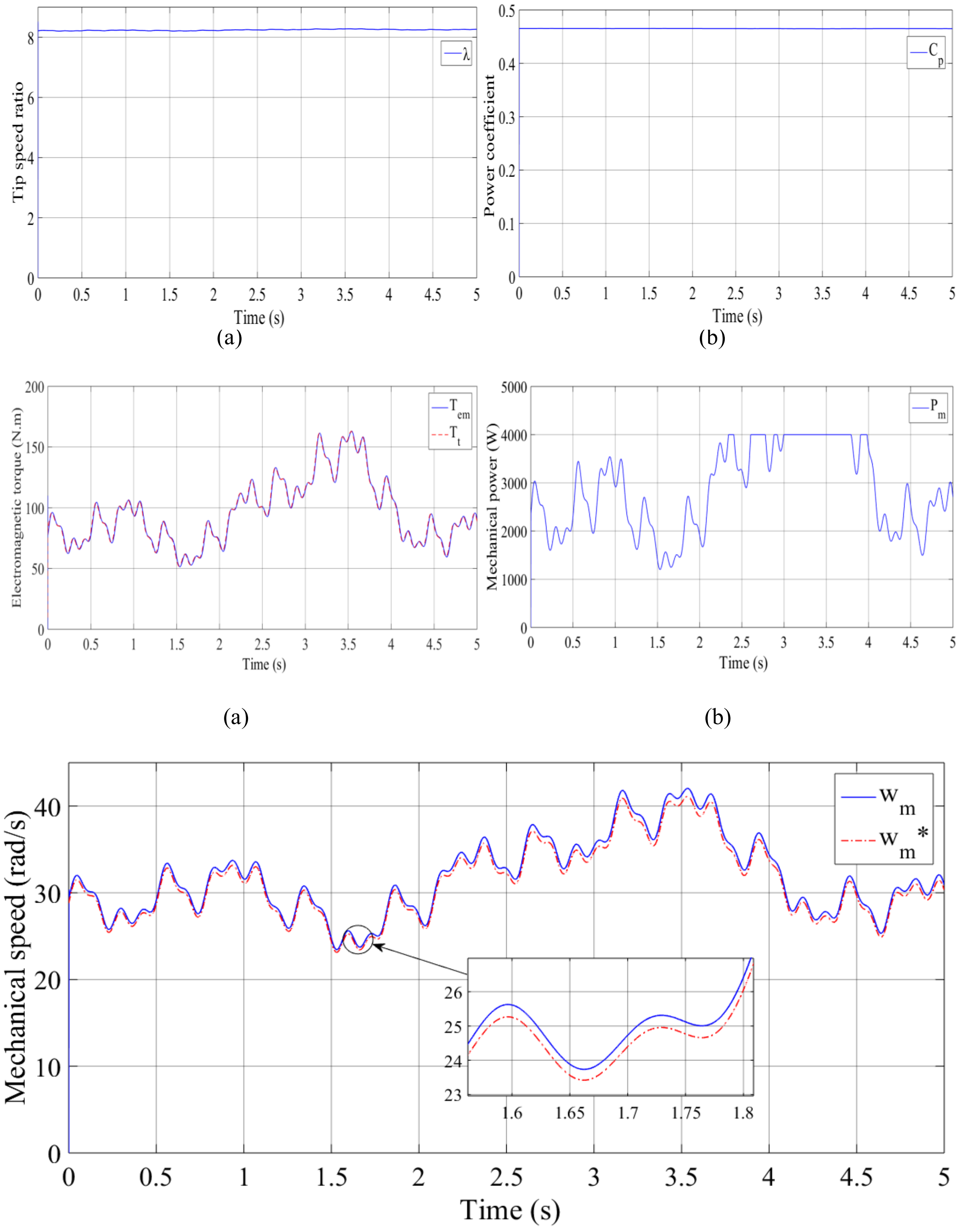

(a) (b)

(a) (b)

(e)

Figure 2.8 MPPT-PI performance: Tip speed ratio (a), Power coefficient (b), Electromagnetic torque (c), Mechanical power (d), Mechanical speed (e).

Figure 2.8(d) shows that the mechanical power (P_m) closely follows the wind speed profile. This correlation highlights that the mechanical power output effectively adapts to fluctuations in wind speed, ensuring the system consistently generates the maximum possible power under varying conditions.

In addition, Figure 2.8(e) shows that the mechanical speed of the SynRG (Ω_m) generally follows the reference wind speed, but there is noticeable deviation from the reference values due to the limitations of the PI controller. Accurate tracking is essential to ensure that the generator operates within its optimal speed range, thereby improving the efficiency of the energy conversion process.

2.3.2 GSC control results

The PI controller effectively tracks the DC bus voltage, as illustrated in Figure 2.9. Despite fluctuations in wind conditions, the DC bus voltage remains stable, which is essential for maintaining consistent and reliable operation of the wind turbine system.

Figures 2.10(a,b) show that the power output closely follows the reference values for PI controller, with acceptable performance in terms of dynamic response.

Figures 2.11(a) and 2.11(b) show the magnification of active and reactive power by the PI controller, which clearly shows significant power ripples. This results in more noticeable fluctuations in the power factor, as depicted in Figure 2.12(a).

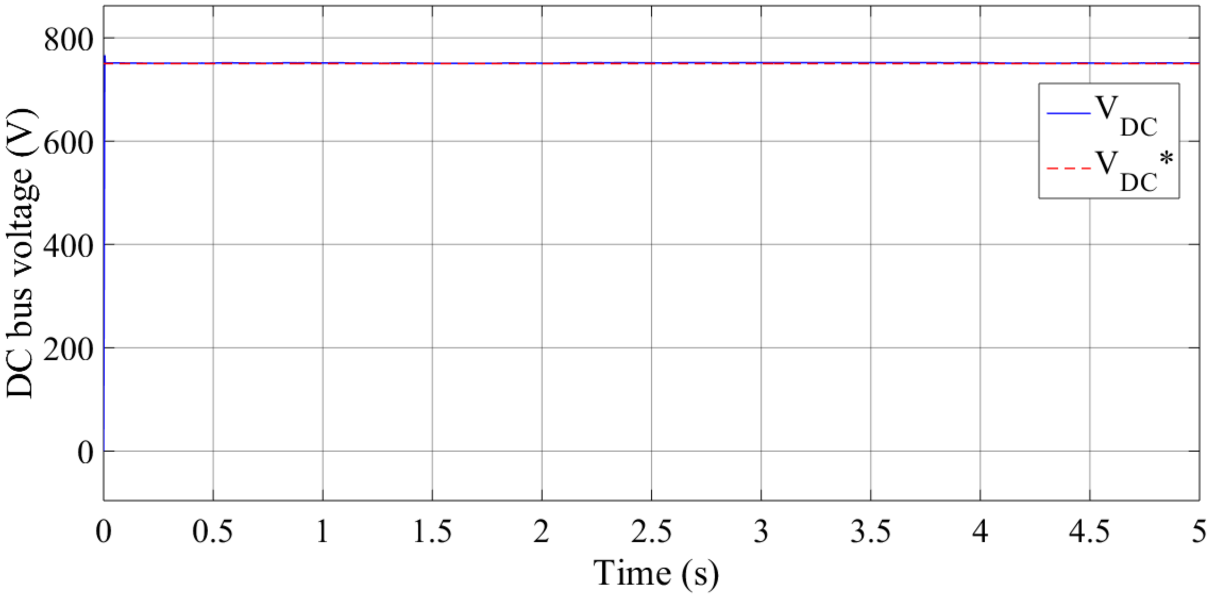

Figure 2.9 DC bus voltage

Figure 2.10(d), 2.11(c) shows the grid currents produced by vector control. This figure indicates that the current is tied to changes in the active power generated and injected into the grid. Since the voltage remains constant and is regulated by the electrical grid, the current varies only when the active power generated fluctuates with changes in wind conditions. Additionally, Figure 2.11(c) shows significant ripple in the current, which can impact grid stability and power quality.

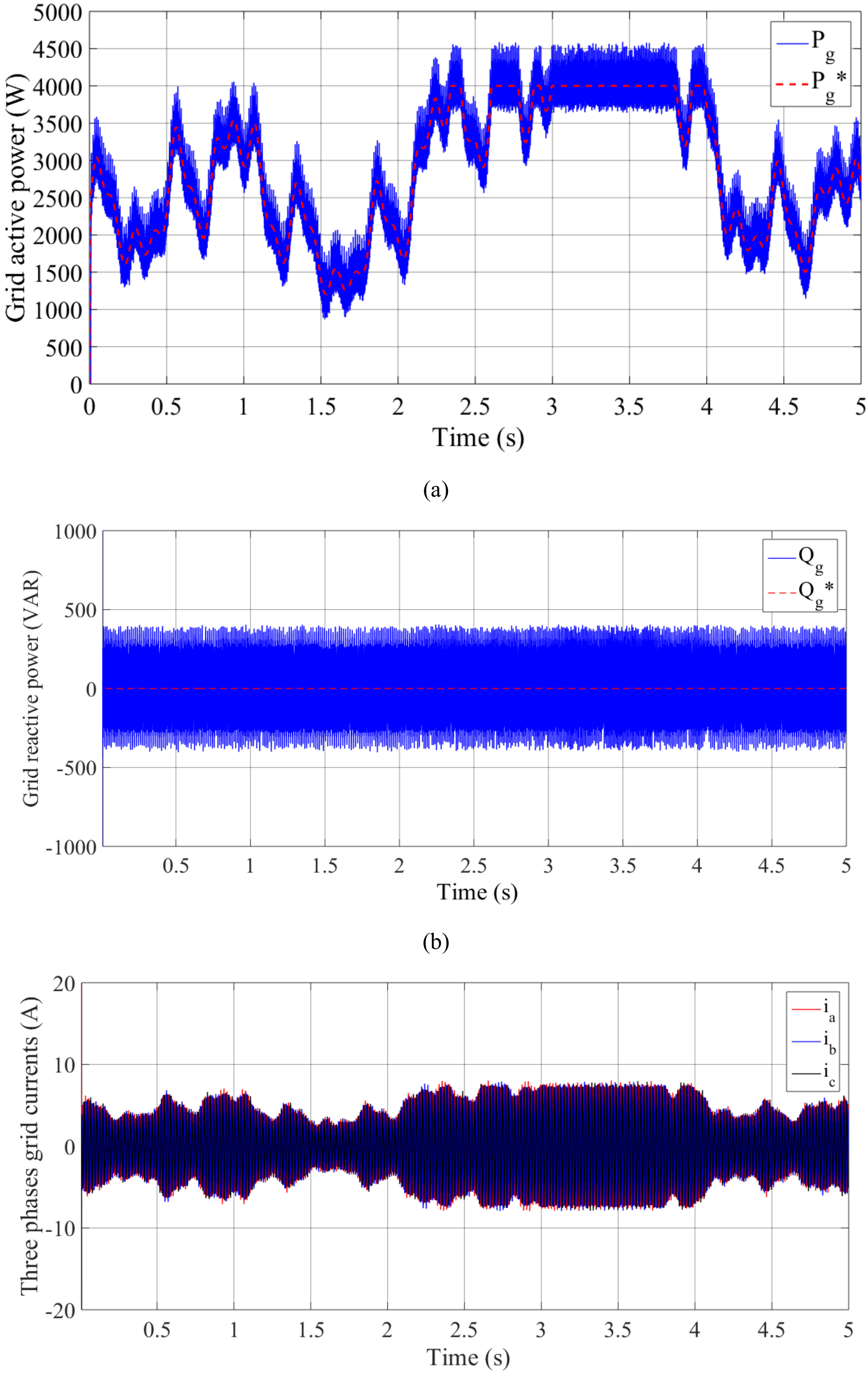

(a)

(b)

(c)

Figure 2.10 PI performance: Active power (a), Reactive power (b), Grid currents (c).

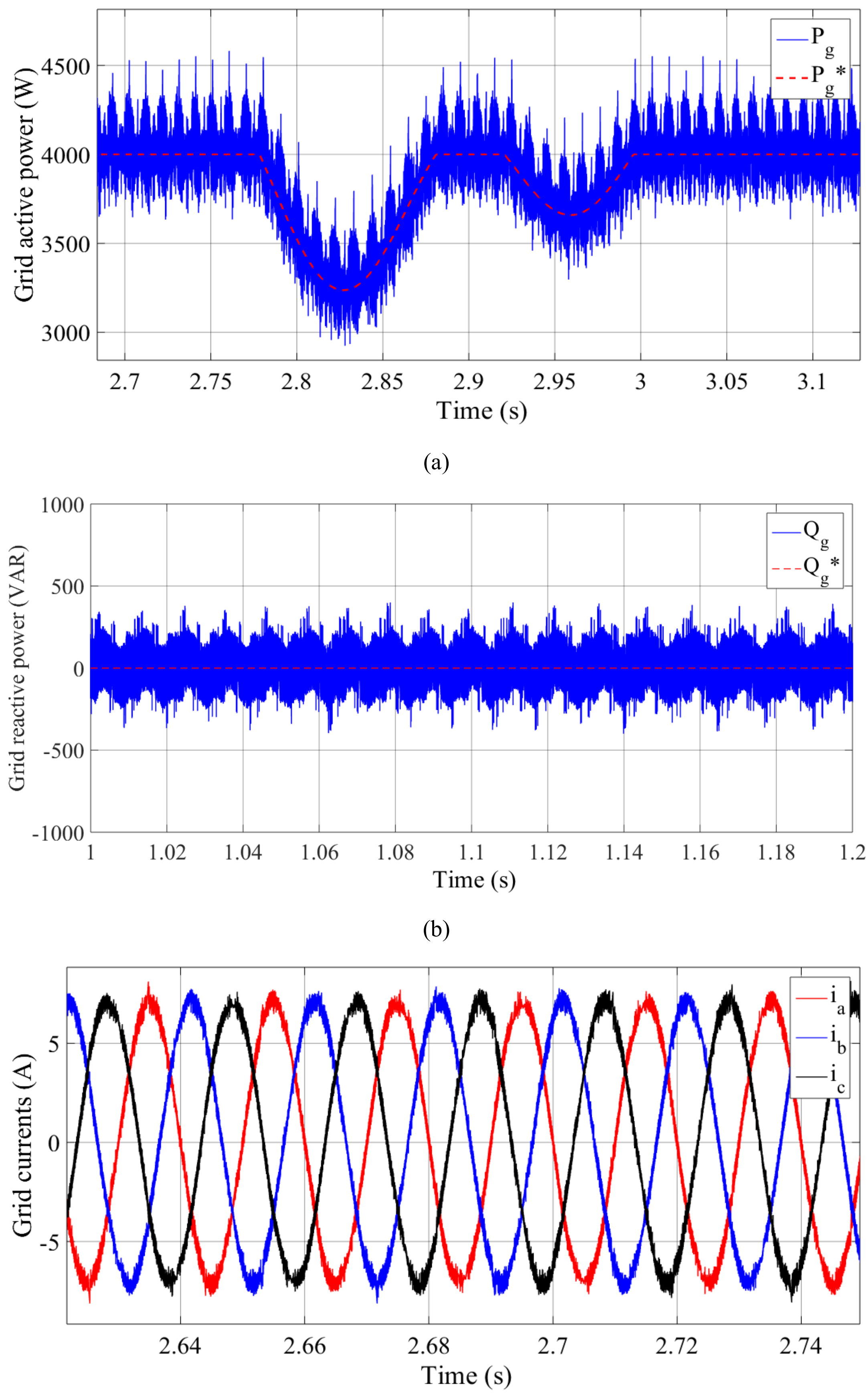

(a)

(b)

(c)

Figure 2.11 Zoom on: Active power (a), Reactive power (b), Grid currents (c).

Figure 2.10(d), 2.11(c) shows the grid currents produced by vector control. This figure indicates that the current is tied to changes in the active power generated and injected into the grid. Since the voltage remains constant and is regulated by the electrical grid, the current varies only when the active power generated fluctuates with changes in wind conditions. Additionally, Figure 2.11(c) shows significant ripple in the current, which can impact grid stability and power quality.

A harmonic analysis of the grid current was conducted to evaluate the impact of the PI controller on signal quality, as illustrated in Figure 2.12(b). The analysis reveals that the PI controller results in a THD 6.20%, indicating a less-than-ideal performance.

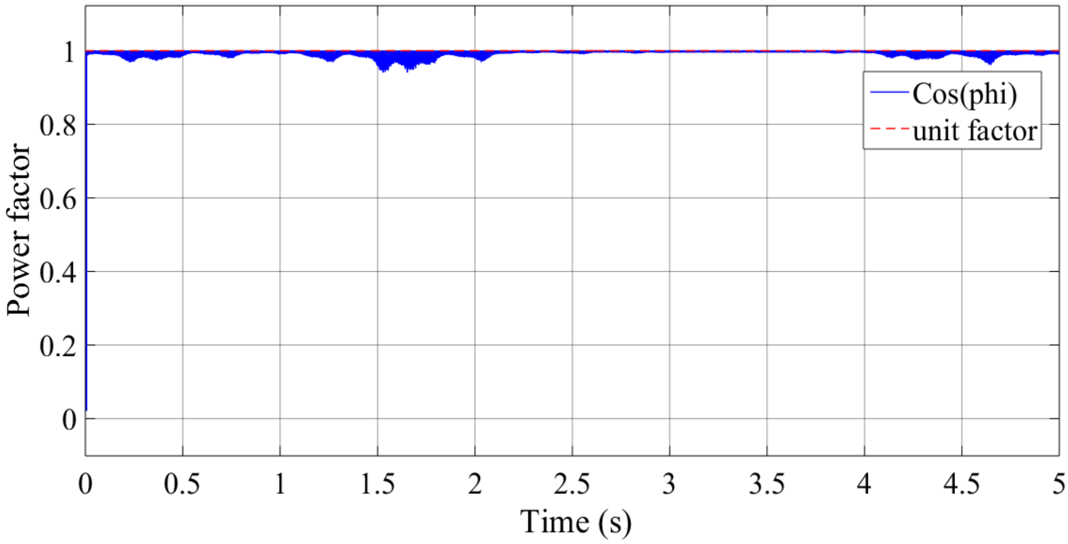

(a)

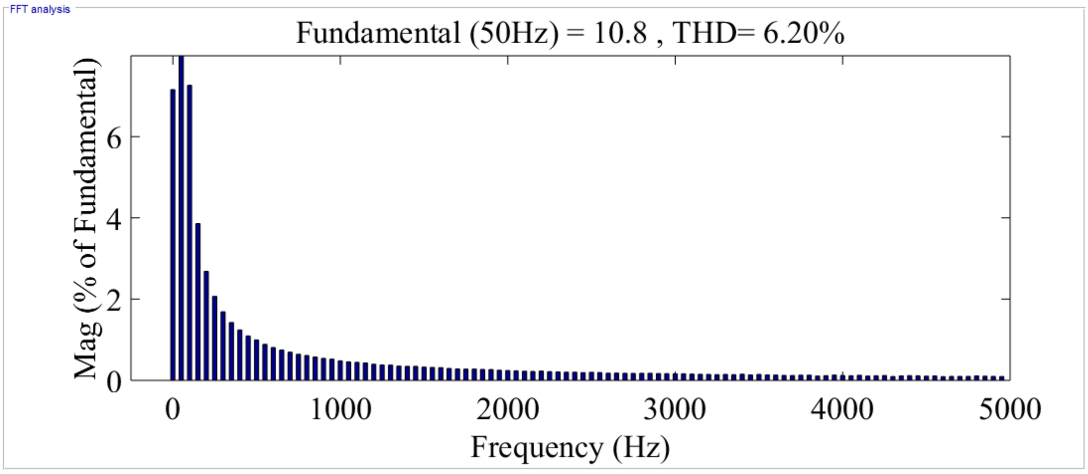

(b)

Figure 2.12 Power factor (a), Grid current THD (b).

In summary, while a PI controller is acceptable in following reference signals, it has difficulties in minimizing power fluctuations and maintaining stability with changing wind speeds. This can restrict its ability to enhance the efficiency and reliability of wind turbine operations.

2.4 Conclusion

This In this chapter, we thoroughly examined the modeling and control mechanisms of a wind energy conversion system centered around a synchronous reluctance generator (SynRG). We emphasized the critical role of maximum power point tracking (MPPT) control in optimizing energy extraction from varying wind conditions, achieved by adeptly regulating the turbine's rotational speed. This fundamental aspect sets the stage for effective energy generation, ensuring that the system can adapt to fluctuations in wind availability.

To enhance the performance of the wind conversion system, we introduced vector control methods. These strategies employ classic proportional-integral (PI) controllers to manage the machine-side converter, which adjusts both the operational speed of the generator and the stator currents. This dual management is essential for maintaining stability and maximizing output, as it allows the system to respond dynamically to changing conditions.

On the other hand, the network-side converter is responsible for maintaining the DC bus voltage while also managing the active and reactive power flow. This coordinated control is vital for ensuring that the system operates within optimal parameters, contributing to both energy efficiency and grid stability.

The results of our analysis can be summarized as follows:

- **Potential of SynRG:** Our findings underscore the viability of the SynRG as a reliable and efficient alternative in wind energy applications. Its design and operational characteristics position it as a strong contender for future wind energy solutions, particularly in environments where traditional systems may falter.
- **Effectiveness of vector control:** The implementation of vector control using PI controllers has proven effective, providing acceptable tracking performance in real-time operations. This success highlights the robustness of classic control strategies, particularly in environments with predictable wind patterns.
- **Challenges identified:** However, while the vector control method demonstrated acceptable robustness, weaknesses were observed on the generator side in speed tracking and on the grid side in increased power fluctuations and higher THD in the grid current. These issues indicate that further refinement of the control strategies is necessary better track and mitigate adverse effects on grid quality and stability.

In conclusion, this chapter has provided a comprehensive overview of the methodologies applied in the modeling and control of SynRG-based wind energy systems. While significant advancements have been made, the challenges of power quality and system fluctuations necessitate ongoing research and innovation. By addressing these challenges, we can enhance the reliability and efficiency of wind energy systems, ultimately contributing to the broader goal of sustainable energy generation. The insights gained here will serve as a foundation for the development of more sophisticated control strategies in subsequent chapters, aimed at improving the overall performance of wind energy conversion systems.

CHAPTER 3: MODEL-FREE CONTROL STRATEGY OF SynRG-BASED WPS

Chapter 3: Model-free control strategy of SynRG-based WPS

3.1 Introduction

In modern wind power systems, the drive for increased efficiency and enhanced performance continues to push the boundaries of control strategies. Traditional control techniques, such as vector control with PI controllers, have long been favored for managing the power output of wind turbines, particularly in systems involving SynRG. These conventional methods ensure that the MSC effectively tracks the generator's speed, maximizing power extraction, while the GSC maintains a stable DC bus voltage and manages the active and reactive power injected into the grid. However, despite their widespread use and proven performance, PI-based controllers have inherent limitations, particularly when dealing with fast dynamics, system uncertainties, and disturbances. One of the most critical issues is the ripple effect, which often leads to fluctuations in power output and reduced system stability. This chapter seeks to address these limitations by introducing a more advanced control approach: model-free control (MFC).

Model-free control represents a paradigm shift in control theory, as it does not rely on an explicit mathematical model of the system being controlled. This feature makes it particularly appealing for applications like wind energy conversion systems, where system dynamics are complex, nonlinear, and subject to continuous variation due to changing wind conditions. The MFC approach offers robustness and adaptability in the face of system uncertainties, making it a highly promising candidate for improving wind turbine performance. In this chapter, we integrate the model-free control strategy into the vector control framework, aiming to enhance the overall system's responsiveness, stability, and efficiency. By replacing the conventional PI controllers in the MSC and GSC with MFC, we aim to significantly reduce the ripple effect and improve power tracking accuracy, particularly in response to fluctuating wind speeds.

A primary goal of this work is to demonstrate how MFC can optimize the performance of the wind energy system, particularly in tracking the reference speed generated by the MPPT algorithm. MPPT algorithms play a crucial role in ensuring that the wind turbine operates at its most efficient point, extracting the maximum possible power from the wind. However, to fully realize the benefits of MPPT, the control system must be able to track rapid changes in wind speed with high precision. The model-free control approach is designed to excel in this aspect, providing faster response times and greater accuracy compared to traditional PI controllers. This is especially important in wind energy systems, where even small improvements in tracking performance can lead to significant gains in power output.

In addition to optimizing the MSC, the model-free control strategy is also applied to the GSC. The GSC plays a vital role in managing the interaction between the wind turbine and the electrical grid. It regulates the DC bus voltage, ensures power quality, and controls the flow of active and reactive power. In conventional PI-controlled systems, the GSC is susceptible to the ripple issues, leading to increased THD and power fluctuations. By implementing MFC, we aim to reduce these disturbances, improving the overall stability of the system and ensuring smoother integration with the grid.

To validate the effectiveness of the proposed control strategy, this chapter presents a series of simulation results. These simulations compare the performance of the wind energy system under both the traditional PI control and the model-free control. The results will demonstrate how MFC not only enhances the system's dynamic response but also improves power efficiency by ensuring smoother and more accurate tracking of the reference speed. Moreover, the ability of MFC to handle disturbances and uncertainties will be showcased, highlighting its robustness and adaptability in real-world wind energy applications.

In conclusion, this chapter aims to showcase the significant advantages of integrating model-free control into the vector control framework of wind energy systems. By addressing the limitations of PI controllers, particularly in terms of ripple and stability, MFC offers a promising solution for optimizing the performance of both the MSC and GSC. Through a detailed analysis of simulation results, we will demonstrate how this advanced control strategy can improve overall system efficiency, stability, and robustness, paving the way for more reliable and efficient wind energy conversion.

3.2 Definition of model-free control

Model-free control (MFC) is a modern approach proposed by M. Fliess et al. [21], based solely on the inputs and outputs of the system to be controlled.

In reality, Model-free control uses a local first-order model, which means a simple model valid for a short period of time that is continuously updated. This approach is applied to an intelligent PID (iPID) control, which can be described as a universal control method.

3.2.1 Local modeling

A physical system can be described by the following general input/output model:

$$y^{(n)} = f\left(t, y, \dot{y}, \dots, \dot{y}^{(n-1)}, u, \dot{u}, \dots, \dot{u}^{(m)}\right) \tag{3.1}$$

where $y(t)$ is the output, and $u(t)$ represents the input. This model is based on a system of differential equations of order n.

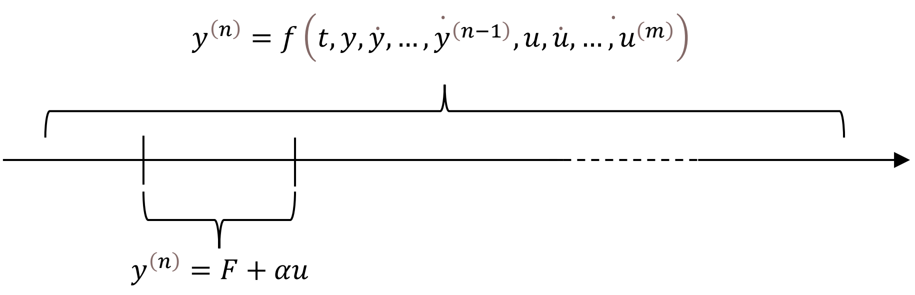

Figure 3.1 The principle of local modeling.

Such a model is often complex and may not be fully known due to uncertainties in parameters, approximated or neglected dynamics, etc. The real physical system may be subject to disturbances, measurements which are often noisy, and inputs could be uncertain.

To address these issues, the complex model (3.1) is replaced by a simpler linear model, valid for a short period of time, described by the following equation (3.2), known as the ultra-local model (Figure 3.1):

$$y^{(v)} = F + \alpha u \tag{3.2}$$

In the context of local modeling, the parameters and terms involved are defined as follows:

- $\boldsymbol{v} \geq 1$: This represents the order of the derivative of the output used in the local model, with $\boldsymbol{v}$ typically being 1 or 2, as chosen by the practitioner.
- $\boldsymbol{y}^{(\boldsymbol{v})}$: This is the $\boldsymbol{v}$-th order derivative of the output, calculated using a numerical differentiator.
- $\boldsymbol{u}$: This denotes the input to the system.
- $\boldsymbol{\alpha}$: This is a constant, non-physical parameter chosen by the practitioner such that $\boldsymbol{\alpha u}$ and $\boldsymbol{y}^{(\boldsymbol{v})}$ are of the same order of magnitude. The value of $\boldsymbol{\alpha}$ is determined through trial and error.
- $\boldsymbol{F}$: This is a constant function assumed to encapsulate all unknown and disturbed parts of the system (with no difference). It is continuously estimated by:

$$F_{est} = {y^{(v)}}_{est} - \alpha u \tag{3.3}$$

3.2.2 Principle of MFC

Model-free control considers two-time intervals as depicted in Figure 3.2. These intervals are:

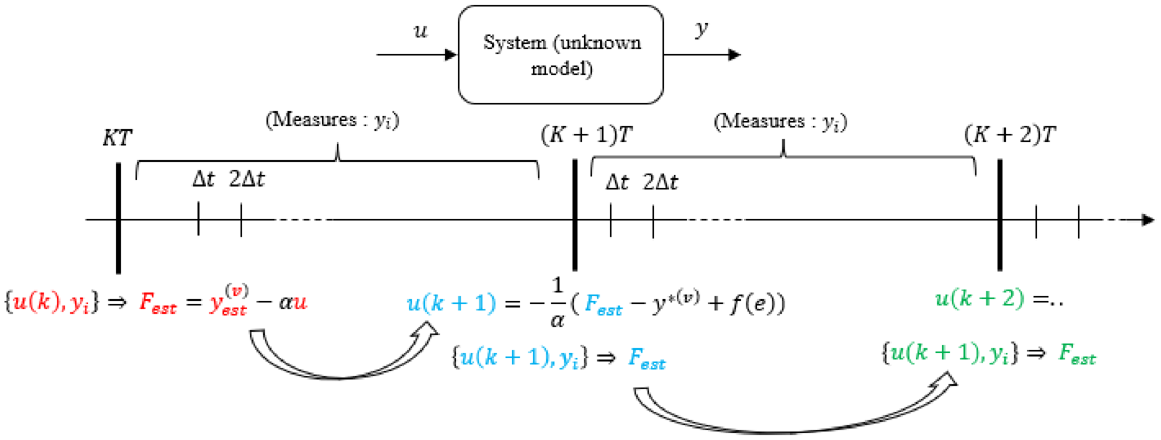

Figure 3.2 Principle of model-free control.

- Control interval T: apply $u(KT)$, where T is the sampling period (measurement frequency).
- Measurement interval Δt: measure y_i and estimate $y_{est}^{(v)}$.

The control law is given at each instant KT by:

$$u(KT) = -\frac{1}{\alpha}\left(F_{est} - y^{*(v)} + f(e)\right) \tag{3.4}$$

where

- y^{*} is the reference trajectory that the output y must match or come close to,
- $f(e)$ is a function dependent on the error $e = y^{*} - y$

By combining equations (3.3) and (3.4), we obtain the following equation:

$$e^{(v)} + f(e) = 0 \tag{3.5}$$

We must choose $e^{(v)} + f(e) = 0$ in such a way that the trajectory y^{*} is ensured.

$$\lim_{t \to +\infty} e(t) \tag{3.6}$$

For example, we use the proportional (P), which is adjustable.

In summary, the model-free control algorithm is as follows:

- Choose v, the order of the derivative of y from equation (3.2), generally $v = 1$ or $v = 2$.
- Choose α to ensure F and αu have the same magnitude.
- Choose the reference trajectory y^{*}.
- Calculate $F = y^{(v)} - \alpha u$, after estimating $y^{(v)}$.
- Apply an PID for controlling the system.

$$f(e) = k_P e(t) \tag{3.7}$$

Obviously, the gain of the P must be adjusted.

3.2.3 F estimation

Two approaches are proposed:

- Simultaneous estimation.
- Direct estimation, which we are focusing on in this chapter.

3.2.3.1 Simultaneous estimation

Consider the equation (3.2) of the ultra-local model with $v = 1$ as an example.

$$\dot{y}(t) = F + \alpha u \tag{3.8}$$

According to the rules of operational (Laplace) domain [73], Equation (3.8) can be expressed as:

$$sY = \frac{F_{est}}{s} + \alpha U + y(0) \tag{3.9}$$

By pre-multiplying both sides of Equation (3.9) by $\frac{d}{ds}$ (i.e., multiplying on the left), the initial condition $y(0)$ is eliminated, as demonstrated in Equation (3.10).

$$Y + s\frac{dY}{ds} = -\frac{F_{est}}{s^2} + \alpha\frac{dU}{ds} \tag{3.10}$$

By pre-multiplying both sides of Equation (14) by s^{-2}, which corresponds to integration [74], noise attenuation is achieved. Given the equivalence between differentiation with respect to $\frac{d}{ds}$ and multiplication by $-t$, this results in the real-time estimate in the time domain.

$$F_{est}(t) = -\frac{6}{\tau^3}\int_{t-\tau}^{t}[(\tau - 2\sigma)y(\sigma) + \alpha\sigma(\tau - \sigma)u(\sigma)]\, d\sigma \tag{3.11}$$

where $\tau > 0$ could be quite small.

Remark 3.1: The expression given in Equation (3.11) can be approximated using finite impulse response (FIR) filters (see, for example, [75]). To enable real-time implementation, backward integration over a short time interval T is utilized.

3.2.3.2 Direct estimation

To estimate F in real time, it is assumed to remain constant between consecutive time instants. It can be estimated using Equation (3.2).

$$F_{est}(k) = y_{est}^{(v)}(k) - \alpha u(k-1) \tag{3.12}$$

where F_{est} represents the online estimate of F, $y_{st}^{(v)}(k)$ is the estimated value of $y^{(v)}$ at time step k, and $u(k-1)$ is the control input at time $k-1$.

Remark 3.2: The MFC maintains the simplicity of a traditional PID controller. Additionally, by identifying and estimating the system's internal dynamics, the MFC achieves self-adaptation and high robustness, which greatly enhances overall control performance.

The MFC schema is described in Figure 3.3.

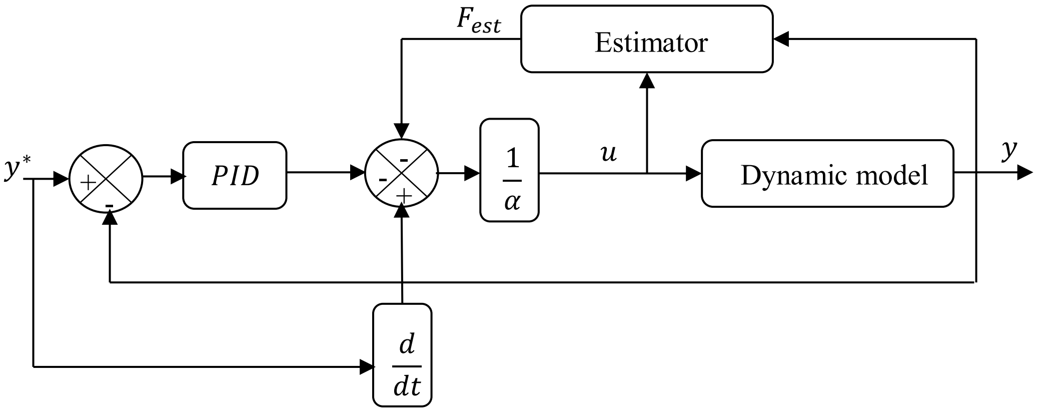

Figure 3.3 MFC scheme.

3.3 Implementing MFC for GSC and MSC

Figure 6 illustrates the block diagram of the system using the MFC controller for both the MSC and GSC.

3.3.1 Control of the MSC

In this section, MSC control is indirectly achieved by regulating the stator currents ($\boldsymbol{i_{sd}}$ and $\boldsymbol{i_{sq}}$) using two MFC controllers. Additionally, MFC used to ensures that the generator speed follows the reference speed, allowing the wind turbine to generate maximum power.

The errors chosen for this control are given by the following equations:

$$e(\Omega_m) = \Omega^*{}_m - \Omega_m \tag{3.13}$$

$$\begin{cases} e(i_{sd}) = i_{sd}{}^* - i_{sd} \\ e(i_{sq}) = i_{sq}{}^* - i_{sq} \end{cases} \tag{3.14}$$

- **Step 1:** MFC control for MPPT

The speed can be written from (2.9) as follows:

$$\frac{d\Omega_m}{dt} = \frac{1}{J}(T_m - T_{em} - f.\Omega_m) \tag{3.15}$$

The functional equation derived by combining Equations (3.2) and (3.15) is as follows:

$$\dot{y}^*{}_{\Omega_m} = \frac{d\Omega_m}{dt} = F_{\Omega_m} + \alpha_{\Omega_m} u_{\Omega_m} \tag{3.16}$$

The value of F, which is valid for only a brief period, is estimated as follows:

$$F_{\Omega_m\, est}(k) = \dot{y}_{\Omega_m\, est} - \alpha_{\Omega_m} u_{\Omega_m}(k-1) \tag{3.17}$$

By closing the loop with a P controller, the control law for the MFC controller, derived from the ultra-local model, is as follows:

$$u_{\Omega_m} = -\frac{F_{\Omega_m\, est} - \dot{y}^*_{\Omega_m} + K_{P\,\Omega_m} e(\Omega_m)}{\alpha_{\Omega_m}} \tag{3.18}$$

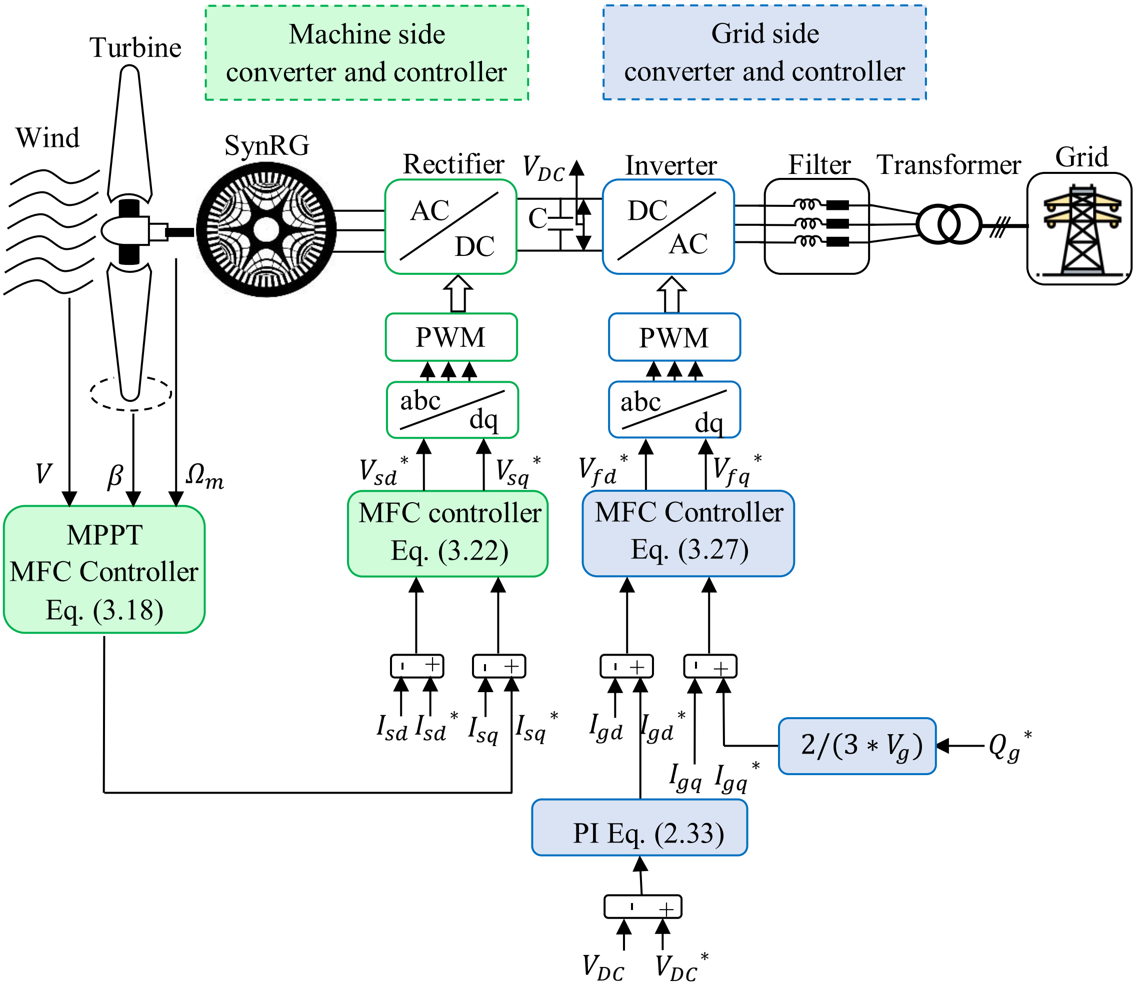

Figure 3.4 System control configuration using MFC controller.

- **Step 2:** MFC control for stator currents

The stator currents are expressed as follows:

$$\begin{cases} \frac{di_{sd}}{dt} = \frac{V_{sd}}{L_{sd}} - \frac{R_s i_{sd}}{L_{sd}} + \frac{\Omega_r \Phi_{sq}}{L_{sd}} \\ \frac{di_{sq}}{dt} = \frac{V_{sq}}{L_{sq}} - \frac{R_s i_{sq}}{L_{sq}} - \frac{\Omega_r \Phi_{sd}}{L_{sq}} \end{cases} \tag{3.19}$$

The functional equation derived by combining Equations (3.2) and (3.19) is as follows:

$$\begin{cases} \dot{y}^*{}_{i_{sd}} = \frac{di_{sd}}{dt} = F_{i_{sd}} + \alpha_{i_{sd}} u_{i_{sd}} \\ \dot{y}^*{}_{i_{sq}} = \frac{di_{sq}}{dt} = F_{i_{sq}} + \alpha_{i_{sq}} u_{i_{sq}} \end{cases} \tag{3.20}$$

The value of F, which is valid for only a brief period, is estimated as follows:

$$\begin{cases} F_{i_{sd}\,est}(k) = \dot{y}_{i_{sd}\,est} - \alpha_{i_{sd}} u_{i_{sd}}(k-1) \\ F_{i_{sq}\,est}(k) = \dot{y}_{i_{sq}\,est} - \alpha_{i_{sq}} u_{i_{sq}}(k-1) \end{cases} \tag{3.21}$$

By closing the loop with a P controller, the control law for the MFC controller, derived from the ultra-local model, is as follows:

$$\begin{cases} u_{i_{sd}} = -\frac{F_{i_{sd}\,est} - \dot{y}^*_{i_{sd}} + K_{P\,i_{sd}} e(i_{sd})}{\alpha_{i_{sd}}} \\ u_{i_{sq}} = -\frac{F_{i_{sq}\,est} - \dot{y}^*_{i_{sq}} + K_{P\,i_{sq}} e(i_{sq})}{\alpha_{i_{sq}}} \end{cases} \tag{3.22}$$

3.3.2 Control of the GSC

Grid-side control is indirectly achieved by regulating the currents (i_{gd} and i_{gq}) using two MFC controllers. Additionally, a PI controller can be used to maintain a constant DC bus voltage.

The errors used for controlling the GSC are listed below:

$$\begin{cases} e(i_{gd}) = i_{gd}{}^* - i_{gd} \\ e(i_{gq}) = i_{gq}{}^* - i_{gq} \end{cases} \tag{3.23}$$

The grid currents are expressed as follows:

$$\begin{cases} \frac{di_{gd}}{dt} = \frac{V_{fd}}{L_f} - \frac{R_f i_{gd}}{L_f} + \omega_g i_{gq} - \frac{V_{gd}}{L_f} \\ \frac{di_{gq}}{dt} = \frac{V_{fq}}{L_f} - \frac{R_f i_{gq}}{L_f} - \omega_g i_{gd} - \frac{V_{gq}}{L_f} \end{cases} \tag{3.24}$$

The functional equation derived by combining Equations (3.2) and (3.24) is as follows:

$$\begin{cases} \dot{y}^*{}_{i_{gd}} = \frac{di_{gd}}{dt} = F_{i_{gd}} + \alpha_{i_{gd}} u_{i_{gd}} \\ \dot{y}^*{}_{i_{gq}} = \frac{di_{gq}}{dt} = F_{i_{gq}} + \alpha_{i_{gq}} u_{i_{gq}} \end{cases} \tag{3.25}$$

The value of F, which is valid for only a brief period, is estimated as follows:

$$\begin{cases} F_{i_{gd}\,est}(k) = \dot{y}_{i_{gd}\,est} - \alpha_{i_{gd}} u_{i_{gd}}(k-1) \\ F_{i_{sq}\,est}(k) = \dot{y}_{i_{gq}\,est} - \alpha_{i_{gq}} u_{i_{gq}}(k-1) \end{cases} \tag{3.26}$$

By closing the loop with a P controller, the control law for the MFC controller, derived from the ultra-local model, is as follows:

$$\begin{cases} u_{i_{gd}} = -\frac{F_{i_{gd}\,est} - \dot{y}^*_{i_{gd}} + K_{P\,i_{gd}} e(i_{gd})}{\alpha_{i_{sd}}} \\ u_{i_{gq}} = -\frac{F_{i_{gq}\,est} - \dot{y}^*_{i_{gq}} + K_{P\,i_{gq}} e(i_{gq})}{\alpha_{i_{gq}}} \end{cases} \tag{3.27}$$

3.4 Results and simulation

To analyze the performance of the method presented in this chapter, specifically vector control using MFC, a wind system based on the SynRM is developed and simulated in the Matlab/Simulink environment for variable wind speeds. Additionally, the performance of the proposed strategies is compared through three tests: a tracking test, a wind speed variation test, and a robustness test. The parameters for the turbine and the SynRM are provided in chapter 2.

Remark 3.3: To ensure a fair comparison between the classical PI controls and our innovative MFC strategy, we used the same set of parameters for both control methods. This approach guarantees that any performance improvements observed can be attributed solely to the inherent advantages of the MFC strategy, rather than variations in controller tuning.

3.4.1 Tracking test

The initial test evaluates the tracking performance of the MFC strategy when exposed to varying wind speeds applied in discrete steps. These results are then compared to those achieved with the conventional approach, which employs PI controllers.

The wind speed profile used for the control process is illustrated in Figure 3.5.

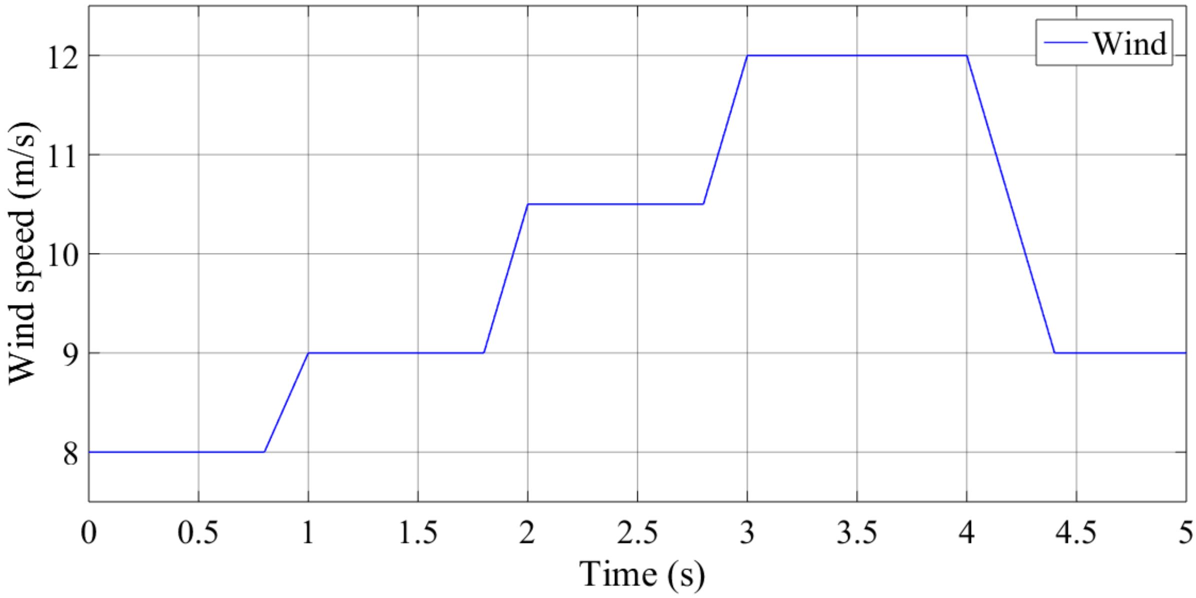

Figure 3.5 Wind speed profile.

3.4.1.1 MSC control results

Figures 3.6(a) and 3.6(b) clearly demonstrate that both the tip speed ratio (λ) and the power coefficient (C_p) consistently align with their optimal reference values—8.1 and 0.47, respectively—throughout the entire simulation period. This precise alignment underscores that the system maintains maximum aerodynamic efficiency and a critical factor in optimizing energy extraction from the wind. By ensuring that the tip speed ratio and power coefficient stay near their ideal values, the turbine operates at peak aerodynamic performance, maximizing energy capture from the wind resource.

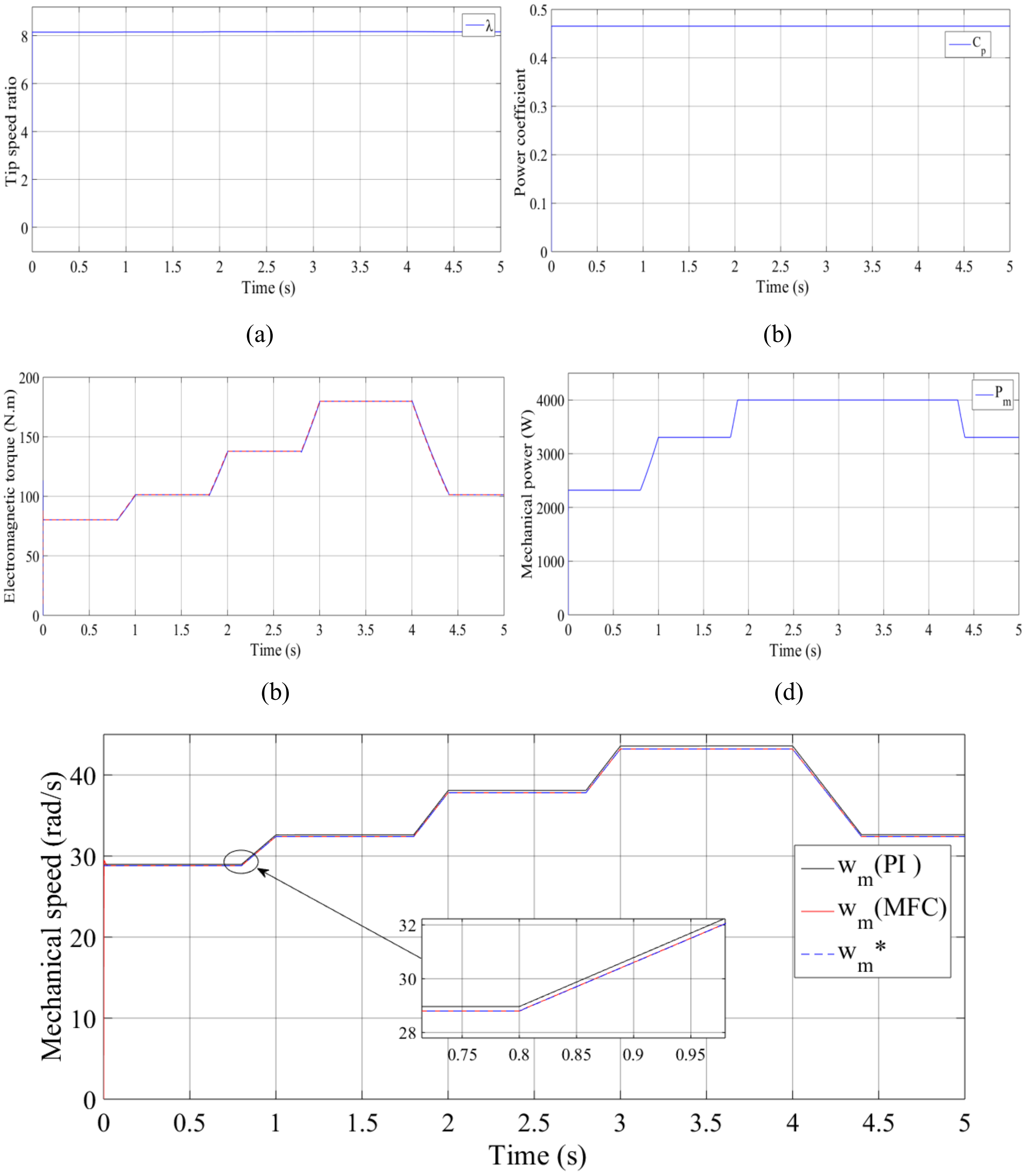

(a) (b)

(b) (d)

(e)

Figure 3.6 MPPT-MFC performance: Tip speed ratio (a), Power coefficient (b), Electromagnetic torque (c), Mechanical power (d), Mechanical speed (e).

In Figure 3.6(c), the electromagnetic torque ($\boldsymbol{T_{em}}$) is shown to precisely follow the optimal torque dictated by the MPPT algorithm. This accurate tracking of the electromagnetic torque is essential for ensuring that power transfer from the wind turbine to the generator occurs efficiently, thereby optimizing electrical power output. The MPPT algorithm's effectiveness in maintaining the ideal torque ensures that the system extracts the maximum possible electrical energy from the available wind power.

Figure 3.6(d) highlights how the mechanical power ($\boldsymbol{P_m}$) closely tracks the wind speed profile throughout the simulation. This strong correlation between mechanical power and wind speed fluctuations indicates that the system is highly adaptive, allowing the turbine to generate the maximum amount of power even as wind conditions change. By adjusting to variations in wind speed, the mechanical power output remains optimized, ensuring that the system consistently operates at peak performance and delivers the highest possible energy yield across a range of wind conditions.

Figure 3.6(e) demonstrates that the turbine speed closely tracks its reference for both indirect control methods (PI and MFC), providing evidence that the MPPT algorithm is functioning as intended. However, as observed in the zoomed-in view of the figure, the MFC method exhibits superior speed control accuracy compared to PI control, thereby enabling a more precise execution of MPPT.

3.4.1.2 GSC control results

Both controllers demonstrate proficiency in accurately tracking the DC bus voltage, as illustrated in Figure 3.7. However, the enlarged view reveals that the MFC method exhibits a faster response time compared to PI control. Regardless of fluctuations in wind conditions, the DC bus voltage remains stable, which is essential for maintaining consistent and reliable operation of the wind turbine system.

Figures 3.8(a,b) provide a comprehensive comparison of the performance of two grid-side control strategies: the PI and the MFC. Both controllers are adept at accurately tracking the active power references ($\boldsymbol{P_g}$), as illustrated in Figures 3.8(a) and 3.10(a), ensuring that the generated power aligns closely with the desired output. This precise tracking is crucial for maintaining grid stability and optimizing the efficiency of power generation.

Additionally, Figures 3.8(b), 3.10(b) and 3.11(c) illustrate how both control strategies effectively maintain a unity power factor ($\cos(phi)$) by ensuring that the grid's reactive power (Q_g) remains consistently close to zero. This is important because it reflects efficient energy production while minimizing losses, thereby improving the overall quality of the generated electrical energy.

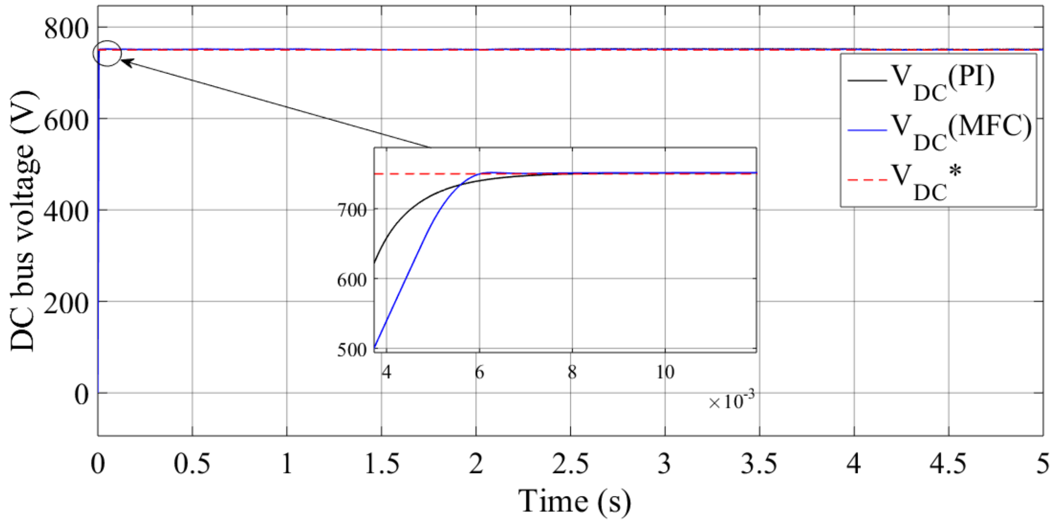

Figure 3.7 DC bus voltage

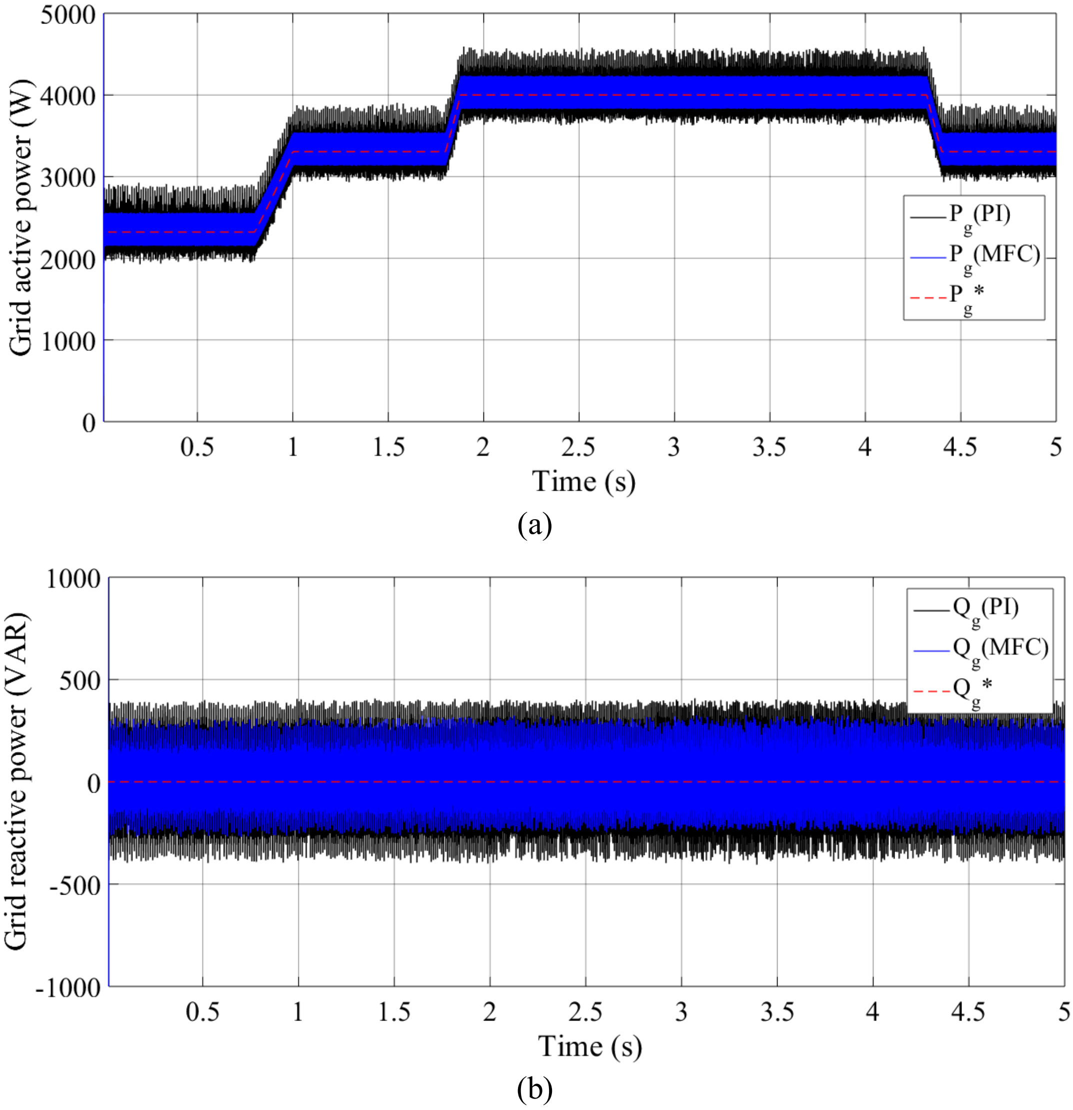

(a)

(b)

Figure 3.8 MFC performance: Active power (a), Reactive power (b),

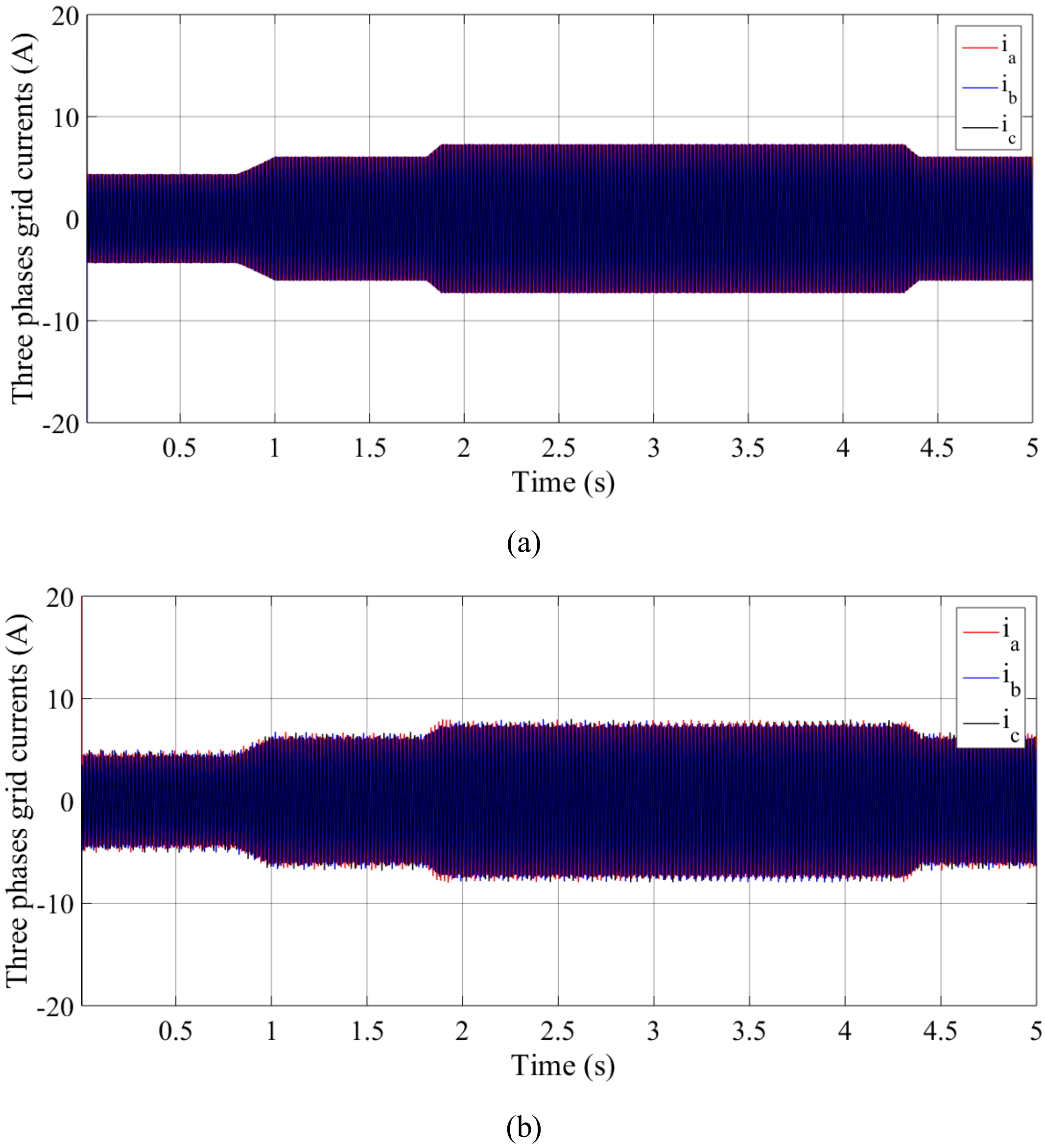

Figure 3.9 Grid currents using MFC (a), grid currents using PI (b).

Figures 3.9(a,b) illustrates that while the amplitude of the injected current varies with wind speed, it consistently maintains a stable frequency of 50 Hz. Under MFC control, the waveform is more sinusoidal and exhibits a lower ripple rate compared to PI control (Figures 3.11(c,d)). This suggests that MFC delivers enhanced performance regarding waveform quality and stability, even amid fluctuations in wind speed.

A harmonic analysis of the grid current was performed to evaluate the effect of the two control methods on the quality of the signal delivered to the grid, as shown in Figure 3.12. The analysis indicates that the THD achieved with MFC (Figure 3.12(a)) is significantly lower at 4.82%, compared to the 10.51% THD observed with PI control (Figure 3.12(b)).

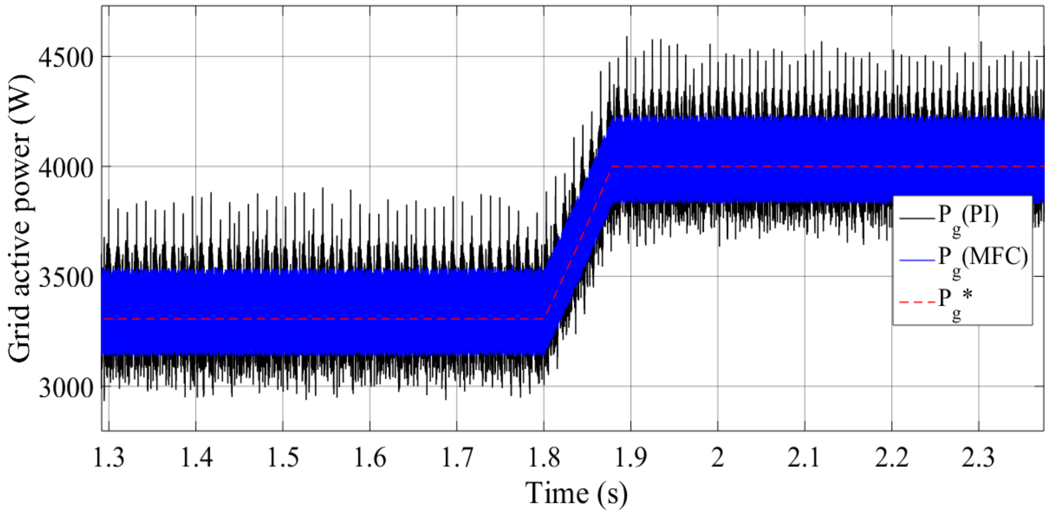

(a)

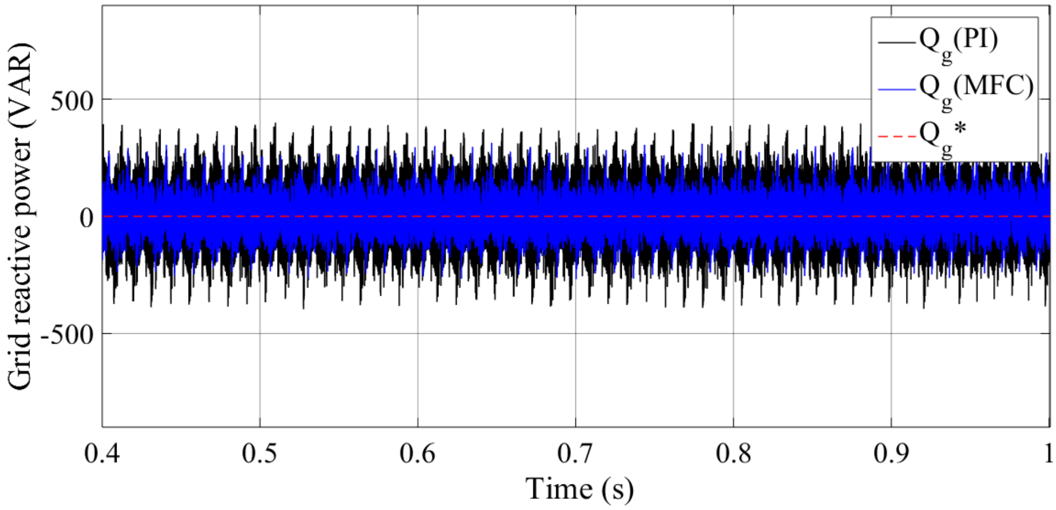

(b)

Figure 3.10 Zoom on: Active power (a), Reactive power (b).

3.4.1.3 Conclusion of the first test

The initial tracking test underscores the superior performance of the MFC strategy over conventional PI control. The MFC effectively tracks the electromagnetic torque set by the MPPT algorithm and maintains stable DC bus voltage despite fluctuations in wind speed.

Moreover, MFC exhibited enhanced speed control accuracy and produced a more sinusoidal waveform with reduced ripple rates, thereby improving power quality. Harmonic analysis further confirmed significantly lower total harmonic distortion for the MFC compared to PI control. Overall, these findings indicate that MFC enhances energy extraction and optimizes the performance of the wind turbine system.

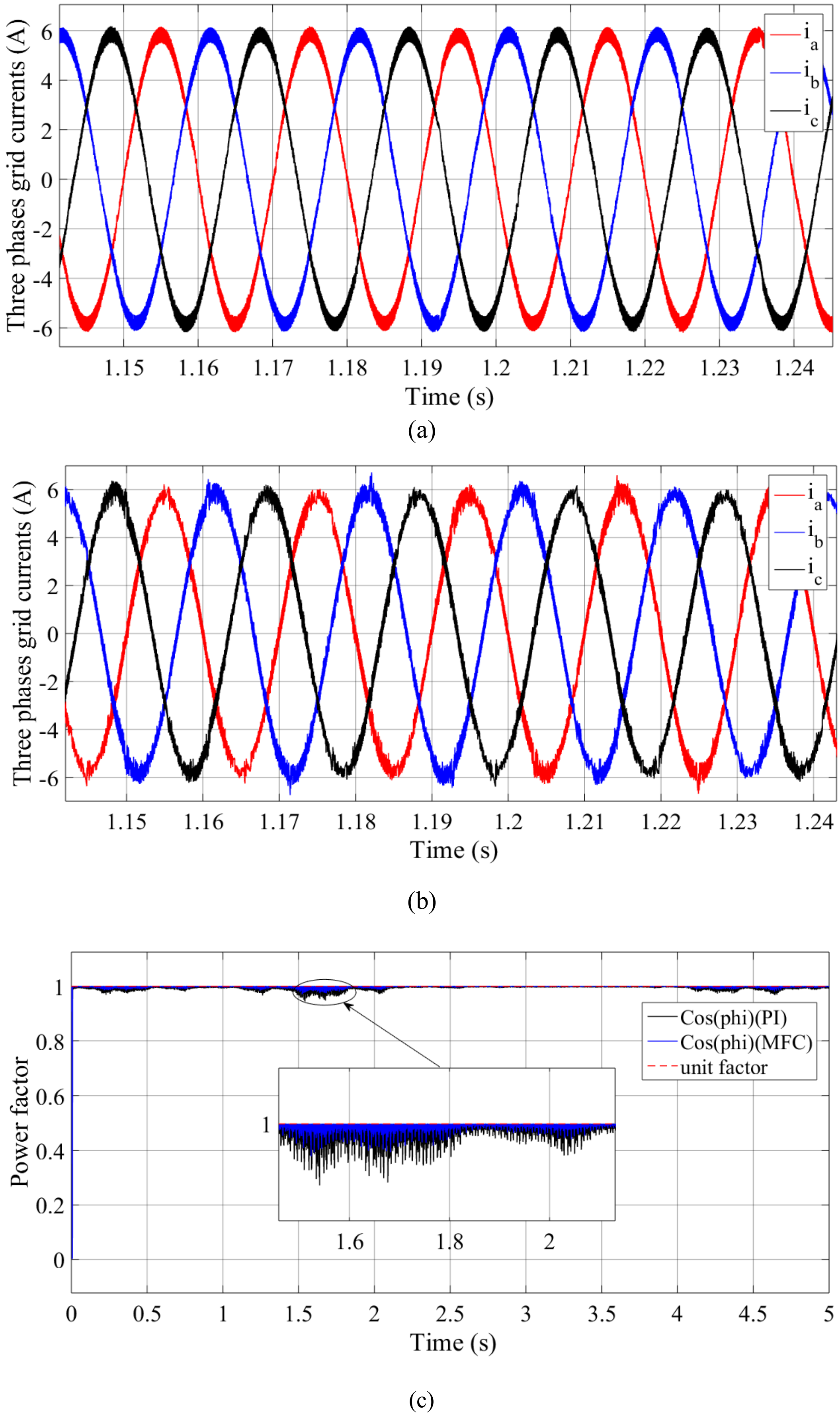

Figure 3.11 Grid currents using MFC (a), Grid currents using PI (b), Power factor (c).

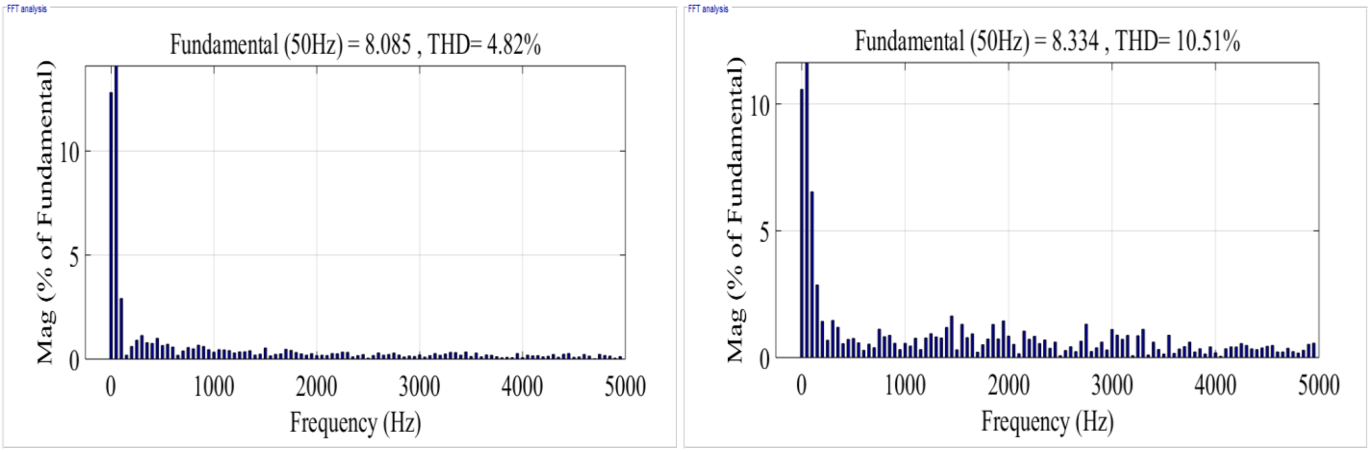

(a) (b)

Figure 3.12 MFC grid current THD (a), PI grid current THD (b).

3.4.2 Wind speed variation test

In this test, a different wind speed pattern was applied compared to the one used in the first test. This variation was introduced to evaluate the impact on the proposed control method. The wind speed profile used in this test is illustrated in Figure 3.13.

3.4.2.1 MSC control results

In this text, the results for the tip speed ratio (λ), power coefficient (C_p), electromagnetic torque (T_{em}), and mechanical power (P_m) show no significant differences in performance. However, Figure 3.14(e) indicates that the turbine speed closely tracks its reference for both control methods (PI and MFC), confirming that the MPPT algorithm is functioning as intended. Importantly, the zoomed-in view of the figure reveals that the MFC method provides superior speed control accuracy compared to PI control, enabling a more precise implementation of the MPPT strategy.

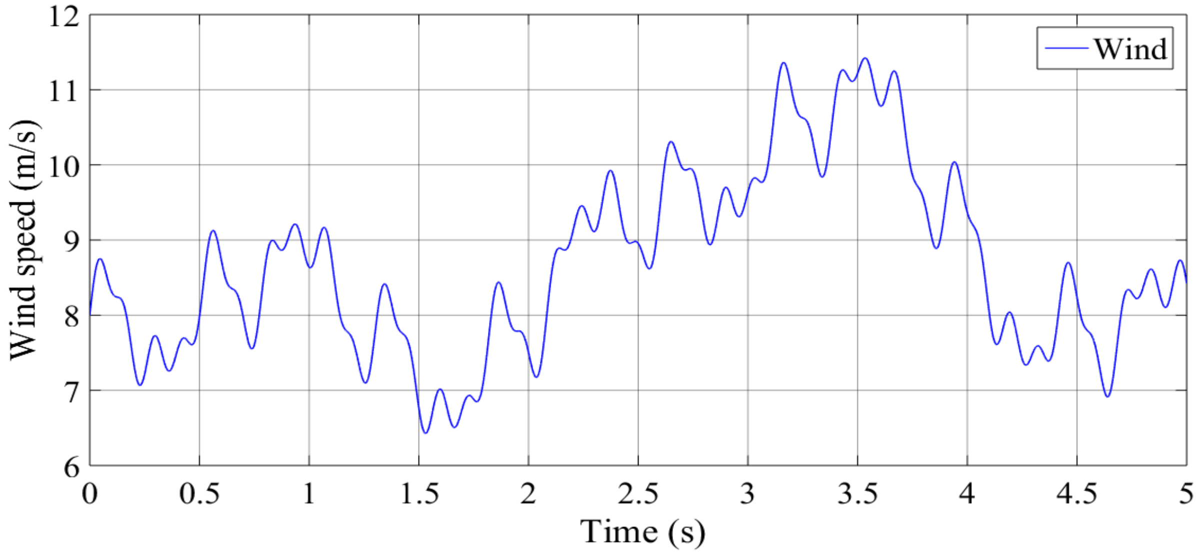

Figure 3.13 Wind speed profile.

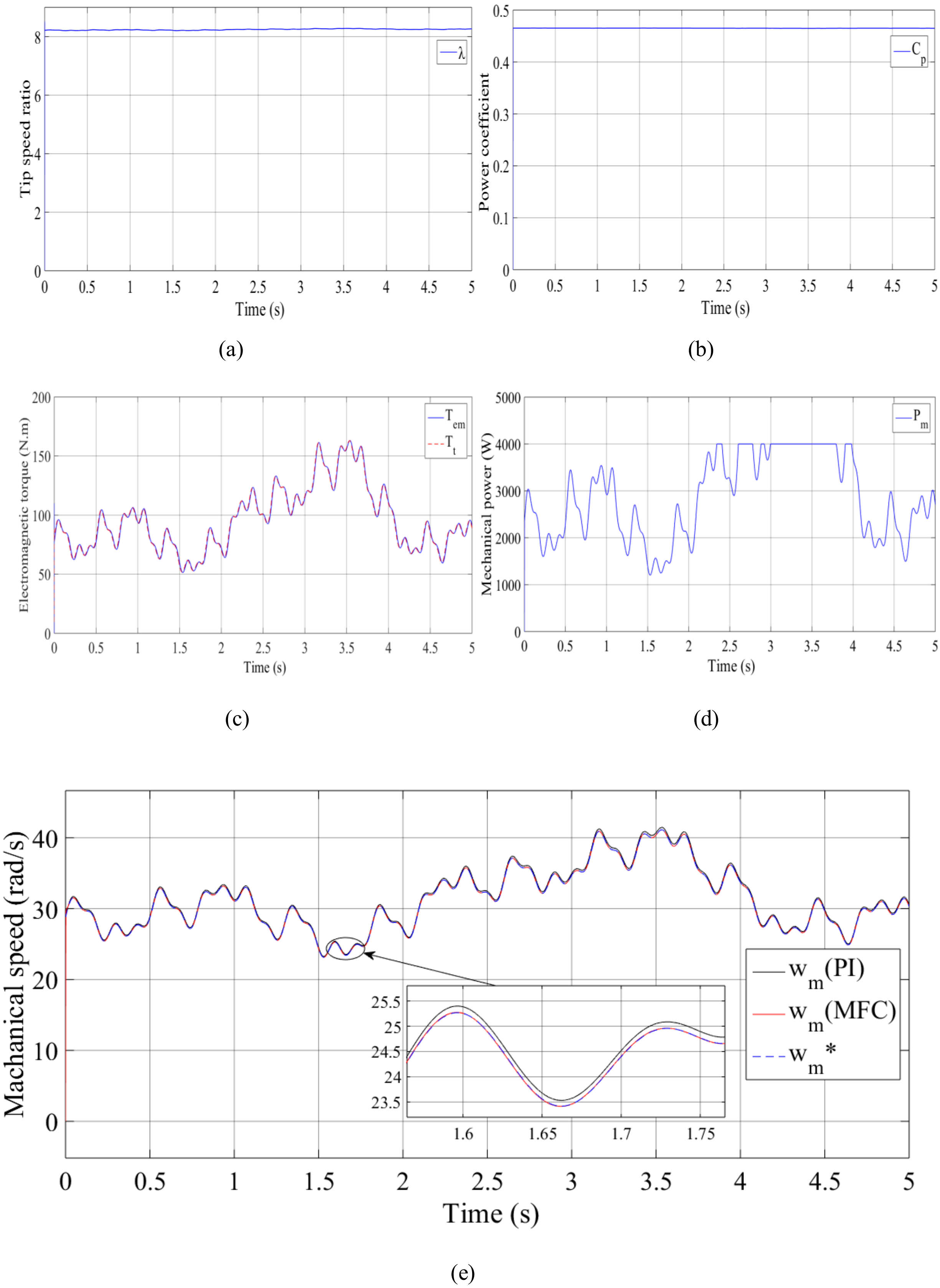

(a) (b)

(c) (d)

(e)

Figure 3.14 MPPT-MFC performance: Tip speed ratio (a), Power coefficient (b), Electromagnetic torque (c), Mechanical power (d), Mechanical speed (e).

3.4.2.2 GSC control results

Both controllers effectively track the DC bus voltage with high accuracy, as shown in Figure 3.15. Despite variations in wind conditions, the DC bus voltage remains stable, which is crucial for ensuring the consistent and reliable operation of the wind turbine system.

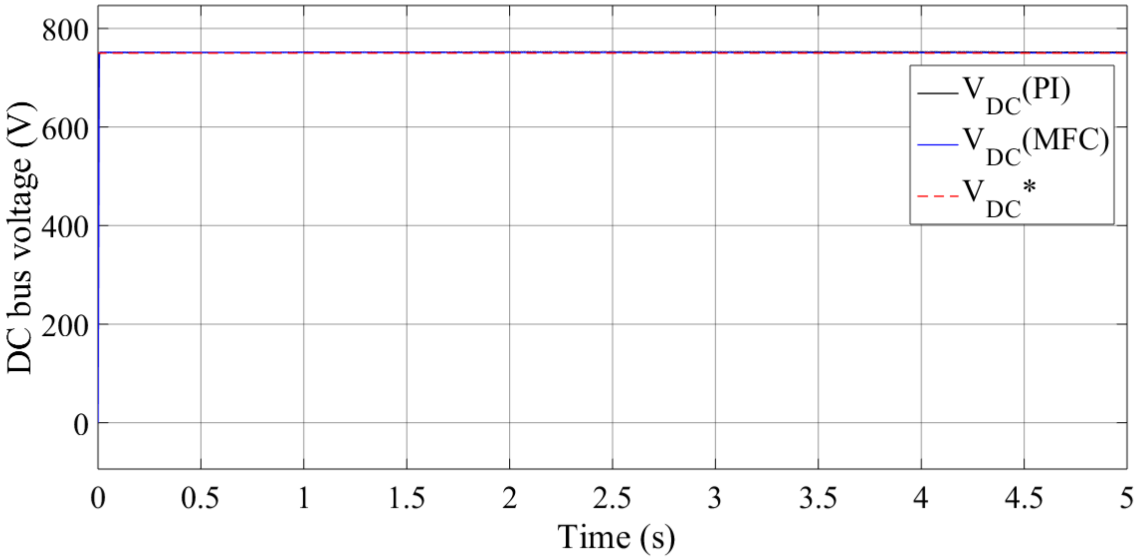

Figure 3.15 DC bus voltage.

Figures 3.16(a) and 3.16(b) present a detailed comparison of the performance of two grid-side control strategies: PI and MFC. Both controllers effectively track the active power references (P_g), as illustrated in Figures 3.16(a) and 3.17(a). However, MFC demonstrates greater robustness, showing less ripple and improved stability compared to the PI controller.

In addition, Figures 3.16(b), 3.17(b) and 3.18(a) highlight the robustness and effectiveness of both control strategies in the second test in maintaining the single power factor ($\cos(phi)$) by keeping the grid reactive power (Q_g) consistently close to zero, with a notable improvement for MFC. This is important because it indicates efficient power generation and reduced losses, thus improving the overall quality of the generated electrical power.

Similarly, in the second test, the MFC demonstrated improved control accuracy and generated a more sinusoidal waveform with lower ripple rates, thereby enhancing power quality. Harmonic analysis further confirmed that the THD with MFC (2.16%) was significantly lower compared to PI control (6.20%). Overall, these findings suggest that MFC optimizes energy extraction and improves the overall performance of the wind turbine system.

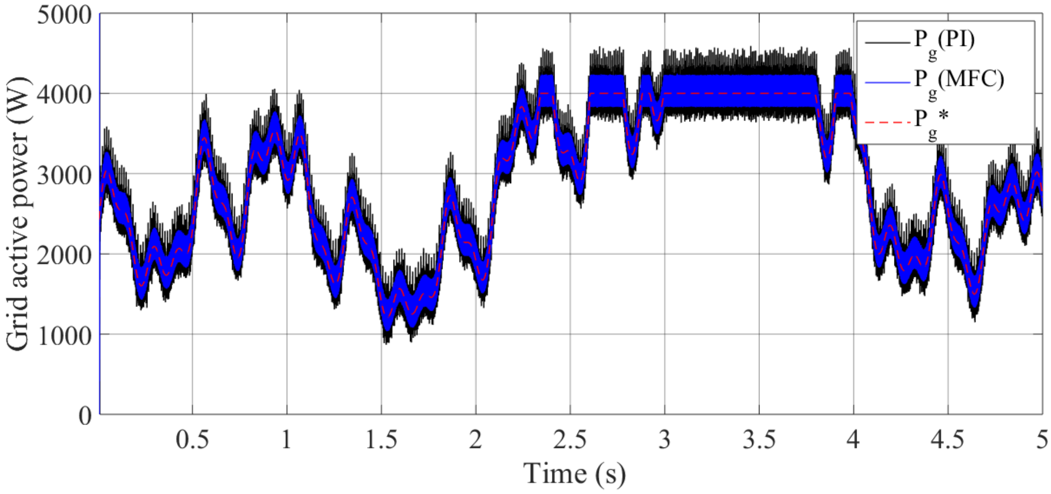

(a)

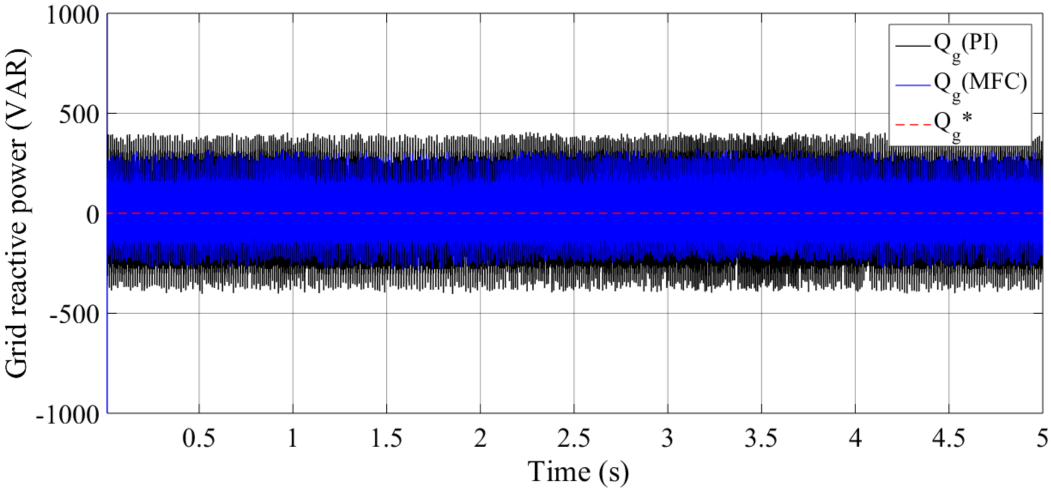

(b)

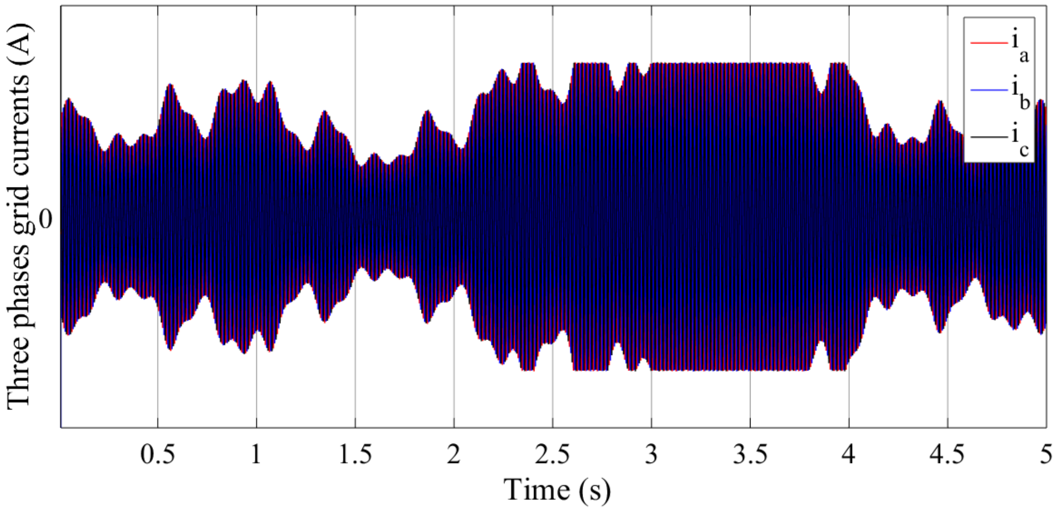

(c)

Figure 3.16 MFC performance: Active power (a), Reactive power (b), Grid currents (c).

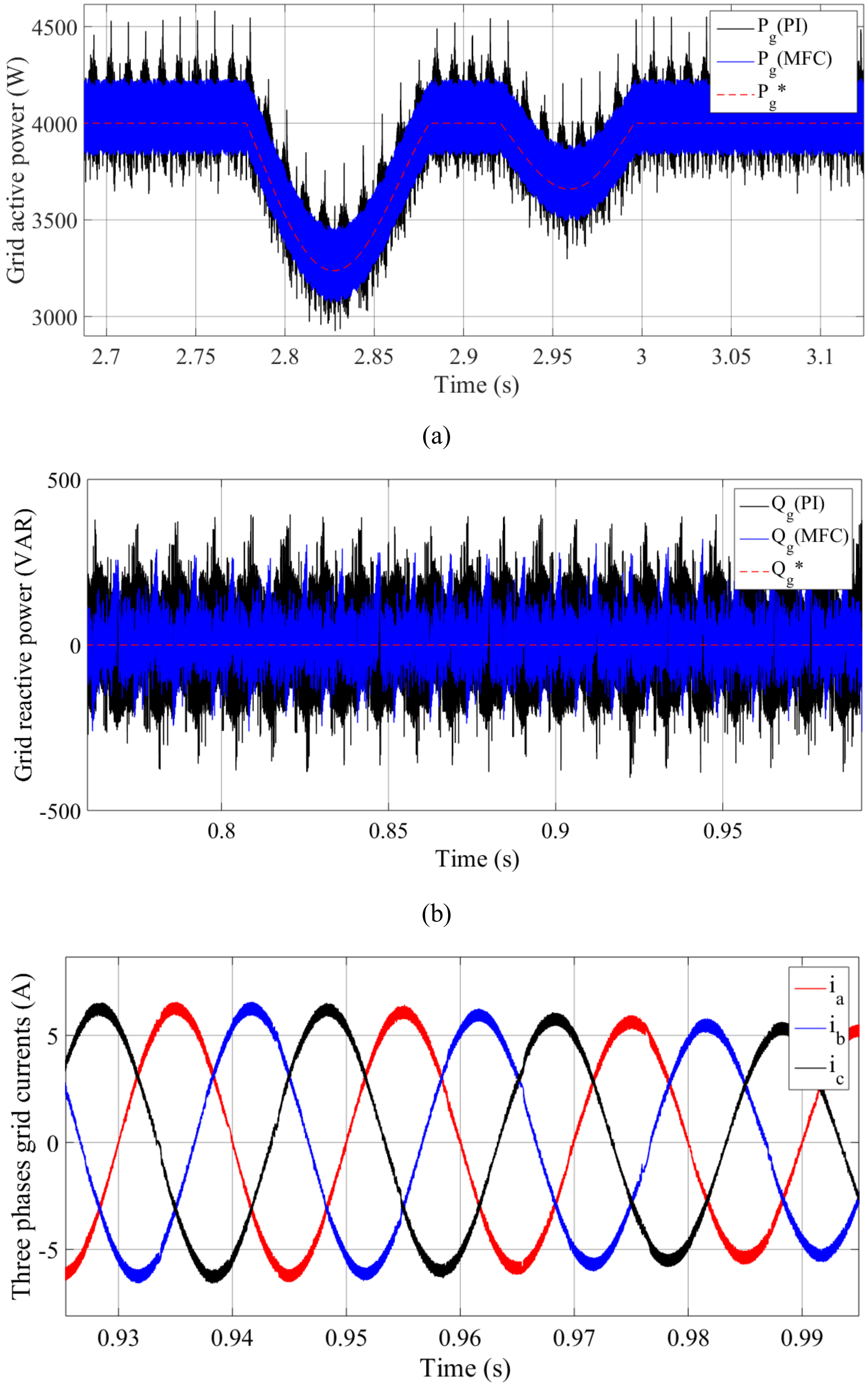

(a)

(b)

(c)

Figure 3.17 Zoom on: Active power (a), Reactive power (b), Grid currents (c).

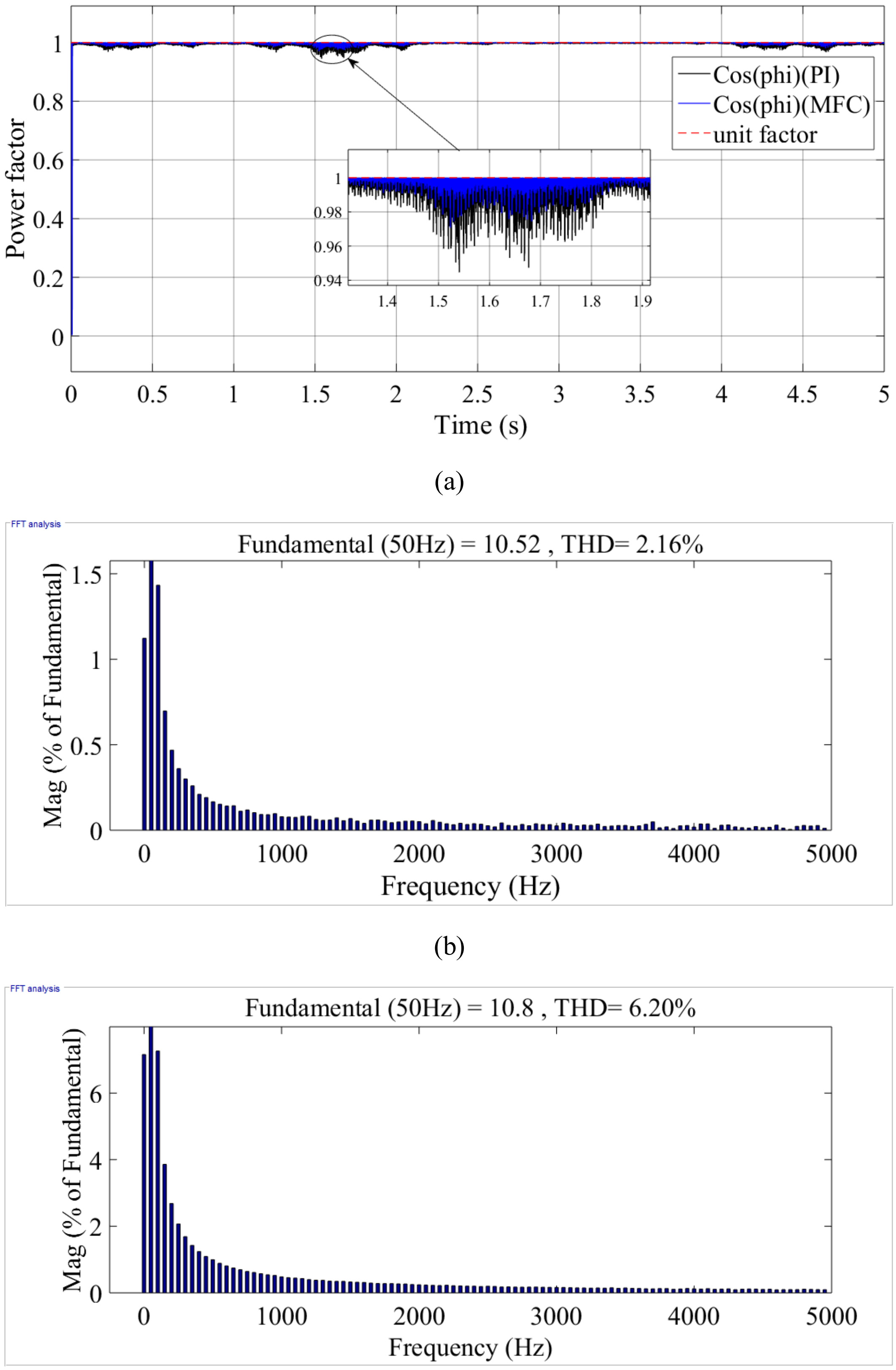

(a)

(b)

(c)

Figure 3.18 Power factor (a), MFC grid current THD (b), PI grid current THD (c).

3.4.2.2 Conclusion for the second test

The second test demonstrates the superior robustness of the MFC control strategy compared to PI control under varying wind conditions. While both controllers performed similarly in tracking the tip speed ratio, power coefficient, torque, and mechanical power, MFC showed better speed control accuracy, ensuring more precise MPPT.

MFC also maintained greater stability, less ripple, and more effective power generation with minimal losses. It achieved a lower total harmonic distortion (THD) of 2.16% compared to 6.20% for PI control, enhancing power quality and overall wind turbine system performance.

3.4.3 Robustness test

This test evaluates the robustness of the proposed control strategy MFC, compared to conventional PI control strategies. The robustness of these controllers is tested by deliberately altering key machine parameters to simulate challenging operating conditions. The specific parameter modifications include:

- Stator resistance: increased by 50% from its nominal value to account for increased losses and potential variations due to temperature changes.
- Stator inductance: reduced by 50% from its nominal value to simulate degraded magnetic properties or winding changes.
- System inertia: increased by 50% to represent a heavier mechanical load or modified system dynamics.

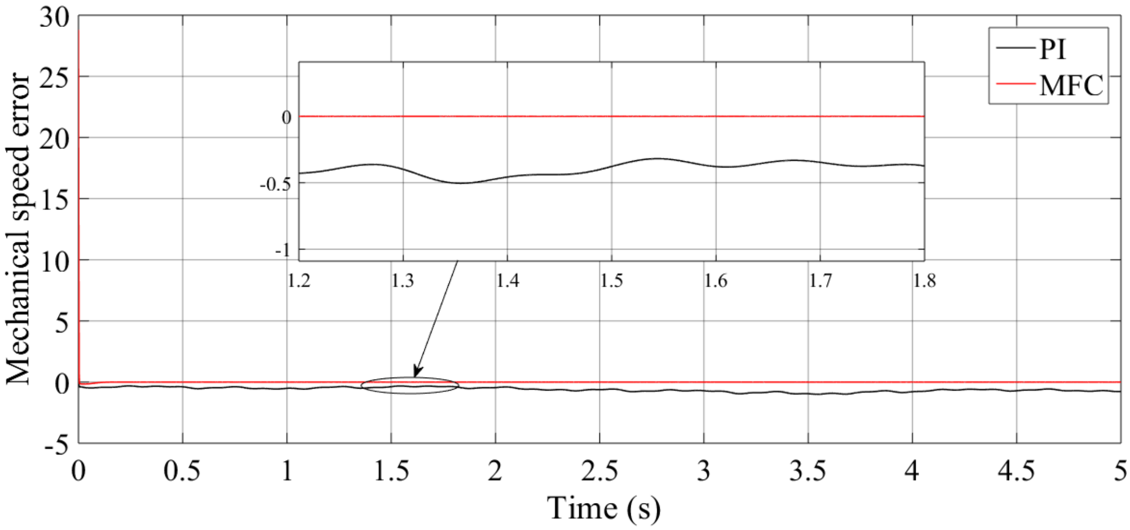

Figure 3.19 Mechanical speed error.

The These adjustments are designed to stress-test the controllers under non-ideal and varying operational conditions, evaluating their adaptability and resilience.

The simulation results, depicted in Figure 2.13, provide a clear comparison of the two control strategies under these challenging conditions:

- The PI controller showed a marked sensitivity to parameter variations, resulting in significant generator speed errors. This indicates a limited capacity to adapt to abrupt system changes or uncertainties.
- The MFC controller exhibited superior robustness, with substantially lower generator speed errors under the same conditions. This underscores its effectiveness in maintaining stable operation despite parameter deviations.

The findings demonstrate that the MFC controller offers enhanced performance and resilience, making it a more reliable option for systems subject to variable and unpredictable environments.

3.5 Conclusion

This chapter has focused on the modeling and control of a wind energy conversion system based on a Synchronous Reluctance Generator (SynRG). We have presented the model-free control (MFC) strategy as an alternative to the traditional vector control method. These control techniques have been applied to regulate the active and reactive power while ensuring accurate maximum power point tracking (MPPT). The goal was to minimize power and current oscillations, leading to an overall improvement in system efficiency and performance.

In particular, the chapter discussed how the MFC-based control was applied to achieve accurate MPPT, reducing fluctuations in both power and current injected into the grid. Through simulation comparisons between the conventional PI controller and the proposed MFC strategy in two different tests, it became evident that MFC offers significant advantages. Notably, MFC ensures more precise power regulation and better tracking of the maximum power point, resulting in enhanced system efficiency. This improvement is maintained even when the system is subjected to robustness tests under varying wind conditions.

The simulation results also clearly demonstrate the superiority and effectiveness of MFC in reducing the ripple effect in both current and active/reactive power delivered to the grid. This reduction in oscillations directly contributes to improved overall system performance, even when compared to conventional PI control methods.

The key findings of this chapter can be summarized as follows:

- Enhanced robustness of MFC: The MFC controllers show superior robustness compared to PI controllers, allowing them to handle variations in wind speed more effectively without significant performance degradation.
- Improved power regulation and MPPT: MFC controllers provide more precise power regulation and MPPT, ensuring that the wind turbine consistently operates at its optimal efficiency point. However, some oscillations were observed due to the ripple effect inherent in the PID.

- Reduced power and current oscillations: Compared to traditional PI controllers, the MFC technique significantly reduces the ripple in power and current, leading to smoother operation and better power quality in the grid.
- Lower total harmonic distortion (THD): The comparison between PI and MFC controllers shows that the latter results in a much lower current THD, improving the quality of power injected into the grid.

In conclusion, the model-free control approach not only provides superior performance in terms of power regulation and efficiency but also addresses some of the limitations of PI controllers, such as increased power oscillations and higher THD. The results obtained from this chapter confirm that MFC is a more effective and robust control strategy for wind energy systems based on SynRG, making it a viable option for enhancing grid stability and maximizing the energy output of wind turbines.

CHAPTER 4: ENERGY OPTIMIZATION USING ADVANCED CONTROL OF SynRG-BASED WPS

Chapter 4: Energy optimization using advanced control techniques of SynRG-Based WPS

4.1 Introduction

This chapter introduces an innovative control approach that combines two distinct methods, building upon the strategie presented in the previous chapter, to create a more advanced and effective control technology. Our goal is to maintain the simplicity of the MFC approach while significantly enhancing performance. Specifically, we aim to minimize the ripples observed in the currents and the active and reactive powers injected into the grid, which are common issues in traditional control methods.

To achieve this, we propose a novel method that integrates two powerful techniques: the MFC and the Ant Colony Optimization (ACO) algorithm. This combination provides an effective solution for controlling and regulating both grid active and reactive powers within the system. The proposed strategy stands out from other approaches due to its fundamental principles, simplicity, ease of implementation, and long-term reliability.

The simulation results for the WPS controlled by the optimized MFC-ACO controller reveal several key advantages. The system demonstrates excellent robustness and exhibits a marked reduction in the oscillations of both currents and powers injected into the electrical grid. These improvements suggest that the new control strategy is not only more sustainable but also offers superior performance compared to conventional control methods, making it an ideal solution for modern wind power systems.

In summary, this chapter presents a cutting-edge control method that leverages the strengths of MFC and ACO algorithms to enhance the stability and efficiency of wind power systems, ensuring high-quality power generation with minimal fluctuations and improved grid integration.

4.2 Ant colony optimization (ACO)

4.2.1 Introduction to ACO

ACO is a bio-inspired computational algorithm based on the foraging behavior of ants. This technique excels at solving complex optimization problems and has found applications in diverse fields such as telecommunications, logistics, and energy systems. In the context of wind power systems, ACO can significantly enhance energy optimization by effectively managing control parameters to improve overall system performance [76].

4.2.2 Operating principle

The ACO technique mimics how ants search for food. Initially, ants move randomly within their environment, but upon discovering food, they return to their colony while leaving a pheromone trail [76]. Other ants may follow this trail, reinforcing the optimal route, particularly if it leads to food. Over time, frequently traveled paths accumulate stronger pheromone levels, while less frequented paths diminish, compelling all ants to adopt the shortest route. This process is visually represented in Figure 4.1.

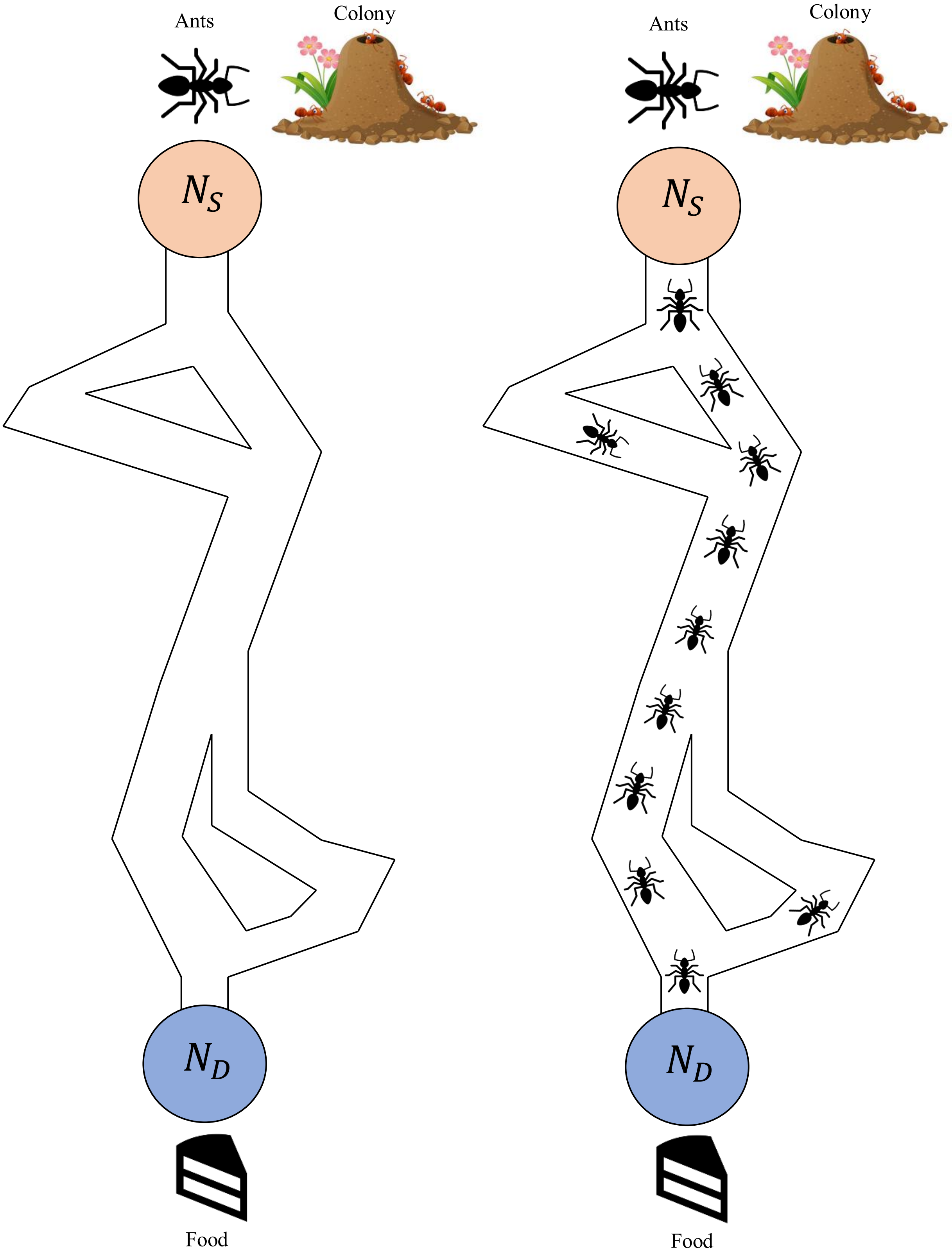

Figure 4.1 Experiment on ants selecting the shortest paths.

Each ant serves as an agent capable of generating solutions, with the decision-making process guided by two key factors:

Visibility factor ($\boldsymbol{\eta_{ij}}$): Also known as the "gluttonous force," this factor represents the attractiveness of a decision point, where iJ denotes the specific decision being evaluated.

Trace factor ($\boldsymbol{\tau_{ij}}$): This factor indicates the amount of pheromone on a given path. A higher value signifies greater historical appeal.

The probability of selecting a decision point ij is mathematically expressed as:

$$P_{ij}^{k}\begin{cases}\dfrac{(\tau_{ij}(t))^{a}(\eta_{ij}(t))^{b}}{\sum ieN_{i}((\tau_{ij}(t))^{a}(\eta_{ij}(t))^{b}} \\ 0\end{cases} \tag{4.1}$$

Where:

- $\tau_{ij}(t)$: The pheromone level on the path between nodes i and j at time t.
- $\eta_{ij}(t)$: The visibility value between nodes i and j, which varies based on problem-specific criteria.
- a: The relative importance of the pheromone trace in influencing decisions.
- b: The importance attributed to the visibility value.
- N_i: The set of nodes that have not yet been selected.

4.2.3 Application in wind power systems

In wind power systems, ACO plays a crucial role in optimizing several key areas, contributing to the overall efficiency and performance of the system:

- Power flow management: ACO can optimize the control parameters to manage both active and reactive power effectively. This ensures that the system operates at its highest efficiency, even under fluctuating wind conditions.
- Reduction of harmonic distortion: ACO also focuses on minimizing THD in the generated power. Lower THD levels translate to higher power quality, reducing electrical noise and improving the reliability and lifespan of the wind turbine components, such as generators and converters.
- Dynamic adjustment: One of the strengths of ACO is its ability to facilitate real-time adjustments. As wind speeds and other environmental factors change, ACO adapts system parameters dynamically, ensuring that the wind power system remains responsive and robust. This dynamic adaptability helps maintain a stable and efficient operation, even in varying conditions.

4.2.4 Advantages of ACO

The table 4.1 concisely presents the advantages of ACO in a clear and organized manner.

Table 4.1 Advantages of ACO

Advantages of ACO	Description

• Flexibility	• ACO adapts to various system configurations and operational conditions, making it a versatile optimization tool.
• Scalability	• The algorithm effectively scales with increasing complexity, enabling it to manage larger and more intricate wind power systems.
• Simplicity of Implementation	• ACO algorithms are relatively straightforward to implement and can be easily integrated with existing control strategies, enhancing their applicability and ease of use.

4.3 Integrating MFC with ACO

4.3.1 PID controller tuning using ACO

Several researchers have explored the optimization of PID controllers through the use of ACO algorithms, employing various approaches to enhance the efficiency of ACO [77-80]. For instance, in [81] utilized ACO to adjust the parameters of a PID controller for a second-order process, evaluating different cost functions. Their results demonstrated a significant improvement compared to traditional tuning methods.

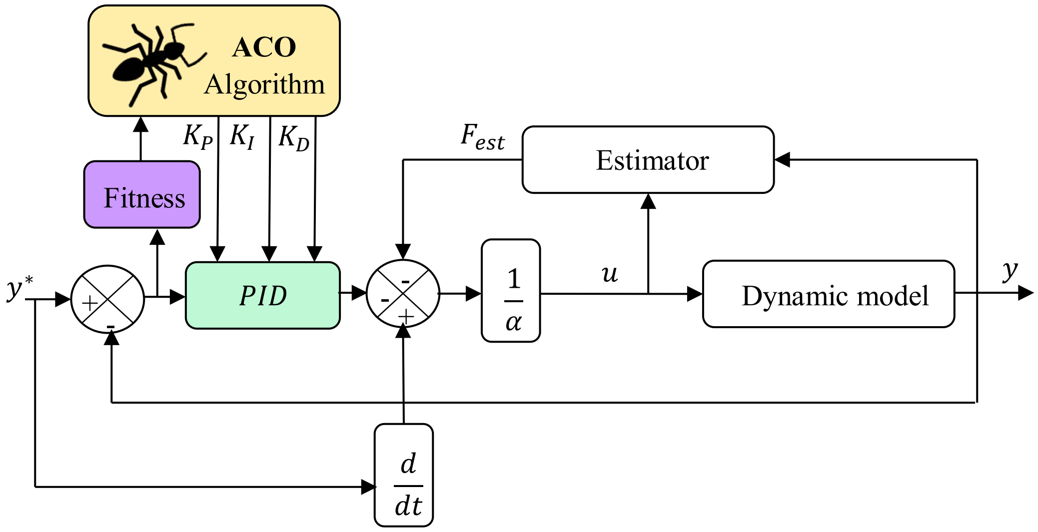

Figure 4.2 ACO-based MFC controller optimization structure.

Figure 4.2 illustrates the ACO-based MFC controller optimization structure. The PID controller design problem, when approached using the ACO algorithm, can be viewed as a network problem (as depicted in Figure 4.3). In this model, three vectors are used to represent the parameter values (K_P, K_I, K_D). These vectors can be likened to roads connecting nests, with each ant required to travel through three nests, selecting the path between the start and end nodes. The goal of ACO is to find the optimal path with the lowest cost function (as shown in Equation 4.7).

Ants deposit pheromones at the beginning of each path, and these pheromones are subsequently updated according to the reinforcement rule. Each ant updates the pheromone trail after completing a tour, following local pheromone update rules, as shown in the following equation:

$$\tau_{ij}(k) = \tau(k-1)_{ij} + \frac{0.01\theta}{A} \tag{4.2}$$

Where:

$\tau_{ij}(k)$: is the pheromone value between nests i and j at iteration k.

θ: is the pheromone updating coefficient.

A: is the cost function for the ant's tour.

For the global pheromone update, paths in the best and worst tours of the ant colony are updated using the following rules:

For the best tour:

$$\tau_{ij}^{best}(k) = \tau_{ij}^{best}(k) + \frac{\theta}{A_{best}} \tag{4.3}$$

For the worst tour:

$$\tau_{ij}^{worst}(k) = \tau_{ij}^{worst}(k) + \frac{0.3\theta}{A_{worst}} \tag{4.4}$$

Here, τ^{best} and τ^{worst} represent the pheromone levels on the paths taken by the ants in the best and worst tours, with cost values A_{best} and A_{worst}, respectively. The pheromones on the paths of the best tours are significantly increased, while those of the worst tours are decreased.

Afterward, pheromone evaporation occurs according to the following equation, allowing the ACO algorithm to forget old paths and direct its search towards new possibilities, preventing it from getting stuck in local optima:

$$\tau_{ij}(k) = \lambda\tau_{ij}(k) + (\tau_{ij}^{best} + \tau_{ij}^{worst}) \tag{4.5}$$

Where $\boldsymbol{\lambda}$ is the evaporation constant [81]. This strategy ensures the algorithm can explore new solutions without being trapped in local minima.

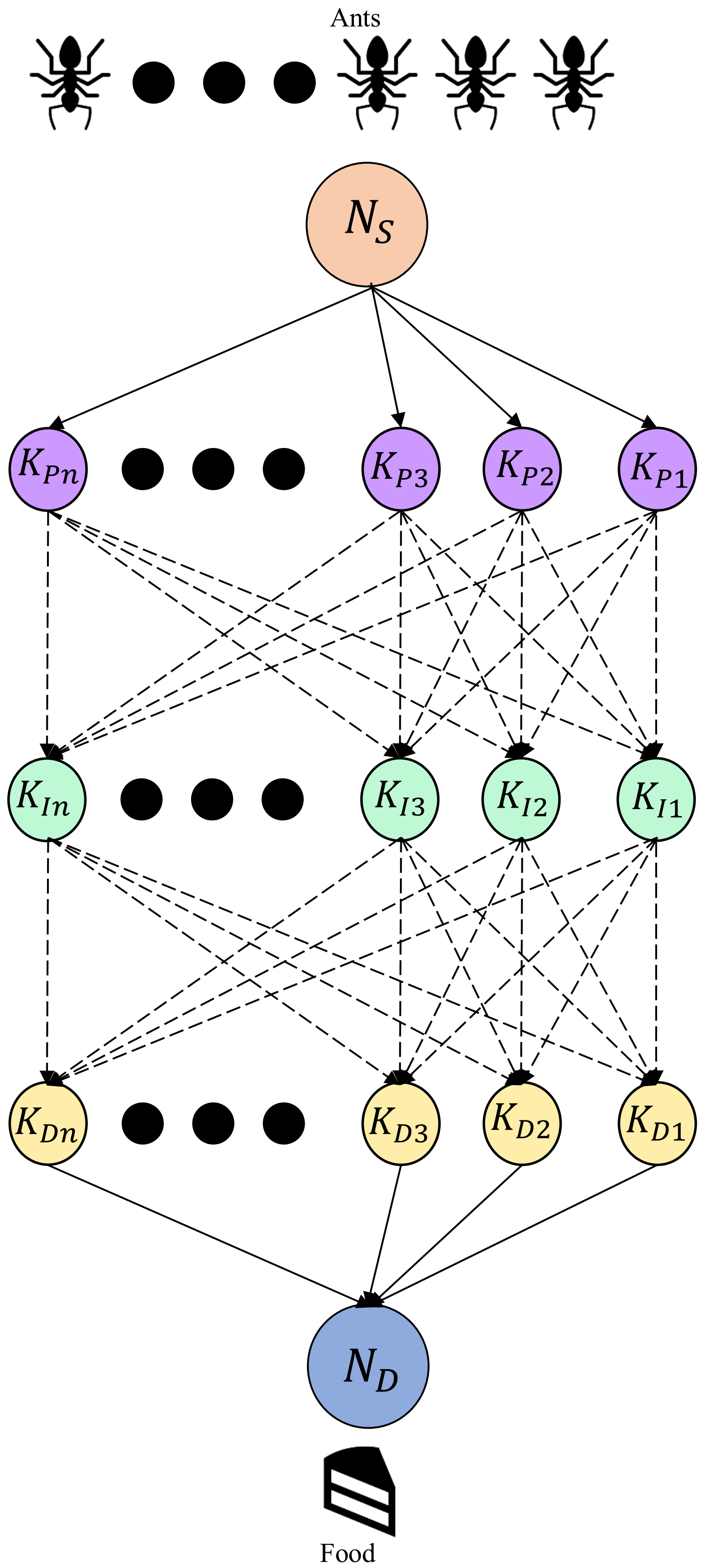

Figure 4.3 Graphical illustration of the ACO-based PID tuning process

4.3.2 Fitness evaluation

A crucial step in the ACO process is the selection of cost functions that determine the fitness or suitability of each node. Various research papers, such as in [82,83], utilize performance indices as cost functions. In [83], the authors compare three performance indices—Integral Time Absolute Error (ITAE), Integral Absolute Error (IAE), and Integral Square Error (ISE)—both separately and in combination.

Among these, ISE has proven to be particularly effective in improving system performance. For this reason, a weighted combination of these indices is adopted in this work to enhance the performance of the ACO and improve the overall system efficiency.
The performance indices are defined as follows [84]:

$$ISE = \int_0^t e(t)^2 dt \tag{4.6}$$

Here, the PID controller is designed to minimize the error signal $e(t)$, thereby reducing the values of these performance indices. The minimization of these indices ensures the formation of optimal nodes within the ACO algorithm. The suitability of each node, or its fitness, is expressed by:

$$Fitness\ Value = \frac{1}{ISE} \tag{4.7}$$

This fitness value plays a key role in guiding the ACO algorithm towards better solutions.

4.3.3 Parameters of ACO

The process of PID optimization using the ACO algorithm involves several crucial steps, as outlined in the algorithm flowchart (Figure 4.4). In this approach, PID controller parameters are represented by 500 nodes, where each node signifies a potential solution for the values of K_P, K_I, and K_D. The more nodes used, the more accurate the optimization process, as more trails are updated.

Through extensive experimentation, optimal ACO parameters were determined: $\theta = 0.04$ and $\lambda = 0.92$. Selecting appropriate ACO parameters is vital for achieving convergence to optimal values in reduced time.

The following parameters of the ACO algorithm must be initialized to large values to increase the probability of finding the best PID values:

- $Var_{Pmax} = 2500,\ Var_{Imax} = 500,\ Var_{Dmax} = 10$
- $Var_{Pmin} = -2500,\ Var_{Imin} = -500,\ Var_{Dmin} = -10$
- $n_{iter} = 50$

Initially, large parameter ranges allow the system to explore a wide range of potential solutions. After convergence, these parameters are reduced to values closer to the optimal gains found, which shortens the iteration count and execution time. A detailed list of ACO parameters can be found in Table 4.1.

```
Algorithm: Ant Colony Optimization for PID Tuning
Begin
  Initialize algorithm parameters:
    • Initialize variables such as $n_{iter}$, $\alpha$, $\beta$, $n_{ant}$, $n_{parameters}$, $LB$, $UB$ and $n_{node}$.
    • Create a pheromone matrix and use a uniform distribution to generate random potential
      solutions for $K_P$, $K_I$, and $K_D$.
  Run simulation:
    • Calculate the fitness based on weighted cost functions.
  Node selection:
    • Select the next node based on probability using Equation (4.1).
  Display optimal parameters:
    • Output the optimum values of $K_P$, $K_I$, and $K_D$.
  Pheromone evaporation:
    • Reinforce the best path and allow for the evaporation of bad choices using Equations (4.3)
      and (4.4).
  Global pheromone update:
    • Update the pheromone levels globally according to the optimal solutions calculated in Step
      5, using Equation (4.5).
  Select the best path:
    • Repeat steps 2 to 6 until the maximum number of iterations is reached. Select the path with
      the highest pheromone concentration.
End
```

Table 4.2 ACO parameters

Symbol	Value
n_{iter}	50
n_{ant}	20
α	0.6
β	0.2
$n_{parameters}$	3
n_{node}	500

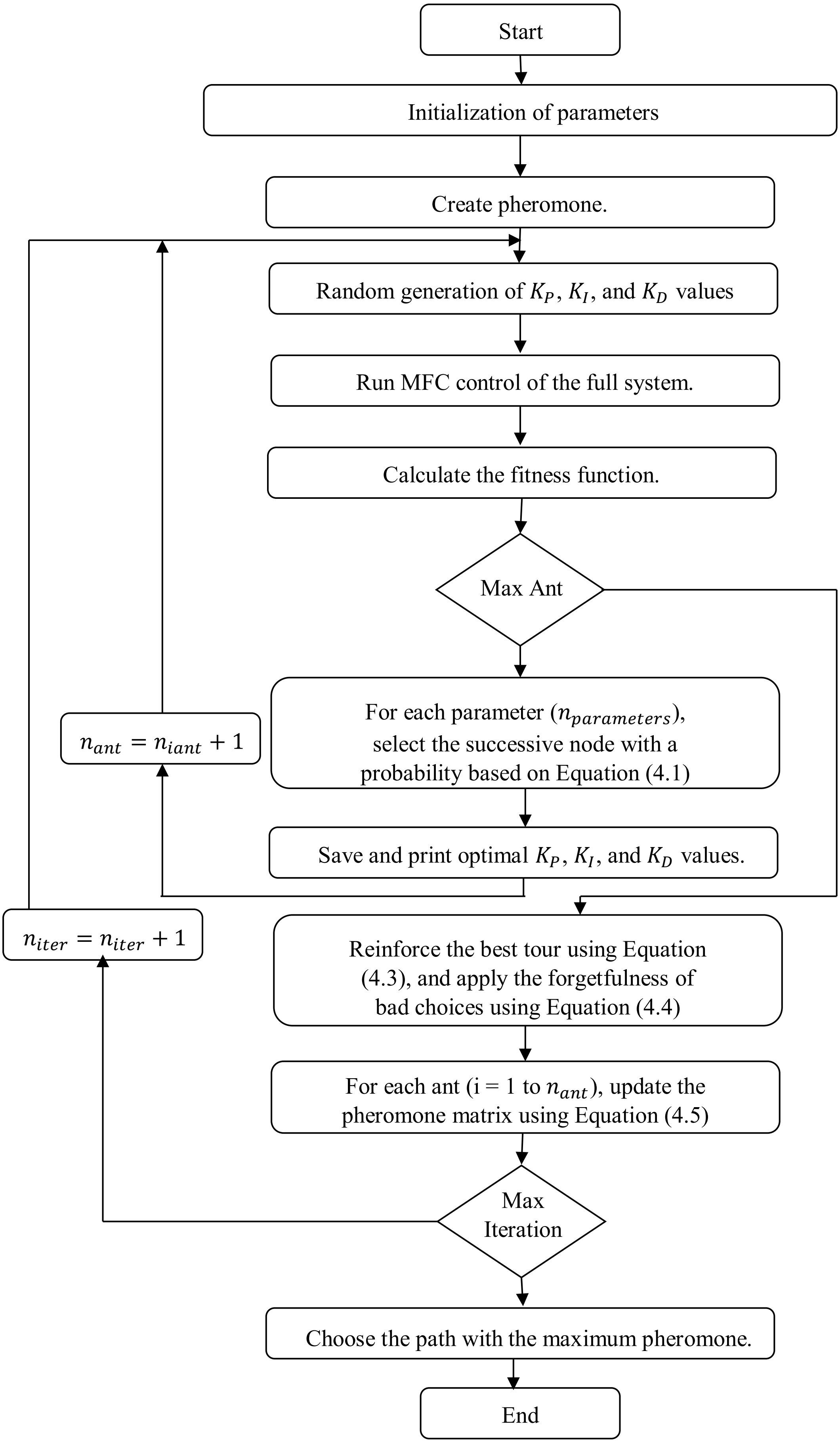

Figure 4.4 The flowchart of the ACO algorithm.

4.4 Implementing MFC-ACO for GSC

In this chapter, the MFC combined with ACO approach, referred to as MFC-ACO, will be applied to the GSC. The overall control structure is depicted in Figure 4.5.

On the machine side, three MFC controllers will be utilized to regulate the direct and quadrature components of the stator current (i_{sd} and i_{sq}), as well as the mechanical speed (Ω_m), as shown in Figure 4.5. These controllers are crucial for ensuring precise control of both the electrical and mechanical performance of the machine, as demonstrated by the results discussed in the previous chapter.

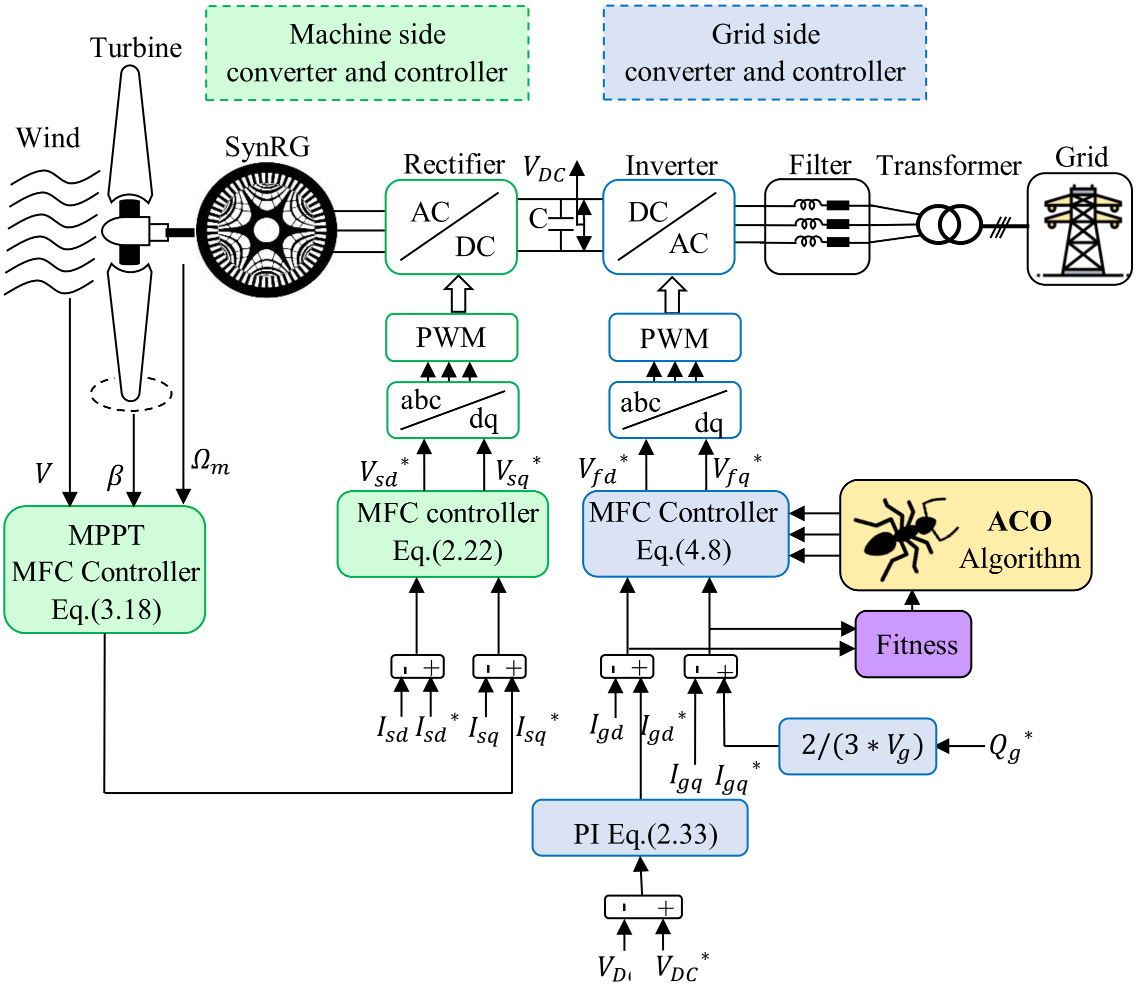

Figure 4.5 System control configuration using MFC-ACO controller.

To stabilize the DC link voltage, a PI controller is used to ensure that the measured voltage V_{DC} follows its reference value V^*_{DC}. In addition, two MFC-ACO controllers have been designed to regulate the direct and quadrature current components (i_{gq}, i_{gq}) of the GSC, as shown in Figure 4.5. These controllers are essential for maintaining grid current control and achieving a unit power factor and minimize power fluctuations.

Using the equations from (3.27), the loop is closed by using a PID controller. The control law for the MFC-ACO controller, derived from the highly localized model, is formulated as follows:

$$\begin{cases} u_{i_{gd}} = -\dfrac{F_{i_{gd}\,est} - \dot{y}^*_{i_{gd}} + K_{P\,i_{gd}} e(i_{gd}) + K_{I\,i_{gd}} \int e(i_{gd}) + K_{D\,i_{gd}} \dot{e}(i_{gd})}{\alpha_{i_{sd}}} \\ u_{i_{gq}} = -\dfrac{F_{i_{gq}\,est} - \dot{y}^*_{i_{gq}} + K_{P\,i_{gq}} e(i_{gq}) + K_{I\,i_{qd}} \int e(i_{qd}) + K_{D\,i_{qd}} \dot{e}(i_{qd})}{\alpha_{i_{gq}}} \end{cases} \tag{4.8}$$

4.5 Results and simulation

In this section, we present the results of controlling the WPS based on the SynRG. The entire wind system has been simulated and controlled using MATLAB/SIMULINK. The aim is to analyze the performance of the MFC-ACO controllers implemented in the GSC for current control loops. Additionally, we will compare the performance of the proposed controller with that of a conventional PI controller and an MFC, focusing on improvements in power quality and robustness.

Remark 4.1: The results for the MSC remain consistent with those presented in the previous chapter. This is because we retained the existing MFC configuration, which had already demonstrated strong performance. Consequently, there have been no changes in the outcomes when integrating the MFC-ACO control strategy.

4.5.1 Tracking test

The initial test assesses the tracking performance of the MFC-ACO strategy under varying wind speeds, applied in discrete steps. The wind speed profile utilized during the control process is depicted in Figure 4.6.

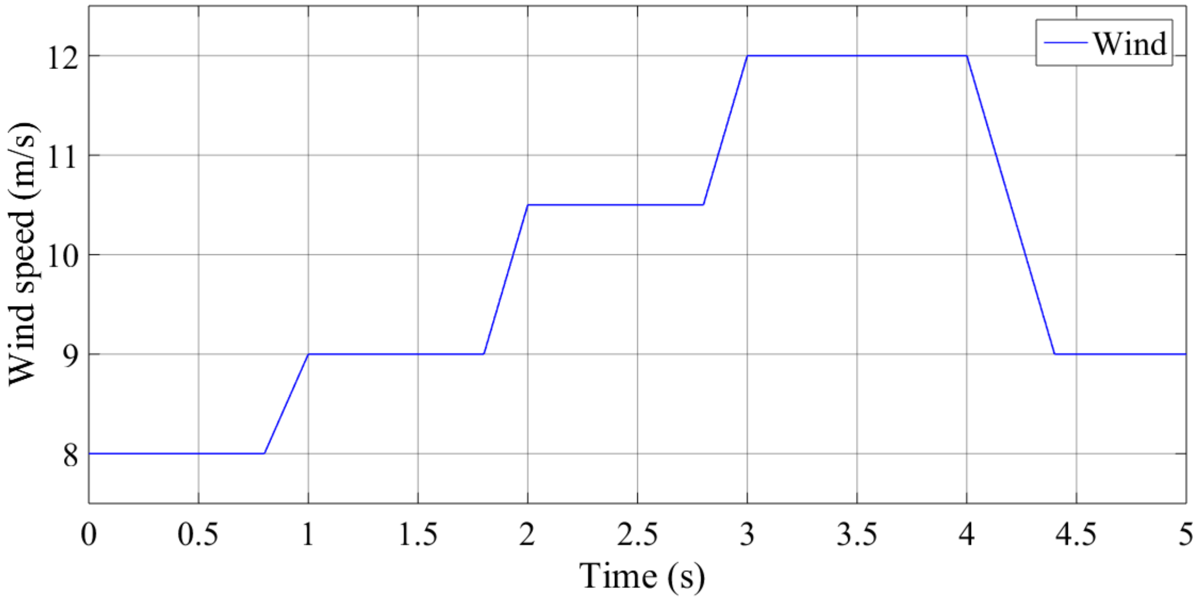

Figure 4.6 Wind speed profile.

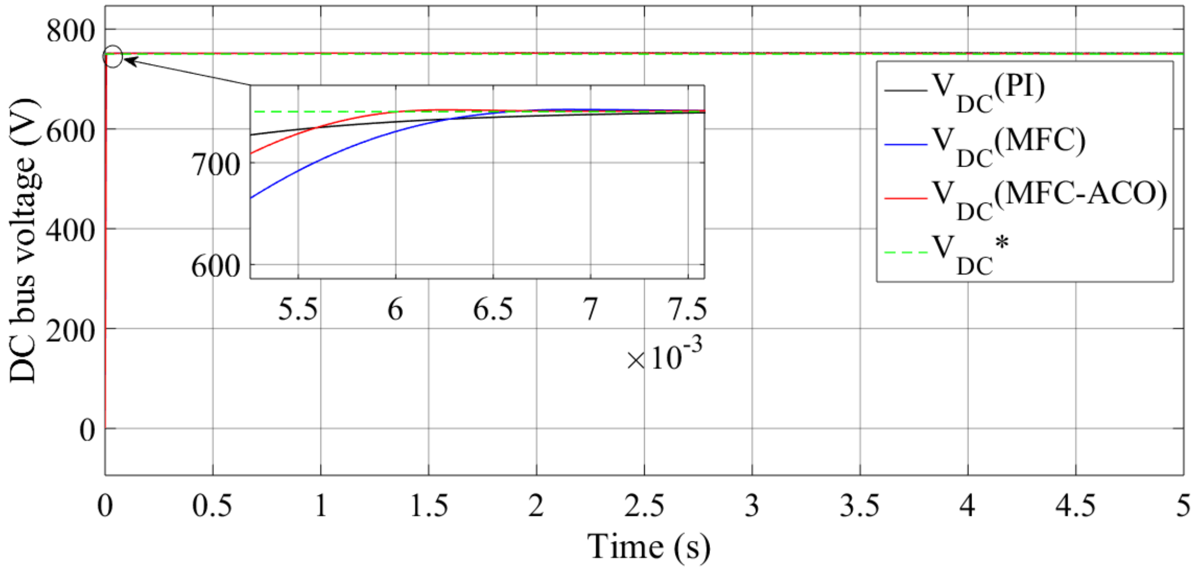

Figure 4.7 DC bus voltage

The tracking performance of the PI, MFC, and MFC-ACO controllers for DC bus voltage demonstrates high precision, as illustrated in Figure 3.7. All three controllers maintain stable DC bus voltage, even under fluctuating wind conditions. This stability is essential for ensuring the reliable and continuous operation of the wind turbine system, as variations in the DC bus voltage could disrupt energy conversion efficiency. The ability of the controllers, especially MFC-ACO, to stabilize the voltage despite environmental changes highlights their effectiveness in maintaining system robustness and operational consistency.

The power outputs closely follow the reference values, though slight ripples are observed in Figures 4.8(a,b) and 4.9(a,b). In Figure 4.8(b), Q_g remains constant, as it is unaffected by changes in wind speed, unlike P_g, which is highly dependent on wind speed. As shown in Figure 4.6, the active power increases with rising wind speed, and conversely, decreases when the wind speed drops. Notably, the conventional control schemes—PI and MFC—exhibit more significant ripples compared to the MFC-ACO approach, which shows reduced ripple levels. These differences in ripple magnitude are summarized in Table 4.2.

Figure 4.8(c) illustrates the grid current, displaying a sinusoidal waveform that aligns with variations in $\boldsymbol{P_g}$. Notably, the PI controller exhibits significant fluctuations in the current, whereas the MFC controller shows improvements, with MFC-ACO performing even better. The MFC-ACO controller's ability to produce a much smoother grid current is particularly evident, contributing to enhanced grid stability and improved power quality. This improvement is clearly depicted in Figures 4.9(a), 4.9(b), and 4.9(c), and validated by the data in Table 4.2. The proposed MFC-ACO approach effectively reduces ripples in both current and power, as demonstrated by the substantial reduction ratios outlined in Table 4.2. This highlights the controller's significant role in minimizing disturbances and optimizing system performance.

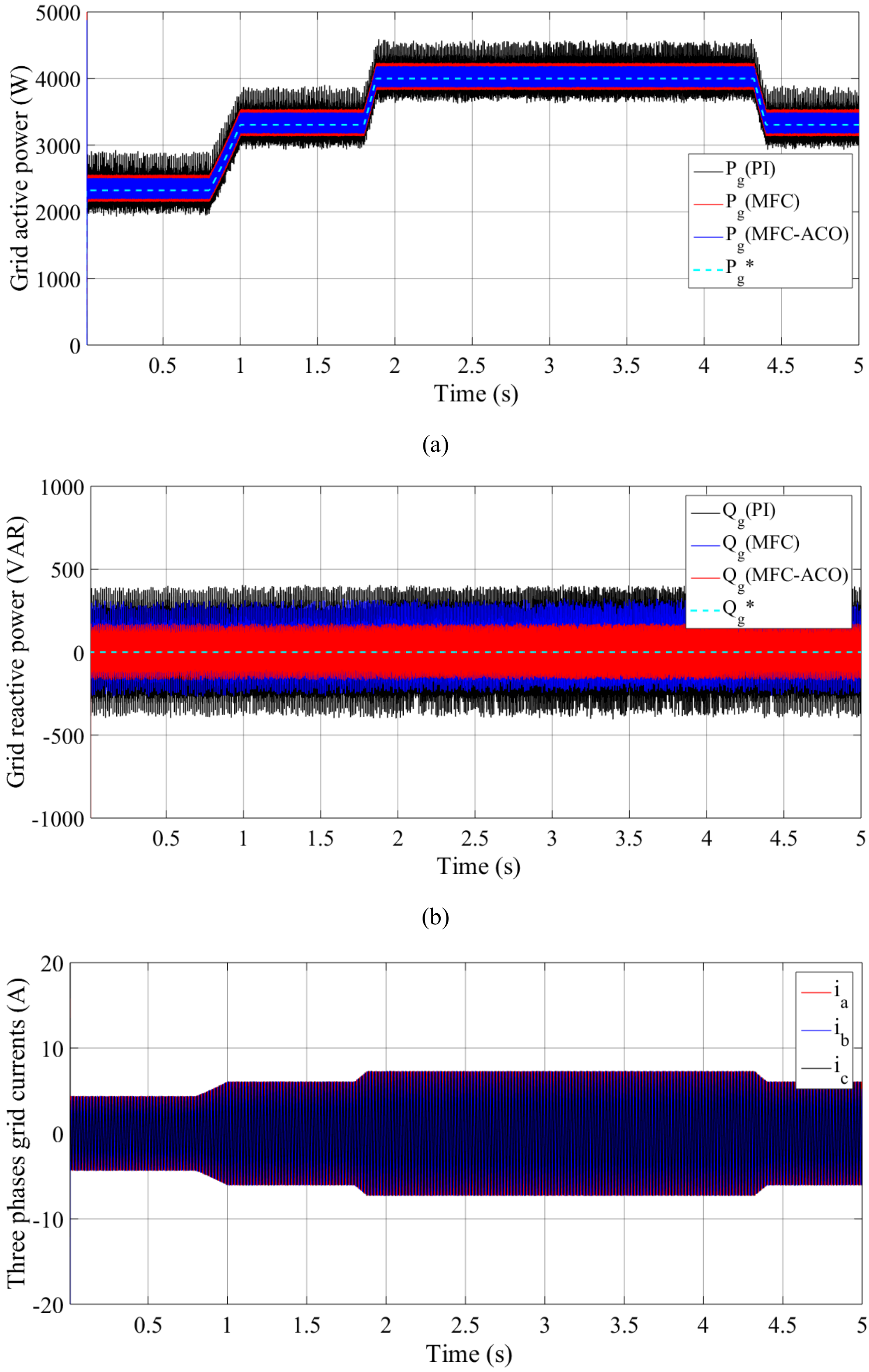

(a)

(b)

(c)

Figure 4.8 MFC-ACO performance: Active power (a), Reactive power (b), Grid currents using (c) (First test).

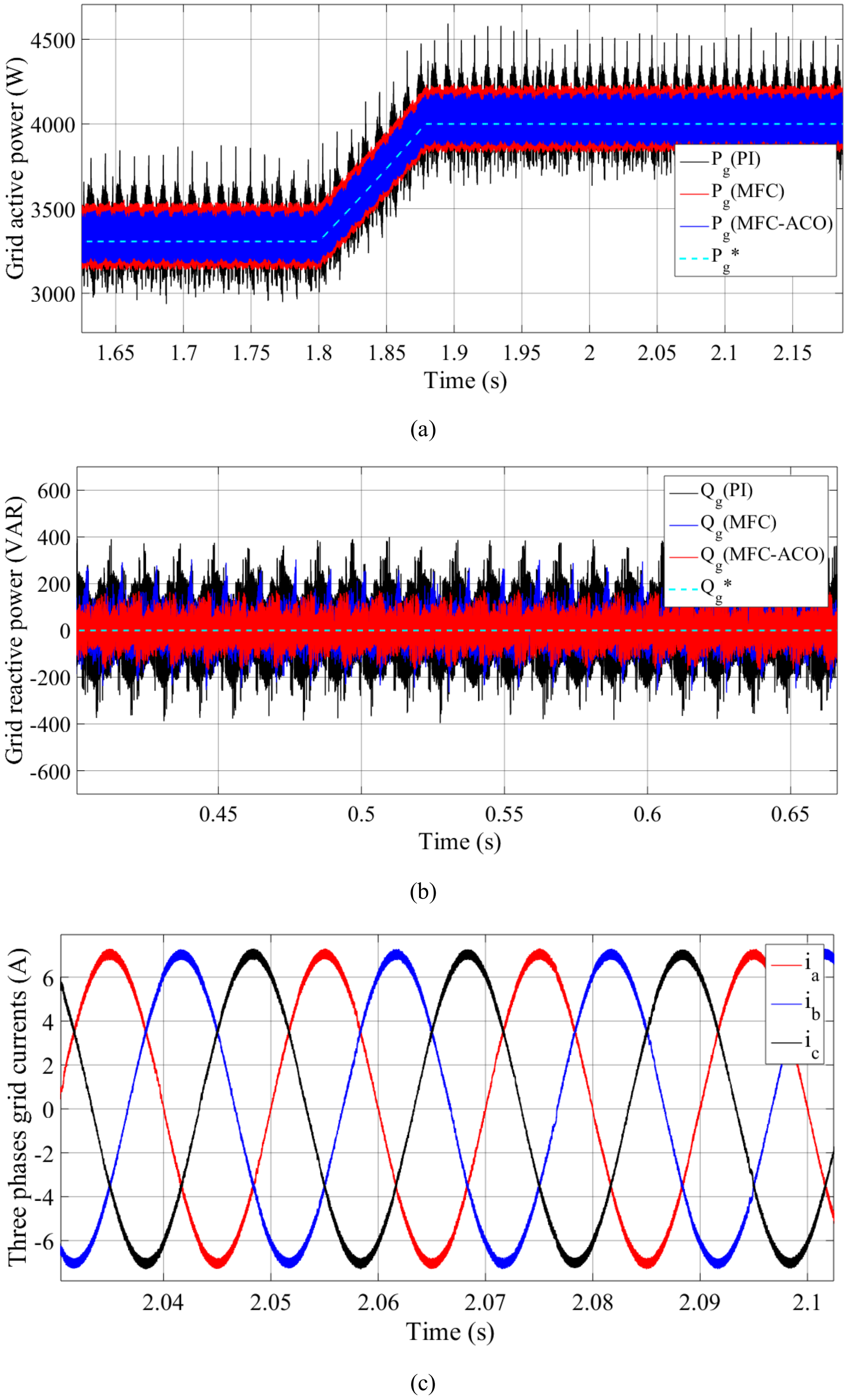

(a)

(b)

(c)

Figure 4.9 Zoom on: Active power (a), Reactive power (b), Grid currents (c) (First test).

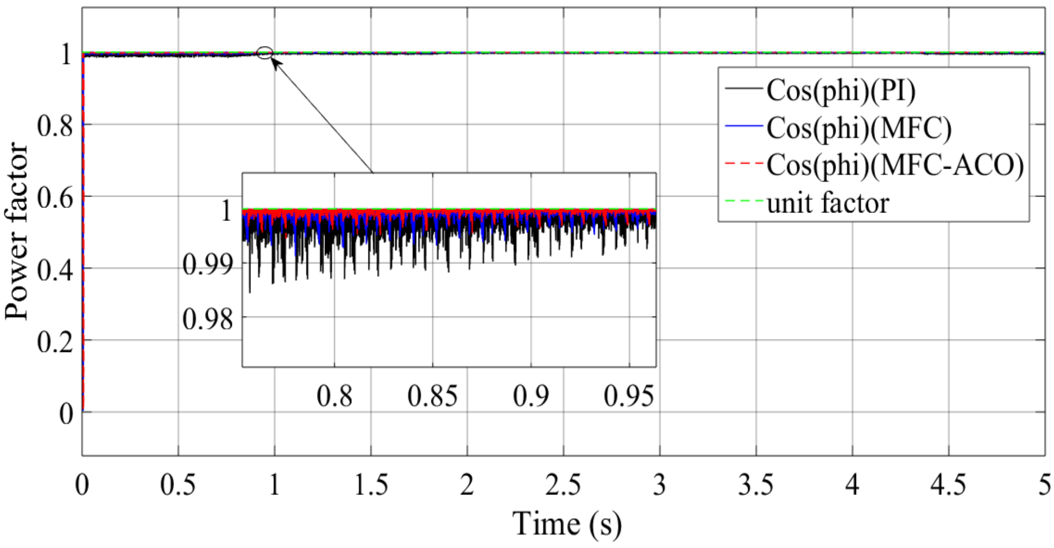

(a)

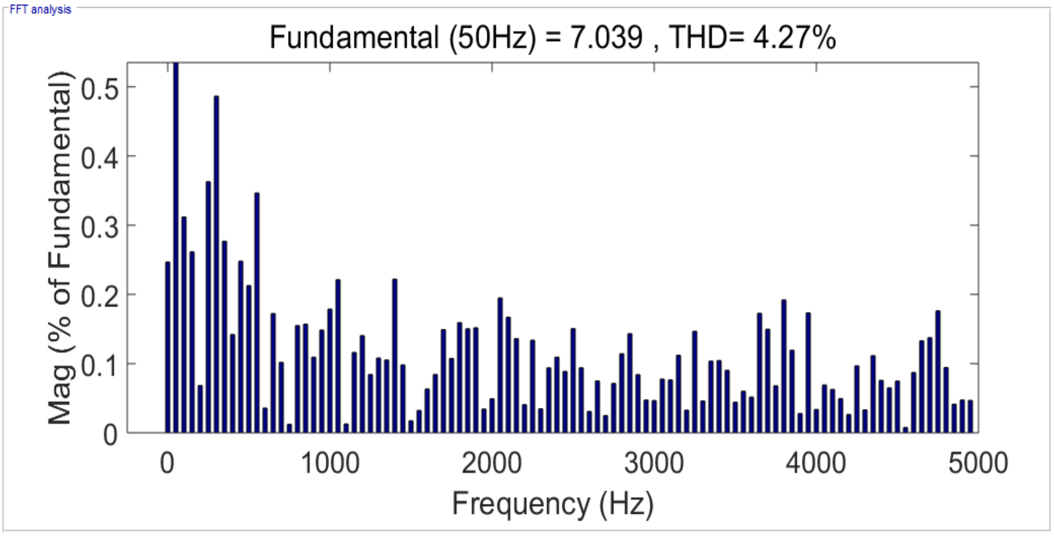

(b)

Figure 4.10 Power factor (a), MFC-ACO grid current THD (b) (First test).

Additionally, Figure 4.10(a) demonstrates how the MFC-ACO strategy effectively maintains a unity power factor ($\cos(phi)$) by keeping Q_g consistently near zero. This is crucial as it indicates efficient energy production with minimal losses, thereby enhancing the overall quality of the electrical energy generated. Maintaining a unity power factor not only improves system efficiency but also ensures that the wind power system operates harmoniously with the grid, reducing reactive power compensation requirements and further optimizing energy delivery.

In Figure 4.10(b), the THD of the grid current is illustrated for the MFC-ACO controller, which achieved a low THD of 4.27%. In comparison, the PI controller and the MFC controller resulted in higher THD values, with 10.51% and 4.82% respectively. This reduction in THD demonstrates the superior performance of the MFC-ACO approach in minimizing harmonic distortion, contributing to improved power quality and greater system efficiency.

4.5.2 Conclusion for the first test

The MFC-ACO strategy effectively maintains stable DC bus voltage and reduces ripple levels under varying wind speeds, outperforming the PI and MFC controllers. It achieves a unity power factor and a low THD of 4.27%, indicating efficient energy production and minimal losses. Overall, MFC-ACO enhances the stability and performance of wind power systems in variable conditions.

4.5.3 Wind speed variation test

In this test, a new wind speed pattern was applied, differing from the one used in the initial evaluation. This variation was introduced to assess the effectiveness and adaptability of the proposed control method under changing conditions. The wind speed profile utilized for this test is depicted in Figure 3.11.

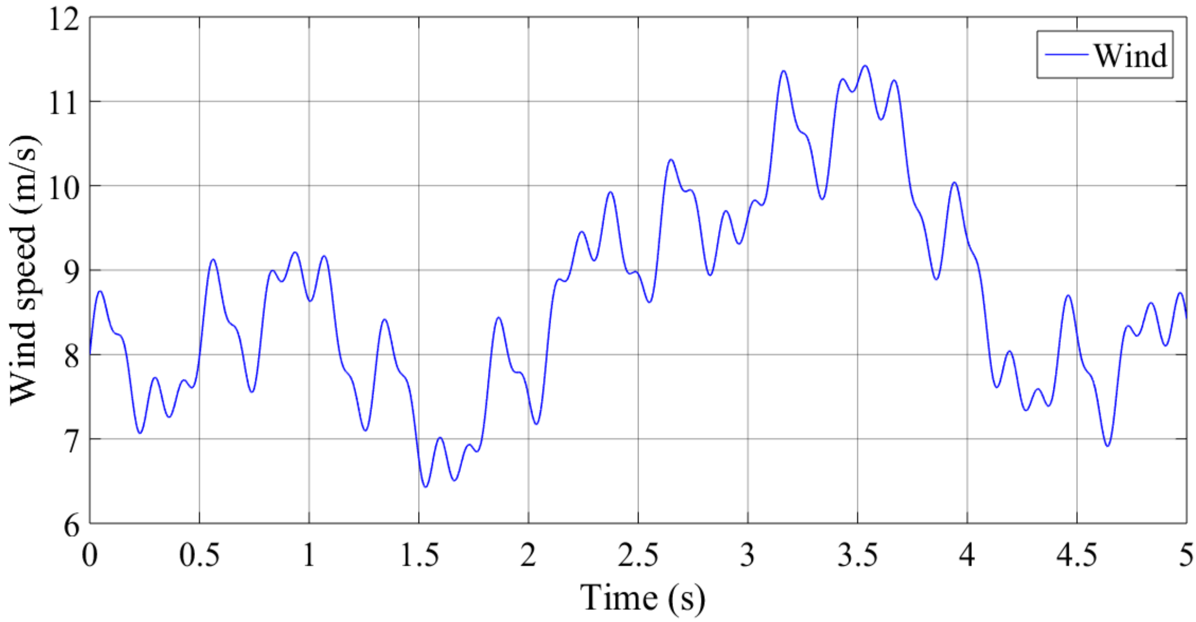

Figure 4.11 Wind speed profile (Second test).

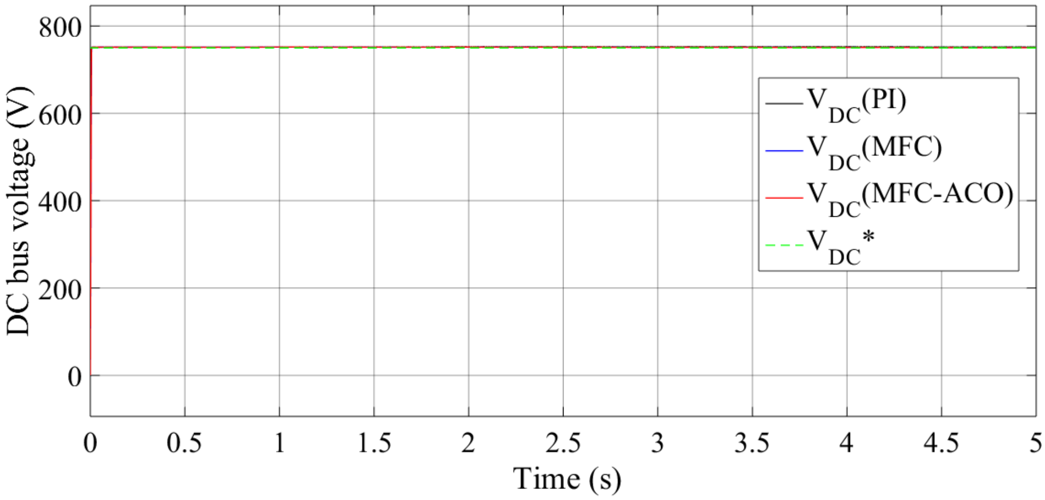

Figure 4.12 DC bus voltage

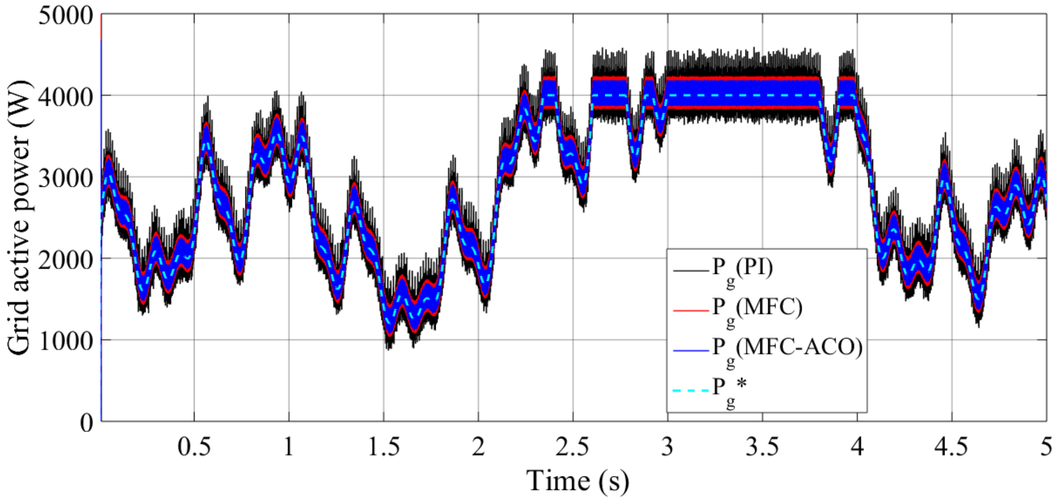

(a)

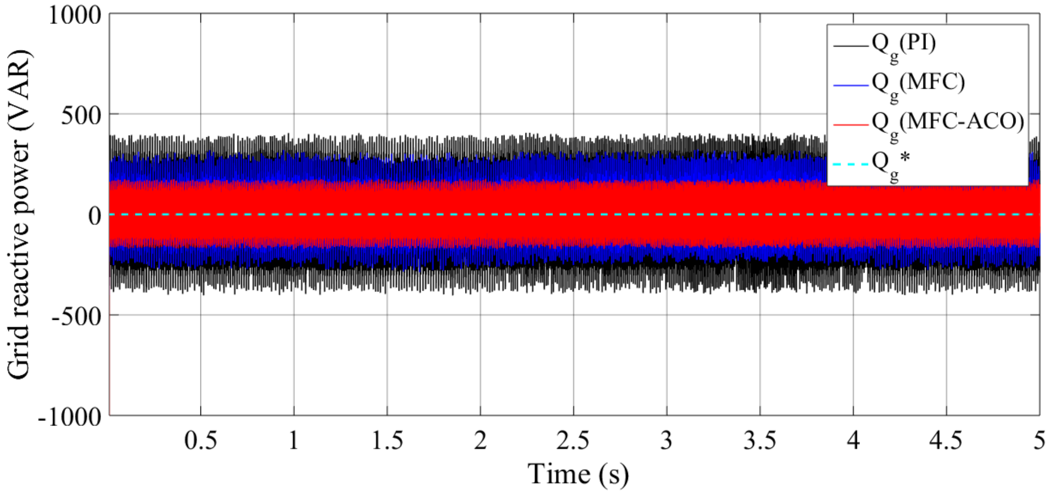

(b)

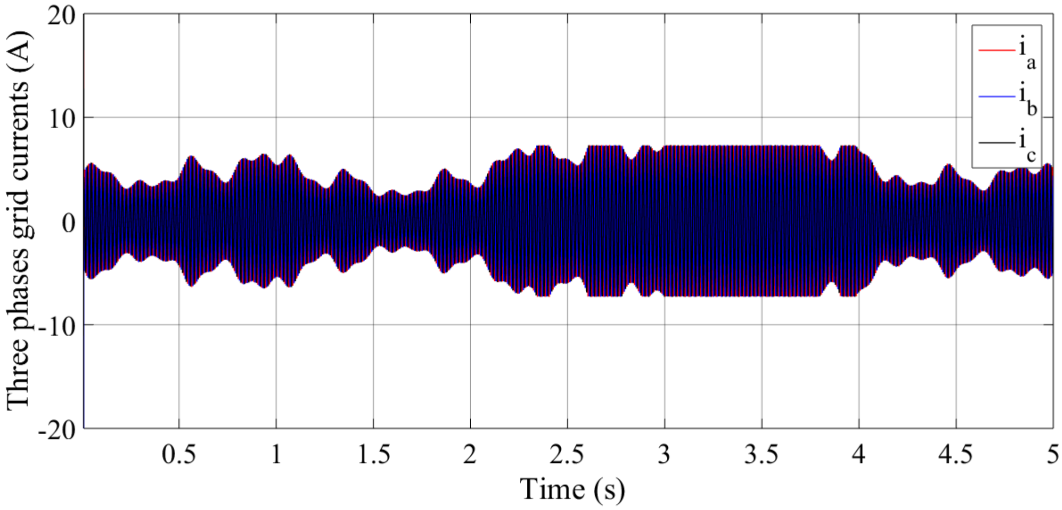

(c)

Figure 4.13 MFC-ACO performance: Active power (a), Reactive power (b), Grid currents using (c) (Second test).

The PI, MFC, and MFC-ACO controllers demonstrate precise tracking of the DC bus voltage, as illustrated in Figure 4.12. Even with fluctuations in wind conditions, the DC bus voltage remains stable.

Figures 4.13(a) and 4.13(b) illustrate P_g and Q_g behavior, respectively. Notably, Q_g remains constant at 0 VAR, unaffected by time or variations in wind speed for both controllers, maintaining perfect alignment with the reference value. However, ripples in the power output are observed, particularly in the PI and MFC controllers, as highlighted in Figures 4.14(a, b) and Table 4.3.

The active power P_g, shown in both Figures 4.13(a) and 4.14(a), displays fewer ripples when using the proposed control strategy (MFC-ACO), indicating smoother power delivery. P_g consistently tracks the reference values, reflecting a highly accurate performance. Moreover, the shape of P_g aligns closely with the wind speed profile, increasing or decreasing in sync with speed variations. As the wind speed decreases, P_g proportionally decreases, confirming the direct relationship between wind speed and active power output. This demonstrates the effectiveness of the MFC-ACO approach in dynamically responding to changing wind conditions while minimizing power fluctuations.

Figures 4.13(c) and 4.14(c) illustrate the grid currents, which follows a clear sinusoidal pattern that synchronizes with the variations in wind speed. The grid current exhibits fewer ripples when using the MFC-ACO controller, indicating smoother and more stable performance compared to other control methods. As P_g increases or decreases, the grid current proportionally adjusts in magnitude, reflecting the close relationship between power output and current flow. This behavior is a strong indicator of improved power quality and enhanced stability in grid integration, emphasizing the effectiveness of the MFC-ACO control strategy.

Figure 4.15(a) shows that the MFC-ACO strategy maintains a unity power factor ($\cos(phi)$) by keeping Q_g near zero, indicating efficient energy production with minimal losses. This unity power factor enhances overall energy quality and allows the wind power system to operate smoothly with the grid, reducing the need for reactive power compensation.

Figure 4.15(b) illustrates the THD of the grid current, with the MFC-ACO controller achieving a low THD of 1.91%. In contrast, the PI and MFC controllers produced higher THD values of 6.20% and 2.16%, respectively. This reduction in THD highlights the MFC-ACO approach's effectiveness in minimizing harmonic distortion, thereby improving power quality and system efficiency.

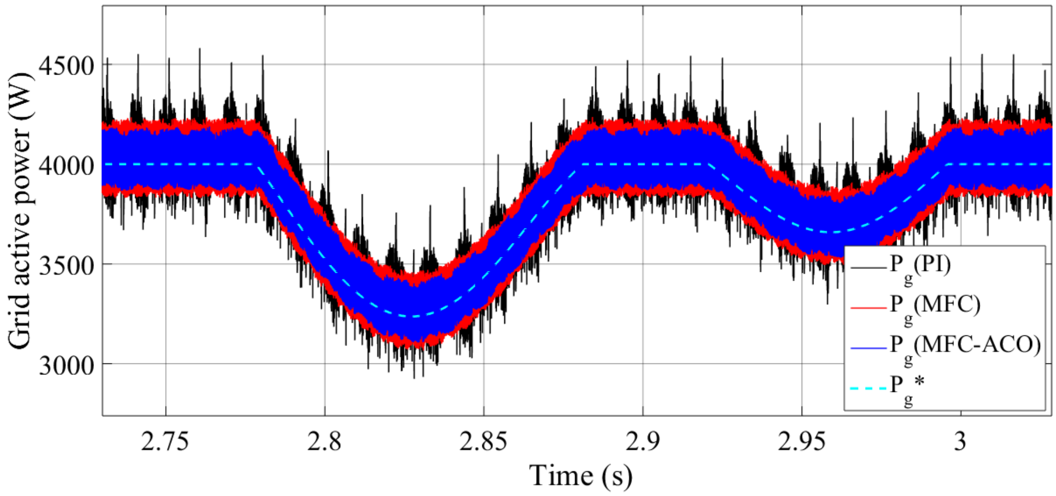

(a)

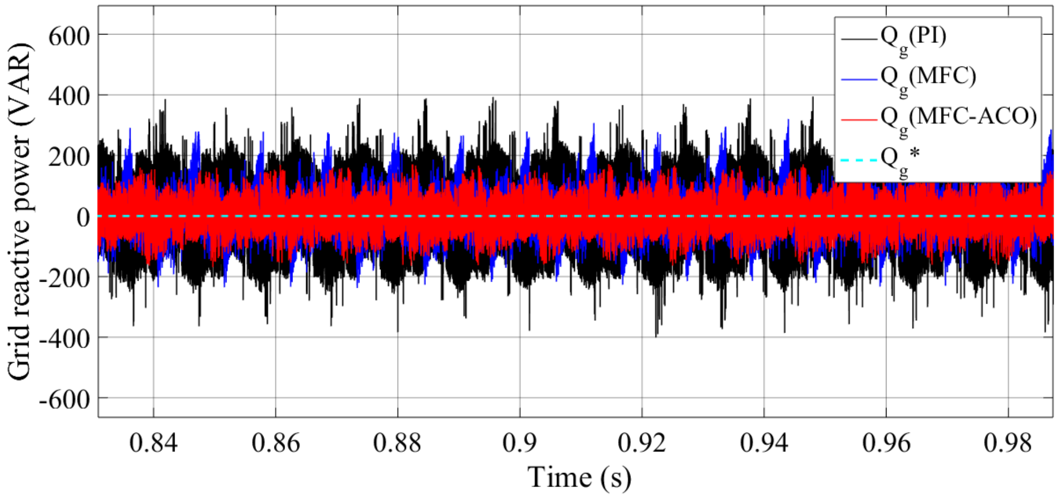

(b)

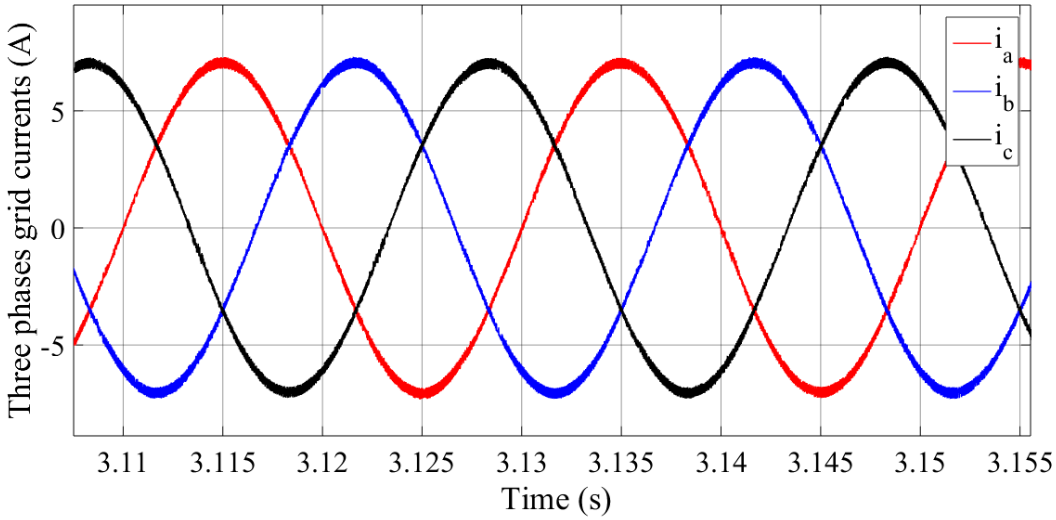

(c)

Figure 4.14 Zoom on: Active power (a), Reactive power (b), Grid currents (c) (Second test).

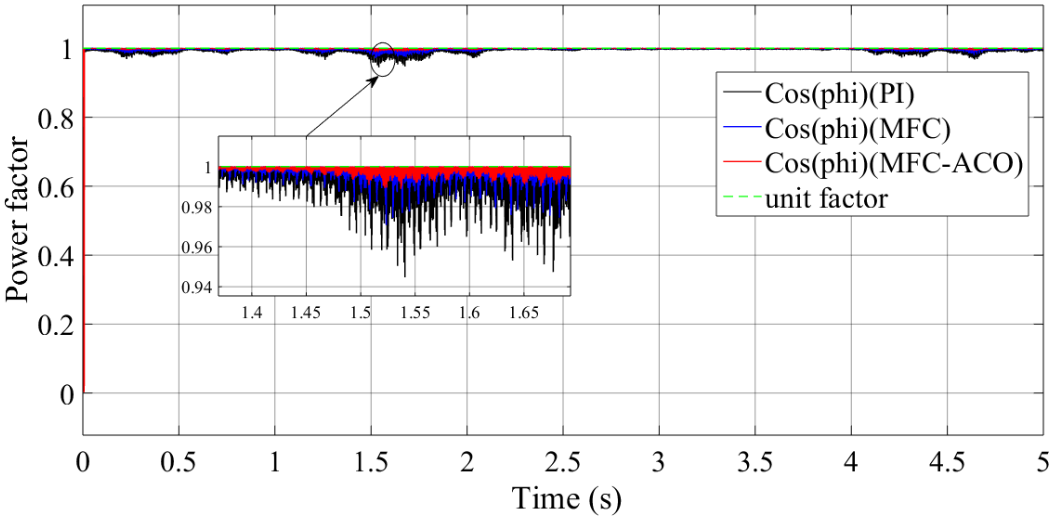

(a)

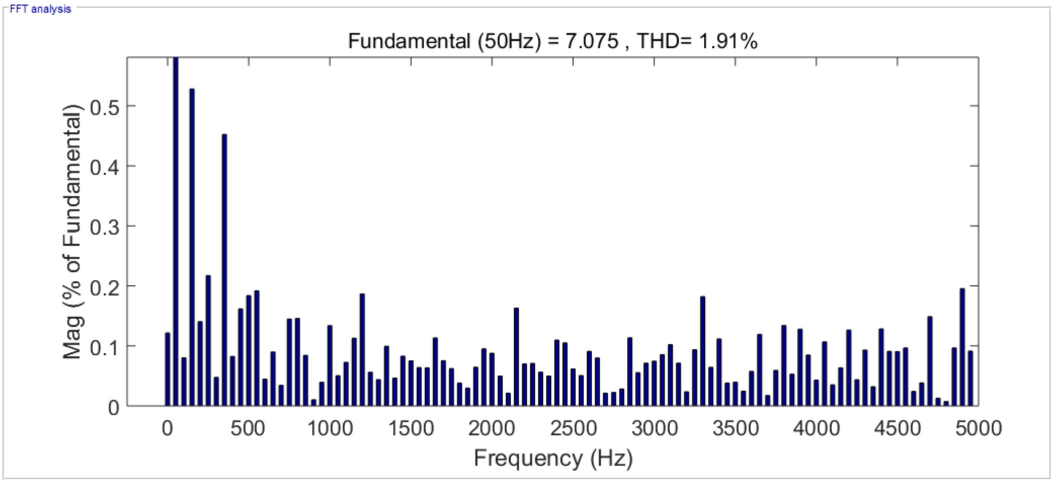

(b)

Figure 4.15 Power factor (a), MFC-ACO grid current THD (b) (Second test).

4.5.4 Conclusion for the second test

The wind speed variation test demonstrates that the MFC-ACO controller effectively maintains stable DC bus voltage and minimizes power ripples under a new wind speed pattern. It achieves a constant Q_g of 0 VAR and tracks P_g closely to reference values, showcasing its adaptability to changing conditions. The grid current exhibits fewer ripples, indicating improved power quality and stability in integration. Additionally, the MFC-ACO strategy achieves a low THD of 1.91%, outperforming PI and MFC controllers, thus highlighting its superior performance in enhancing system efficiency and reducing harmonic distortion.

Table 4.3 MFC-ACO performance comparison (peak to peak).

Performance Comparison	P_g (W)	Q_g (VAR)	i_{ga}	THD (%)
First Test				
PI	971	812	0.71	10.51
MFC	416	586	0.47	4.82
MFC-ACO	323	354	0.40	4.27
Ratios (%)	66.73	56.40	43.66	59.37
Second Test				
PI	970	807	0.67	6.20
MFC	422	599	0.44	2.16
MFC-ACO	324	352	0.34	1.91
Ratios (%)	66.59	56.38	49.25	69.19

4.6 Conclusion

In this chapter, we presented a novel control strategy that integrates MFC with the ACO algorithm to address the challenges of WPS using SynRG. This approach was designed to improve stability, efficiency, and robustness while overcoming the limitations of traditional PI controllers, which often struggle with the nonlinear and dynamic nature of wind energy systems.

The combination of MFC and ACO eliminates the need for precise mathematical modeling and adapts effectively to fluctuating wind conditions. This adaptability is essential for optimizing performance under varying wind speeds. The simulation results confirmed that the MFC-ACO strategy significantly reduces current and power oscillations, improving grid stability and ensuring more reliable energy output.

A key advantage of this method is its simplicity and ease of implementation, making it a practical choice for real-world applications where minimizing complexity and cost is critical. The ACO algorithm enhances the system’s ability to find optimal solutions in real time, further improving control precision.

In conclusion, the MFC-ACO control strategy represents a significant advancement in wind energy systems. It provides precise power control, reduces fluctuations, and enhances robustness, offering a powerful solution for the next generation of wind power technologies. The results suggest great potential for future research and widespread adoption, contributing to more efficient and sustainable renewable energy generation.

GENERAL CONCLUSION

General conclusion

This thesis presents significant advancements in the modeling and control of wind power systems (WPS) using synchronous reluctance generators (SynRG). The primary objective was to develop a robust control strategy that enhances system stability, efficiency, and reliability while effectively addressing the challenges posed by the nonlinear and dynamic nature of wind energy systems.

In our exploration, we first established the critical role of maximum power point tracking (MPPT) in optimizing energy extraction from varying wind conditions. By focusing on precise regulation of the turbine's rotational speed, we laid a solid foundation for efficient energy generation. The introduction of vector control methods, specifically using proportional-integral (PI) controllers, demonstrated acceptable management of speed and active/reactive power. However, while traditional control strategies showed acceptable performance under predictable conditions, they revealed limitations, particularly in their responsiveness to fluctuating wind patterns and their tendency to generate power oscillations and higher total harmonic distortion (THD). These challenges underscored the necessity for more advanced control approaches.

To this end, we developed the model-free control (MFC) strategy, which successfully mitigated the drawbacks of PI controllers. By eliminating the need for precise mathematical modeling, MFC allowed for greater adaptability to changing wind conditions, leading to enhanced power regulation and improved MPPT. Simulation results clearly indicated that MFC significantly reduced current and power oscillations, thereby optimizing system performance and contributing to improved power quality in the grid.

The culmination of our research introduced a novel integration of MFC with the ant colony optimization (ACO) algorithm, creating a hybrid control strategy that further enhanced the adaptability and efficiency of WPS. This MFC-ACO approach not only simplified implementation but also demonstrated superior performance in real-time optimization of control parameters. The results illustrated that this strategy effectively reduces fluctuations and improves the robustness of energy output, making it a compelling solution for the next generation of wind power technologies.

In summary, this thesis provides a comprehensive framework for understanding and improving the performance of wind energy systems based on SynRG. The findings highlight the viability of advanced control strategies in overcoming the limitations of traditional methods, paving the way for more efficient and reliable renewable energy generation. Future research avenues, including the exploration of alternative control techniques and the application of these strategies to different types of wind power systems, promise to further enhance the sustainability and efficiency of wind energy technologies.

Ultimately, the insights gained from this work contribute not only to the field of renewable energy but also to the broader goal of transitioning towards a more sustainable energy landscape. By advancing the operational capabilities of wind energy systems, we take important steps toward addressing global energy demands and fostering a cleaner, more sustainable future.

The results obtained and the noted observations open interesting and useful research perspectives that could contribute to a better utilization of wind turbines and SynRG:

- Explore alternative control techniques, such as high-order sliding mode control.
- Implement control methods to enhance SynRG performance under fault conditions.
- Utilize multi-objective optimization techniques to optimize multiple parameters. simultaneously, facilitating the identification of various optimal solutions tailored to specific requirements.
- Apply the proposed controller to other WPS based on PMSG and DFIG

Bibliographic References

[1] Aubrée, R. (2014). Stratégies de commande sans capteur et de gestion de l'énergie pour les aérogénérateurs de petite puissance (Doctoral dissertation, Nantes).

[2] Poitiers, F. (2003). Etude et commande de génératrices asynchrones pour l'utilisation de l'énergie éolienne-machine asynchrone a cage autonome-machine asynchrone a double alimentation reliée au réseau (Doctoral dissertation, Université de Nantes).

[3] Camblong, H. (2003). Minimisation de l'impact des perturbations d'origine éolienne dans la génération d'électricité par des aérogénérateurs à vitesse variable (Doctoral dissertation, Paris, ENSAM).

[4] Liserre, M., Cardenas, R., Molinas, M., & Rodriguez, J. (2011). Overview of multi-MW wind turbines and wind parks. IEEE Transactions on Industrial electronics, 58(4), 1081-1095.

[5] Chen, Z., Guerrero, J. M., & Blaabjerg, F. (2009). A review of the state of the art of power electronics for wind turbines. IEEE Transactions on power electronics, 24(8), 1859-1875.

[6] Blaabjerg, F., Chen, Z., & Kjaer, S. B. (2004). Power electronics as efficient interface in dispersed power generation systems. IEEE transactions on power electronics, 19(5), 1184-1194.

[7] Cherfia, N., & Kerdoun, D. (2018). Etude d'une chaine de conversion de l'energie Eolienne (Doctoral dissertation, Université Frères Mentouri-Constantine 1).

[8] Barazarte, R. Y., Gonzalez, G., & Hall, E. (2011). Comparison of electrical generators used for wind power generation. IEEE Latin America Transactions, 9(7), 1040-1044.

[9] Pena, R., Cárdenas, R., Proboste, J., Clare, J., & Asher, G. (2008). Wind–diesel generation using doubly fed induction machines. IEEE Transactions on Energy Conversion, 23(1), 202-214.

[10] Zhao, Y., Wei, C., Zhang, Z., & Qiao, W. (2013). A review on position/speed sensorless control for permanent-magnet synchronous machine-based wind energy conversion systems. IEEE journal of emerging and selected topics in power electronics, 1(4), 203-216.

[11] Moncada, R. H., Tapia, J. A., & Jahns, T. M. (2009). Analysis of negative-saliency permanent-magnet machines. IEEE transactions on industrial electronics, 57(1), 122-127.

[12] Eriksson, S., & Bernhoff, H. (2012, September). Rotor design for PM generators reflecting the unstable neodymium price. In 2012 XXth International Conference on Electrical Machines (pp. 1419-1423). IEEE.

[13] Lendenmann, H., Moghaddam, R. R., Tammi, A., & Thand, L. E. (2011). Motoring Ahead. ABB Rev Corp Tech J., vol. 1, pp. 56-61.

[14] Alnasir, Z., & Kazerani, M. (2013). An analytical literature review of stand-alone wind energy conversion systems from generator viewpoint. Renewable and Sustainable Energy Reviews, 28, 597-615.

[15] Moncada, R. H., Pavez, B. J., Tapia, J. A., & Pyrhönen, J. (2014, September). Operation analysis of synchronous reluctance machine in electric power generation. In 2014 International Conference on Electrical Machines (ICEM) (pp. 2734-2739). IEEE.

[16] Roshanfekr, P., Lundmark, S., Thiringer, T., & Alatalo, M. (2014, April). A synchronous reluctance generator for a wind application-compared with an interior mounted permanent magnet synchronous

generator. In 7th IET International Conference on Power Electronics, Machines and Drives (PEMD 2014) (pp. 1-5). IET.

[17] Wang, Y., Li, H., Liu, R., Yang, L., & Wang, X. (2020). Modulated model-free predictive control with minimum switching losses for PMSM drive system. IEEE Access, 8, 20942-20953.

[18] Lyu, Z., Wu, X., Gao, J., & Tan, G. (2021). An improved finite-control-set model predictive current control for IPMSM under model parameter mismatches. Energies, 14(19), 6342.

[19] Lin, C. K., Agustin, C. A., Yu, J. T., Cheng, Y. S., Chen, F. M., & Lai, Y. S. (2021). A modulated model-free predictive current control for four-switch three-phase inverter-fed SynRM drive systems. Ieee Access, 9, 162984-162995.

[20] Fliess, M. (2009). Model-free control and intelligent PID controllers: towards a possible trivialization of nonlinear control?. IFAC Proceedings Volumes, 42(10), 1531-1550.

[21] Fliess, M., & Join, C. (2013). Model-free control. International journal of control, 86(12), 2228-2252.

[22] Omar, M., Soliman, M., Ghany, A. A., & Bendary, F. (2013). Optimal tuning of PID controllers for hydrothermal load frequency control using ant colony optimization. International journal on electrical engineering and informatics, 5(3), 348-360.

[23] Philippe, R. (2008). L’énergie du Vent : Les éoliennes au service des hommes et de leur planète. Philippe Rocher.

[24] Serrar, A., & Bouhnik, A. A. Optimisation d'énergie d’un système éolien avec stockage (Doctoral dissertation, UNIVERSITY OF KASDI MERBAH OUARGLA).

[25] Medjber, A., Moualdia, A., Mellit, A., & Guessoum, M. A. (2012). Commande Vectorielle Indirecte d‛‛ un Générateur Asynchrone Double Alimenté Appliqué dans un Système de Conversion Eolien. Manuscript received August, 18.

[26] Mohamed, M. (2020). Commande d’une génératrice synchrone à aimants permanents dédiée à la conversion de l’énergie éolienne (Doctoral dissertation, Université Ibn Khaldoun-Tiaret).

[27] Dlimi, F., Djelaili, Z., & Harrouz, A. (2020). Etude et contrôle d'une turbine éolienne a axe verticale couple a un générateur éolien (Doctoral dissertation, universite Ahmed Draia-ADRAR).

[28] Bounadja, E. (2017). Commande d’une machine asynchrone à double alimentation en régime sature (Doctoral dissertation, Ecole Nationale Polytechnique, Algeria).

[29] Mourad, L. (2016). Synthèse de lois de commande non-linéaires pour le contrôle d’une machine asynchrone à double alimentation dédiée à un système aérogénérateur (Doctoral dissertation, Ph. D. thesis, Université Aboubakr Belkaid–Tlemcen–Faculté de Technologie).

[30] Ennis, B. L., & Bacelli, G. (2018). Floating Offshore Vertical-Axis Wind Turbine System Design Studies and Opportunities (No. SAND2018-8138C). Sandia National Lab.(SNL-NM), Albuquerque, NM (United States).

[31] Adeyeye, K. A., Ijumba, N., & Colton, J. (2021, June). The effect of the number of blades on the efficiency of a wind turbine. In IOP Conference Series: Earth and Environmental Science (Vol. 801, No. 1, p. 012020). IOP Publishing.

[32] Tekobon, J. (2016). Système multi physique de simulation pour l'étude de la production de l'énergie basée sur le couplage éolien offshore-hydrolien (Doctoral dissertation, Université du Havre).

[33] Bensalah, A., Barakat, G., & Amara, Y. (2022). Electrical generators for large wind turbine: Trends and challenges. Energies, 15(18), 6700.

[34] Chemidi, A. (2015). Analyse, modélisation et commande avancée d'une éolienne utilisée dans une ferme (Doctoral dissertation).

[35] Hau, E., & von Renouard, H. (2006). Wind Turbine Installation and Operation. Wind Turbines: Fundamentals, Technologies, Application, Economics, 653-701.

[36] Camblong, H. (2003). Minimisation de l'impact des perturbations d'origine éolienne dans la génération d'électricité par des aérogénérateurs à vitesse variable (Doctoral dissertation, Paris, ENSAM).

[37] Hannan, M. A., Al-Shetwi, A. Q., Mollik, M. S., Ker, P. J., Mannan, M., Mansor, M., ... & Mahlia, T. I. (2023). Wind energy conversions, controls, and applications: a review for sustainable technologies and directions. Sustainability, 15(5), 3986.

[38] Belharazem, W. T., & BENDEDDOUCHE, I. (2023). Etude, Modélisation et commande robuste d'une éolienne (Doctoral dissertation).

[39] Heng, T. Y., Ding, T. J., Chang, C. C. W., Ping, T. J., Yian, H. C., & Dahari, M. (2022). Permanent Magnet Synchronous Generator design optimization for wind energy conversion system: A review. Energy Reports, 8, 277-282.

[40] Mahmoud, M. M., Khalid Ratib, M., Aly, M. M., & Abdel-Rahim, A. M. M. (2022). Wind-driven permanent magnet synchronous generators connected to a power grid: Existing perspective and future aspects. Wind Engineering, 46(1), 189-199.

[41] Nasiri, M., Mobayen, S., & Arzani, A. (2021). PID-type terminal sliding mode control for permanent magnet synchronous generator-based enhanced wind energy conversion systems. CSEE Journal of Power and Energy Systems, 8(4), 993-1003.

[42] Bouderbala, M., Bossoufi, B., Lagrioui, A., Taoussi, M., Aroussi, H. A., & Ihedrane, Y. (2019). Direct and indirect vector control of a doubly fed induction generator based in a wind energy conversion system. International Journal of Electrical and Computer Engineering, 9(3), 1531.

[43] Mazouz, F., Belkacem, S., Colak, I., Drid, S., & Harbouche, Y. (2020). Adaptive direct power control for double fed induction generator used in wind turbine. International Journal of Electrical Power & Energy Systems, 114, 105395.

[44] Moncada, R. H., Young, H. A., Pavez-Lazo, B. J., & Tapia, J. A. (2015, May). A commercial-off-the-shelf synchronous reluctance motor as a generator for wind power applications. In 2015 IEEE International Electric Machines & Drives Conference (IEMDC) (pp. 6-12). IEEE.

[45] Hassanain, N. E. A., Abbas, A. Y., & Hussien, A. S. G. (2015). Performance Analysis of Isolated Self-Excited Reluctance Generators Connected to Diode Bridge Rectifier.

[46] Basak, R., & Bhuvaneswari, G. (2018, March). Low voltage ride-through of a synchronous reluctance generator based variable speed wind energy conversion system. In 2018 IEEMA Engineer Infinite Conference (eTechNxT) (pp. 1-6). IEEE.

[47] Alnajjar, M., & Gerling, D. (2016, September). Synchronous reluctance generator with FPGA control of three-level neutral-point-clamped converter for wind power application. In 2016 IEEE International Power Electronics and Motion Control Conference (PEMC) (pp. 498-504). IEEE.

[48] Selma, B., Bounadja, E., Belmadani, B., & Selma, B. (2024). Improving dynamic response and stability of three-phase synchronous reluctance machines with a novel higher-order field-oriented sliding mode control. International Journal of Dynamics and Control, 1-10.

[49] Selma, B., Bounadja, E., Belmadani, B., Selma, B., & Abouaïssa, H. (2023). Model-free control-based vector control of synchronous reluctance motor. International Journal of Dynamics and Control, 11(6), 3062-3073.

[50] Selma, B., Bounadja, E., Belmadani, B., & Selma, B. (2024). Improved performance and robustness of synchronous reluctance machine control using an advanced sliding mode and direct vector control. Advanced Control for Applications: Engineering and Industrial Systems, 6(1), e178.

[51] Kumar, G. V., Chuang, C. H., Lu, M. Z., & Liaw, C. M. (2020). Development of an electric vehicle synchronous reluctance motor drive. IEEE Transactions on Vehicular Technology, 69(5), 5012-5024.

[52] Selma, B., Bounadja, E., Belmadani, B., & Selma, B. (2023, November). Exploring the Potential of Synchronous Reluctance Generator in Grid-Connected Wind Energy Conversion Systems: A Comprehensive Feasibility Study and Control Analysis. In 2023 2nd International Conference on Electronics, Energy and Measurement (IC2EM) (Vol. 1, pp. 1-6). IEEE.

[53] Selma, B., Bounadja, E., & Belmadani, B. (2023, May). MATLAB/Simulink Modeling and Control of Two Synchronous Reluctance Generators for a Grid Connected Wind Farm. In 2023 1st International Conference on Renewable Solutions for Ecosystems: Towards a Sustainable Energy Transition (ICRSEtoSET) (pp. 1-5). IEEE.

[54] Lubin, T. (2003). Modélisation et commande de la machine synchrone à réluctance variable: prise en compte de la saturation magnétique (Doctoral dissertation, Université Henri Poincaré; Nancy I).

[55] Moghaddam, R. R. (2007). Synchronous reluctance machine (SynRM) design. KTH Electrical Engineering.

[56] Mariani, G. B. (2016). Machine synchrone à réluctance: modèles équivalents à réseau de réluctances pour la simulation et l'optimisation (Doctoral dissertation, Université Grenoble Alpes).

[57] Hamza, B., Mokhtar, L., & Djamel, M. Nouveau paradigme de la transitioN énergétique à l'ère du développement durable: cas de l'algérie.

[58] Ministry of Energy and Mines, https://www.energy.gov.dz

[59] Renewable Energy and Energy Efficiency Program, Ministry of Energy and Mines, Design and Implementation by SATINFO, a Subsidiary of Sonelgaz Group, 2011.

[60] Naima, B. B. (2017). Potentiel et développement des énergies renouvelables en Algérie. Communication Science & technology, 19, 120-132.

[61] Hamiti, D. (2022). État des lieux des énergies renouvelables et de la stratégie d'efficacité énergétique en Algérie. Revue d'études juridiques et économiques, 5(2), 1397-1423.

[62] Regional Impact of Renewable Energies on the Labor Market in Algeria, Case Studies of ADRAR and ILIZI, GWS Research Report, Study commissioned by the Ministry of Energy Transition and Renewable Energies, 2021.

[63] LOUKRIZ, A. (2022). Contribution au développement de Techniques de Recherche de la Topologie Optimale d'un Générateur Photovoltaïque (Doctoral dissertation, Faculté des Sciences et de la technologie).

[64] Lafont, F., Balmat, J. F., Pessel, N., & Fliess, M. (2015). A model-free control strategy for an experimental greenhouse with an application to fault accommodation. Computers and Electronics in Agriculture, 110, 139-149.

[65] Abouaïssa, H., Fliess, M., & Join, C. (2017). On ramp metering: Towards a better understanding of ALINEA via model-free control. International Journal of Control, 90(5), 1018-1026.

[66] Selma, B., Bounadja, E., Belmadani, B., Selma, B., & Fliess, M. (2024). A novel intelligent control approach for wind energy conversion systems with synchronous reluctance generators. International Journal of Circuit Theory and Applications, 52(8), 3967-3987.

[67] Pande, J., Nasikkar, P., Kotecha, K., & Varadarajan, V. (2021). A review of maximum power point tracking algorithms for wind energy conversion systems. Journal of Marine Science and Engineering, 9(11), 1187.

[68] Dahbi, A., Nait-Said, N., & Nait-Said, M. S. (2016). A novel combined MPPT-pitch angle control for wide range variable speed wind turbine based on neural network. International journal of hydrogen energy, 41(22), 9427-9442.

[69] Majout, B., El Alami, H., Salime, H., Zine Laabidine, N., El Mourabit, Y., Motahhir, S., ... & Bossoufi, B. (2022). A review on popular control applications in wind energy conversion system based on permanent magnet generator PMSG. Energies, 15(17), 6238.

[70] Bossoufi, B., Karim, M., Lagrioui, A., Taoussi, M., & Derouich, A. (2015). Observer backstepping control of DFIG-Generators for wind turbines variable-speed: FPGA-based implementation. Renewable Energy, 81, 903-917.

[71] Majout, B., Bossoufi, B., Bouderbala, M., Masud, M., Al-Amri, J. F., Taoussi, M., ... & Karim, M. (2022). Improvement of PMSG-based wind energy conversion system using developed sliding mode control. Energies, 15(5), 1625.

[72] Zinelaabidine, B. (2015). Etude et commande d'un système de production d'électricité renouvelable locale (énergie éolienne et photovoltaïque) (Doctoral dissertation).

[73] Join, C., Bernier, J., Mottelet, S., Fliess, M., Rechdaoui-Guérin, S., Azimi, S., & Rocher, V. (2017). A simple and efficient feedback control strategy for wastewater denitrification. IFAC-PapersOnLine, 50(1), 7657-7662.

[74] Fliess, M. (2006). Analyse non standard du bruit. Comptes rendus. Mathématique, 342(10), 797-802.

[75] Rabiner, L. R., & Gold, B. (1975). Theory and Application of Digital Signal Processing:(by) Lawrence R. Rabiner (and) Bernard Gold. Prentice-Hall.

[76] Chiha, I., Liouane, N., & Borne, P. (2012). Tuning PID controller using multiobjective ant colony optimization. Applied Computational Intelligence and Soft Computing, 2012(1), 536326.

[77] Baghli, F. Z., Lakhal, Y., & El Kadi, Y. A. (2023). The Efficiency of an Optimized PID Controller Based on Ant Colony Algorithm (ACO-PID) for the Position Control of a Multi-articulated System. Journal of Robotics and Control (JRC), 4(3), 289-298.

[78] Zhang, X. L., & Zhang, Q. (2021, March). Optimization of PID parameters based on ant colony algorithm. In 2021 International Conference on Intelligent Transportation, Big Data & Smart City (ICITBS) (pp. 850-853). IEEE.

[79] Ali, M., Afandi, A. N., Nurohmah, H., Rukslin, R., Haikal, M. A., & Djalal, M. R. (2023, May). Optimization of wind-turbine control using the hybrid ANFIS-PID method based on ant colony optimization. In AIP Conference Proceedings (Vol. 2536, No. 1). AIP Publishing.

[80] Jagatheesan, K., Samanta, S., Boopathi, D., & Anand, B. (2021, December). Frequency stability analysis of microgrid interconnected thermal power generating system with GWO tuned PID controller. In 2021 9th IEEE international conference on power systems (ICPS) (pp. 1-5). IEEE.

[81] Varol, H. A., & Bingul, Z. (2004). A new PID tuning technique using ant algorithm. Proceedings of the American Control Conference, 3, 2154-2159.

[82] Devasahayam, V., & Veluchamy, M. (2017). An enhanced ACO and PSO based fault identification and rectification approaches for FACTS devices. International Transactions on Electrical Energy Systems, 27(8), e2344.

[83] Herlambang, T., Rahmalia, D., & Yulianto, T. (2019, April). Particle swarm optimization (pso) and ant colony optimization (aco) for optimizing pid parameters on autonomous underwater vehicle (auv) control system. In Journal of Physics: Conference Series (Vol. 1211, No. 1, p. 012039). IOP Publishing.

[84] Kanojiya, R. G., & Meshram, P. M. (2012, August). Optimal tuning of PI controller for speed control of DC motor drive using particle swarm optimization. In 2012 international conference on advances in power conversion and energy technologies (APCET) (pp. 1-6). IEEE.